이학박사 학위논문

Preclinical study of human mesenchymal stem cells with enhanced antioxidant capacity for treating asthma

중간배엽줄기세포의 항산화능 조절기전 연구를 통한 만성 천식질환 줄기세포 치료 고도화 연구

울산대학교대학원

의 과 학 과

윤 홍 덕

A thesis of the Doctor's degree

Preclinical study of human mesenchymal stem cells with enhanced antioxidant capacity for treating asthma

The Department of Biomedical Sciences

University of Ulsan

College of Medicine

HongDuck Yun

중간배엽줄기세포의 항산화능 조절기전 연구를 통한 만성 천식질환 줄기세포 치료 고도화 연구

지도교수 신 동 명

이 논문을 이학박사 학위 논문으로 제출함

2023년 8월

울산대학교대학원

의 과 학 과

윤 홍 덕

윤홍덕의 이학박사학위 논문을 인준함

심사위원장 최 경 철 (인)

심사위원 손 재 경 (인)

심사위원 문 경 준 (인)

심사위원 정 의 만 (인)

심사위원 신 동 명 (인)

울 산 대 학 교 대 학 원

2023 년 8 월

Preclinical study of human mesenchymal stem cells with enhanced antioxidant capacity for treating asthma

Thesis Director: Dong-Myung Shin

A thesis submitted to the Department of Biomedical Sciences in partial fulfillment of the requirements for the Degree of Doctor of Philosophy in Medical Science at University of Ulsan College of Medicine

August 2023

The Department of Biomedical Sciences

University of Ulsan

College of Medicine

HongDuck Yun

ABSTRACT

Chapter 1. Activating transcription factor-2 supports the antioxidant capacity and ability of human mesenchymal stem cells to prevent asthmatic airway inflammation

Glutathione (GSH), an abundant nonprotein thiol antioxidant, participates in several biological processes and determines the functionality of stem cells. A detailed understanding of the molecular network mediating GSH dynamics is still lacking.

Here, we show that activating transcription factor-2 (ATF2), a cAMP-response element binding protein (CREB), plays a crucial role in maintaining the level and activity of GSH in human mesenchymal stem cells (MSCs) by cross talking with nuclear factor erythroid-2 like-2 (NRF2), a well-known master regulator of cellular redox homeostasis.

Priming with ascorbic acid 2-glucoside (AA2G), a stable vitamin C derivative, increased the expression and activity of ATF2 in MSCs derived from human embryonic stem cells and umbilical cord. Subsequently, activated ATF2 cross talked with the CREB1-NRF2 pathway to preserve the GSH dynamics of MSCs through the induction of genes involved in GSH synthesis [glutamate-cysteine ligase catalytic subunit (GCLC) and glutamate-cysteine ligase modifier subunit (GCLM)] and redox cycling [Glutathione reductase (GSR) and Peroxiredoxin -1 (PRDX1)]. Accordingly, shRNA-mediated silencing of ATF2 significantly impaired the self-renewal, migratory, proangiogenic, and anti-inflammatory capacities of MSCs, and these defects were rescued by supplementation of the cells with GSH. In addition, silencing ATF2 attenuated the ability of MSCs to alleviate airway inflammatory responses in an ovalbumin-induced mouse model of allergic asthma.

Consistently, activation of ATF2 by overexpression or the AA2G-based priming procedure enhanced the core functions of MSCs, improving the in vivo therapeutic efficacy of MSCs for treating asthma. Collectively, these results suggest that ATF2 is a novel modulator of GSH

dynamics that determines the core functionality and therapeutic potency of MSCs used to treat allergic asthma.

Keywords

Glutathione, ATF2, AA2G, CREB1-NRF2 pathway, GSH dynamics, redox cycling, allergic asthma, Human Embryonic Stem Cell–Derived Multipotent MSC, Human Umbilical Cord-derived Mesenchymal Stem Cell

*This work is published in Experimental and Molecular Medicine (2023). PMID :36765266

Chapter 2. A preclinical study of human embryonic stem cell-derived mesenchymal stem cells for treating detrusor underactivity by chronic bladder ischemia

The therapeutic effects of human embryonic stem cell-derived multipotent mesenchymal stem cells (M-MSCs) were evaluated for detrusor underactivity (DUA) in a rat model with atherosclerosis-induced chronic bladder ischemia (CBI) and associated mechanisms.

Sixteen-week-old male Sprague–Dawley rats were divided into five groups (n = 10). The DUA groups underwent 30 bilateral repetitions of endothelial injury to the iliac arteries to induce CBI, while the sham control group underwent a sham operation. All rats used in this study received a 1.25 % cholesterol diet for 8 weeks. M-MSCs at a density of 2.5, 5.0, or 10.0×10^5 cells (250 K, 500 K, or 1000 K; K = a thousand) were injected directly into the bladder 7 weeks post-injury, while the sham and DUA group were treated only with vehicle (phosphate buffer solution). One week after M-MSC injection, awake cystometry was performed on the rats. Then, the bladders were harvested, studied in an organ bath, and prepared for histological and gene expression analyses.

CBI by iliac artery injury reproduced voiding defects characteristic of DUA with decreased micturition pressure, increased micturition interval, and a larger residual volume. The pathological DUA properties were improved by M-MSC treatment in a dose-dependent manner, with the 1000 K group producing the best efficacy. Histological analysis revealed that M-MSC therapy reduced CBI-induced injuries including bladder fibrosis, muscular loss, and apoptosis. Transplanted M-MSCs mainly engrafted as vimentin and NG2 positive pericytes rather than myocytes, leading to increased angiogenesis in the CBI bladder. Transcriptomes of the CBI-injured bladders were characterized by the complement system, inflammatory, and ion transport-related pathways, which were restored by M-MSC therapy. Single injection of M-MSCs directly into the bladder of a CBI-induced DUA rat model improved voiding profiles and repaired the bladder muscle atrophy in a dose-dependent manner.

Keywords

Detrusor underactivity, Chronic bladder ischemia, Multipotent mesenchymal stem cells, Embryonic stem cells

*This work is published in Stem Cell Reviews and Reports (2021). PMID :34189670

CONTENTS

LIST OF FIGURES AND TABLES

Chapter 1

Chapter 2

LIST OF ABBREVIATION

Activating Transcription Factor 2 (ATF2)

Ascorbic Acid 2-Glucoside (AA2G)

Analysis of Variance (ANOVA)

Arterial Injury (AI)

Aluminum hydroxide (Alum)

Alpha smooth muscle actin (α-SMA)

Angiopoietin 1 (Angpt-1)

Angiopoietin-1 receptor, Tyrosine-protein kinase receptor (ANG1 also known as TEK)

Bronchoalveolar Lavage Fluid (BALF)

Bladder Capacity (BC)

cAMP-Responsive Element-Binding Protein-1 (CREB1)

Chronic Bladder Ischemia (CBI)

Cholinergic receptor muscarinic-2 (Chrm2)

Cholinergic receptor muscarinic-3 (Chrm3)

Claudin-23 (Cldn23)

Colony stimulating factor-3 receptor (Csf3r)

Colony-Forming Unit-Fibroblast (CFU-F)

Conditioned Medium (CM)

Complement factor-H (CfH)

C-X-C motif chemokine ligand-2 (Cxcl2)

C-X-C motif chemokine ligand-3 (Cxcl3)

C2 complement (C2)

Detrusor Underactivity (DUA)

Detrusor Overactivity (DO)

Differentially Expressed Genes (DEGs)

Dulbecco's Modified Eagle's Medium (DMEM)

Electrical Field Stimulation (EFS)

Embryonic Stem Cells (ESCs)

Extracellular matrix (ECM)

Fluorescent Real-time Thiol Tracer (FreSHtracer)

Forskolin (FSK)

Fibroblast growth factor-2 (FGF2)

Fluorescence ratio (FR)

Fetal Bovine Serum (FBS)

Fc fragment of immunoglobulin G receptor-IIb (Fcgr2b)

Fluorescence activated cell sorting (FACS)

Glutathione (GSH)

Glutathione reductase (GSR)

GSH-recovering capacity (GRC)

GSH ethyl ester (GSH-EE)

GSH index (GI)

Glutamate-cysteine ligase catalytic subunit (GCLC)

Glutamate-cysteine ligase modifier subunit (GCLM)

Gs alpha subunit protein (Gαs)

G protein-coupled receptor (GPCR)

G protein subunit α I1 (GNAI1)

Gene Ontology (GO)

Gene Set Enrichment Analysis (GSEA)

Human beta 2-Microglobulin (hB2M)

Human Embryonic Stem Cell-Derived Multipotent MSC (hES-MSC)

Human Umbilical Cord-Derived Mesenchymal Stem Cell (hUC-MSC)

Hypoxia Inducible Factor-1 (HIF-1)

Hydroxy tryptamine Receptor 2B (HTR2B)

Hematoxylin and eosin (H&E)

Interstitial cystitis/bladder pain syndrome (IC/BPS)

Interferon Gamma Receptor-1 (Ifngr1)

Interferon induced protein with tetratricopeptide repeats 1B-like (Ifit1bl)

Interferon induced protein with tetratricopeptide repeats-1 (Ifit-1, also known as Ifi-56)

Interferon gamma receptor-1 (Ifngr-1)

Interleukin-17 (IL-17)

Induced pluripotent stem cell (iPSC)

Intra-vesical pressure (IVP)

Intra-abdominal pressure (IAP)

Integrin subunit α-V (ITGAV)

Interleukin-33 (Il-33)

Intravenous injection (i.v.)

Intraperitoneal injection (i.p.)

Intranasal injection (i.n.)

Knock-Down (KD)

Lipopolysaccharide (LPS)

L1 cell adhesion molecule (L1cam)

Multipotent MSCs (M-MSCs)

Mesenchymal Stem Cell (MSC)

Micturition Interval (MI)

Micturition Volume (MV)

Neural/glial antigen 2 (NG2)

NFKB Inhibitor-alpha (Nfkbia)

Nuclear Factor Erythroid 2 Like 2 (NRF2)

Ovalbumin (OVA)

Open reading frame (ORF)

Primed/Fresh/OCT4 (PFO)

Pluripotent stem cells (PSCs)

Platelet-Derived Growth Factor (PDGF)

Programmed Death-Ligand 1 (PD-L1 & B7-H1)

Peroxiredoxin-1 (PRDX1)

Phospholipase A2 Group IIA (Pla2g2a)

Platelet-Derived Growth Factor Receptor (PDGFR)

Phosphate-buffered saline (PBS)

Pro surfactant protein C (SFTPC)

Phosphorylated ATF2 (p-ATF2)

Reactive Oxygen Species (ROS)

Real time quantitative PCR (RQ-PCR)

Residual Volume (RV)

Short hairpin RNA (shRNA)

S100 calcium binding protein-A9 (S100a9)

Sphingosine-1-phosphate (S1P)

Standard error of the mean (SEM)

Total ATF2 (t-ATF2)

Transferrin (Tf)

T helper 2 (Th2)

Threonine 69 (Thr69)

Threonine 71 (Thr71)

Tumor Necrosis Factor-α (TNF-α)

Transferase dUTP nick end labeling (TUNEL)

Transforming growth factor β-1 (TGFB1)

Transmembrane Channel Like 7 (Tmc7)

Vascular Endothelial Damage (VED)

Vascular Endothelial Growth Factor-A (Vegfa)

Vitamin-C (Vit C)

Valproic acid (VPA)

VEGF receptor-1 (VEGFR1)

CHAPTER 1

Activating transcription factor-2 supports the antioxidant capacity and ability of human mesenchymal stem cells to prevent asthmatic airway inflammation

INTRODUCTION

Asthma is the most common chronic disease of the lungs in children and adults. The prevalence of asthma has doubled in the past decade, leading to a substantial global health and economic burden. Asthma is an allergic disease that is characterized by a combination of inflammation and structural remodeling in the airways [1]. The resulting airway obstruction causes breathing difficulties, wheezing, shortness of breath, and coughing. Immune responses mediated by innate lymphoid cells and T helper 2 (Th2) cells contribute to allergic airway inflammation and fibrosis, causing permanent deterioration in pulmonary function [2–4]. Asthma patients are grouped into one of four or five categories and are treated in a stepwise manner, depending on symptom severity or extent of disease. Inhaled corticosteroids, long-acting β2-adrenergic receptor agonists, long-acting muscarinic antagonists, and leukotriene receptor antagonists are used as asthma-control drugs, and an IgE-specific monoclonal antibody is used to treat the most severe form of the disease [5]. Although this stepwise approach has improved the management of asthma and reduced dependency on inhaled short-acting bronchodilators for symptom relief, none of the currently available treatments can alter the progression of the disease; hence, there is an urgent need to develop novel therapies. Preclinical and clinical studies have suggested beneficial effects of mesenchymal stem cells (MSCs) in treating incurable allergic asthma [6–10]. These progenitor cells are typically derived from adult tissues, such as the bone marrow, adipose tissue, and umbilical cord (UC) or UC blood, and can also be established by differentiation from pluripotent stem cells (PSCs), including embryonic stem cells (ESCs) and induced PSCs (iPSCs) [11–14]. The therapeutic effects of MSCs are thought to be attributable to their multipotency and ability to directly regenerate damaged cells in target tissues. In addition, MSCs can have indirect effects by providing growth factors, mediating cell–cell interactions, and supplying matrix proteins to modulate the microenvironment of damaged target tissues and facilitate regeneration [15,16]. In particular, the anti-inflammatory and immunomodulatory functions of MSCs are achieved by inhibiting the activation, proliferation, and function of immune cells, including T cells, B cells, innate lymphoid cells, natural killer cells, and antigen-presenting cells [17,18]. Despite the multifactorial benefits of MSCs, their clinical application has been hindered by limited

therapeutic efficacy and a lack of knowledge of their precise mode of action. The high therapeutic potency of primitive MSCs is reportedly lost after large-scale ex vivo expansion, which is required to obtain a sufficient number for therapeutic purposes, due to an accumulation of epigenetic abnormalities and oxidative stress provoked by supraphysiological stimulations [19]. We have described several ex vivo expansion methods to preserve the primitiveness of MSCs, including i) enriching and preserving small-sized cells [20], ii) enhancing the antioxidant capacity by real-time monitoring of glutathione (GSH) dynamics [9,21], and iii) enhancing cell migration and engraftment activity by priming with small molecules [22]. In addition, we recently reported that supplementation with small compounds without genetic manipulation enables the enrichment and expansion of small primitive MSCs with a high antioxidant and engraftment capacity, which was termed the Primed/Fresh/OCT4 (PFO) enrichment procedure [23]. All of these procedures enhance the levels and dynamics of GSH, which is essential to maintain the stemness and therapeutic efficacy of human MSCs [9,21,23]. Mechanistically, MSCs with high GSH dynamics display activation of the cyclic adenosine monophosphate (cAMP)-response element (CRE) binding protein-1 (CREB1) and nuclear factor erythroid-2 like-2 (NRF2) pathway, leading to the induction of genes involved in GSH synthesis (GCLC and GCLM) and redox cycling (GSR and PRDX1) [10,21,23]. The intracellular levels and dynamics of GSH in MSCs can be improved by pretreatment/priming with forskolin (FSK), a CREB1 activator, or by priming with ascorbic acid 2-glucoside (AA2G), a stable vitamin-C (Vit C) derivative that activates CREB1 and in turn upregulates NRF2 target genes responsible for GSH synthesis and redox cycling [10,21]. The biological effects of these GSH-enhancing conditions stimulate the core functions of MSCs derived from various sources, including human ESCs and adult tissues such as the UC and bone marrow. Notably, in previous studies, the in vivo therapeutic effects of MSCs were enhanced by improving GSH dynamics in an experimental asthma animal model and a humanized graft-versus host disease mouse model [10,23]. In this study, we demonstrate that activating transcription factor-2 (ATF2), a member of the leucine zipper domain containing CREB/ATF transcription factor family, plays a key role in modulating GSH dynamics and determining the core functionality and therapeutic potency of MSCs used to treat allergic asthma.

MATERIALS AND METHODS

Study approval

Human UC samples were obtained from healthy full-term newborns after obtaining written informed consent. All procedures were performed in accordance with the guidelines of the Ethics Committee on the Use of Human Subjects at Asan Medical Center (IRB#: 2015-0303). All animal experiments were approved by and performed in accordance with the guidelines and regulations of the Institutional Animal Care and Use Committee of the University of Ulsan College of Medicine (IACUC-2019-12-221 and IACUC-2019-12-325).

Culture of MSC

Human ESC-derived MSCs (hES-MSCs) were established by differentiation from H9 hESCs [11,12] and were maintained in EGM2-MV medium (Lonza, San Diego, CA, USA) on plates coated with rat tail collagen type I (Sigma Aldrich, St. Louis, MO, USA), as described previously [9,10,13]. Human UC MSCs (hUC-MSCs) were isolated from UCs, as described previously [24], and were grown in low-glucose DMEM containing 10 % heat-inactivated fetal bovine serum (HyClone, Pittsburgh, PA, USA), 5 ng/mL human epidermal growth factor (Sigma-Aldrich), 10 ng/mL basic fibroblast growth factor, and 50 ng/mL long-R3 insulin-like growth factor-1 (ProSpec, Rehovot, Israel), as described previously [10,21,22]. All MSCs used in this study were expanded for fewer than seven passages to ensure their functionality and were maintained at 37 °C in a humidified atmosphere containing 5 % CO_2. For GSH-enhancing priming, MSCs were plated at a density of 7×10^4 cells/mL in culture medium with the indicated concentration of AA2G (Sigma-Aldrich) for 3 days or 2 μM FSK (Sigma-Aldrich) for the indicated number of hours. The intracellular GSH level was rescued by supplementation with 0.125 μM GSH ethyl ester (GSH-EE; Sigma-Aldrich) for 4 h. The PFO procedure was performed by supplementation with AA2G, followed by treatment with low

concentrations of sphingosine-1-phosphate (S1P) and valproic acid (VPA), as previously described [23]. In brief, MSCs were plated at a density of 7×10^4 cells/mL and maintained in culture medium with 0.74 mM (Sigma-Aldrich) for two days. One day before the functional evaluation, 50 nM S1P and 0.5 mM VPA (Sigma-Aldrich) were added to the culture medium containing 0.74 mM AA2G.

RNA interference and ectopic expression of ATF2

RNA interference and ectopic expression of ATF2 For knockdown (KD) of ATF2, three independent shRNAs targeting human ATF2 were cloned into the pLenti6/Block-iT lentiviral vector (Invitrogen/Thermo Fisher Scientific, Waltham, MA, USA). For ectopic expression, the open reading frame (ORF) of human ATF2 in the pDONR223 plasmid (Addgene plasmid # 82889) was cloned into the pEZ-Lv235 (#EZ016, GeneCopoeia, Rockville, MD, USA) plasmid using the Gateway Technology reaction in accordance with the manufacturer's instructions (Invitrogen/Thermo Fisher Scientific). Lentiviruses carrying each ATF2 shRNA or human ATF2 ORF were produced and used to infect hES-MSCs or hUC-MSCs, as described previously [25]. The ORF of human ATF2 was kindly provided to us by Jesse Boehm, Matthew Meyerson, and David Root.

In vitro cell proliferation, self-renewal, multipotency, and migration of MSCs

Several in vitro assays were performed to assess the cellular activities of MSCs. An MTT assay (Sigma-Aldrich) was used to assess cell proliferation, and a colony forming unit-fibroblast (CFU-F) assay was used to assess self-renewal. Multipotency (in vitro differentiation into chondrogenic, osteogenic, or adipogenic lineages) and trans well migration in response to platelet-derived growth factor (PDGF; 10 ng/mL PDGF-AA, R&D Systems, Minneapolis, MN, USA) were also assessed. Angiogenesis was quantified using Matrigel, and in vitro anti-inflammation was analyzed as described previously [8-10,20,21]. The digital

images generated in these assays were assessed quantitatively using Image-Pro 5.0 software (Media Cybernetics, Rockville, MD, USA).

Real-time monitoring of the GSH-recovery capacity of living MSCs

Real-time monitoring of the GSH-recovering capacity (GRC) of every living cell under different culture conditions was achieved using an Operetta High-Content Imaging System (HH12000000; PerkinElmer, Waltham, MA, USA) at ×200 or ×400 magnification, as described previously [21]. This system provides a nondestructive, integrated, and image-based high throughput method for analyzing the qualitative and quantitative aspects of GSH dynamics in living MSCs. The GRC assay was based on the unique properties of FreSHtracer (Fluorescent real-time thiol tracer; Cell2in, Inc., Seoul, Korea), a reversible chemical probe for GSH [9,26]. Upon reacting with GSH, FreSHtracer shows a spectral shift in the λ_{max} of its ultraviolet–visible absorption from 520 nm to 430 nm, resulting in decreased fluorescence emission intensity at 580 nm (F_{580}, λ_{ex} 520 nm) and increased fluorescence intensity at 510 nm (F_{510}, λ_{ex} 430 nm) [9,26]. Thus, to determine the fluorescence ratios of FreSHtracer, fluorescence emissions were measured at 510 and 580 nm after excitation at 430 and 520 nm, respectively. These fluorescence signals were analyzed using Harmony High-Content Imaging and Analysis Software 3.1 (PerkinElmer) in confocal mode.

Asthma animal model

Asthma was induced in 6-week-old female BALB/c mice (JA Bio, Suwon, Korea) by sensitization with intraperitoneal injections of 100 μg of ovalbumin (OVA, Sigma-Aldrich) and 2 mg of aluminum hydroxide (Alum, Sigma-Aldrich) on Days 0 and 7, followed by allergen challenge via intranasal injection of 50 μg of OVA on Days 14, 15, 16, 21, 22, and 23, as reported previously [27]. After 17 days, 3×10^5 hUC-MSCs stably expressing a control (shCTR), or ATF2-specific (shATF2) shRNA construct were suspended in 100 μL of

phosphate-buffered saline (PBS) and injected via the tail vein. The same procedure was applied for the administration of hUC-MSCs or hES-MSCs, which were expanded under normal (naïve) culture conditions or using the PFO procedure. PBS alone was injected as a control (sham and asthma groups). Mice were randomly allocated to treatment groups, and the order of allergen sensitization or challenge and injection of MSCs or vehicle was randomized. Treatment groups were masked to investigators who participated in the therapeutic evaluation procedures.

Analysis of airway inflammation

For mechanistic insights into MSC therapy, airway inflammation was evaluated by histological examination and bronchoalveolar lavage fluid (BALF) analysis, as well as via analyses of the expression levels of cytokine genes and proteins in the lung, as reported previously [9,10]. Therapeutic outcomes were analyzed using two independent sets of five animals per group. All histological, BALF, and cytokine analyses were performed by blinded investigators.

For analysis of engraftment of the hUC-MSCs, human β2-microglobulin (hB2M) was detected using a mouse monoclonal antibody (SC80668; Santa Cruz Biotechnology, Santa Cruz, CA, USA) and an Alexa Fluor 488-labeled anti-mouse secondary antibody (Invitrogen). Differentiation lineage was determined by co-staining for hB2M and prosurfactant protein C (SFTPC) rabbit polyclonal antibody (ab90716; Abcam, Cambridge, UK) and visualization with an Alexa Fluor 546- labeled anti-rabbit secondary antibody (Invitrogen). Nuclei were counterstained using DAPI (Sigma-Aldrich). Digital images were selected at random from each slide and used for quantification using Image-Pro 5.0 software.

For gene expression analyses, total RNA was isolated from frozen lung tissues using the RNeasy Mini Kit (Qiagen, Hilden, Germany) and treated with DNase I (Qiagen). Total RNA (800 ng) was reverse-transcribed with TaqMan Reverse Transcription Reagent (Applied

Biosystems, Foster City, CA), and the threshold cycle (Ct) was subsequently determined via real time quantitative PCR (RQ-PCR), as described previously [28]. The relative expression level of each target gene was determined using the $2^{-\Delta\Delta Ct}$ method, with Gapdh as the endogenous control gene.

Statistical analysis

Statistical significance was evaluated by the nonparametric Mann–Whitney test and one-way or two-way ANOVA with the Bonferroni post hoc test using GraphPad Prism 7.0 software (GraphPad Software, La Jolla, CA, USA); $p < 0.05$ was considered statistically significant.

RESULTS

Priming to enhance GSH levels activates ATF2 in MSCs

In a previous transcriptome analysis, a population of hES-MSCs with a high level of GSH (GSH^{High}) was characterized by upregulation of the genes encoding ATF2 and other structurally related activating protein-1 (AP1) proteins, such as JUN, JUNB, and FRA1 [21,29]. This finding was validated by increased levels of the proteins encoded by these genes, as well as their phosphorylated active counterparts, in GSH^{High} hES-MSCs [21]. ATF2 forms a heterodimer with several AP1 proteins, binds to the CRE to regulate gene expression and is activated by several extracellular stimuli, such as hypoxia, oxidative stress, and DNA damage [29–31]. Therefore, we examined whether priming to enhance GSH levels could activate cAMP-dependent ATF2 and affect the CREB1-NRF2 signaling cascade in MSCs derived from different sources (Fig. 1-1a). To this end, we examined the expression level and activity of ATF2 in hES-MSCs and hUC-MSCs cultured in medium with different concentrations (0, 0.37, 0.74, and 1.48 mM) of AA2G for 72 h. RQ-PCR and western blot analyses showed that the transcript and protein levels of ATF2 were increased by AA2G priming in both hES-MSCs and hUC-MSCs (Fig. 1b–d), peaking at the 0.74 mM AA2G concentration. This upregulation was accompanied by an increase in the level of active ATF2 protein, which is phosphorylated at threonine 69 (Thr69) and threonine 71 (Thr71) via mitogen-activated protein kinases such as p38, JNK, and ERK [32]. Consistent with these results, the expression levels of a subset of ATF2 target genes, including PDGFRA, MMP2, and PLAU, were increased following AA2G priming, and this effect was greater in hUC-MSCs than in hES-MSCs (Fig. 1-1e).

We previously reported that further stimulation of AA2G-primed MSCs with a low concentration of S1P and VPA was beneficial for preserving primitive MSCs, characterized morphologically by their small size and high GSH dynamics [23]. In this regard, we examined whether the expression of ATF2 could be affected by the PFO procedure based on the combination of three small molecules, AA2G, S1P, and VPA (Fig. 1-1f). The PFO procedure increased ATF2 transcript and protein expression levels in both hES- and hUC-MSCs (Fig. 1-1g, 1h), resulting in the upregulation of ATF2 target genes.

Next, we examined the effect of FSK priming on ATF2 expression. FSK treatment of hUC-MSCs increased the ATF2 transcript level only minimally but significantly increased the levels of total and phosphorylated ATF2 proteins, with peaks occurring 4 and 2 h after FSK priming, respectively. In hES-MSCs, FSK priming had slight effects on the levels of the ATF2 transcript and protein. Overall, these data demonstrate that GSH-enhancing priming conditions can regulate the expression and activity of ATF2 in human MSCs, depending on the particular cell context and priming factors used. Since AA2G treatment stably activated ATF2 in both hES-MSCs and hUC-MSCs, we used the optimal dose of 0.74 mM AA2G in subsequent studies.

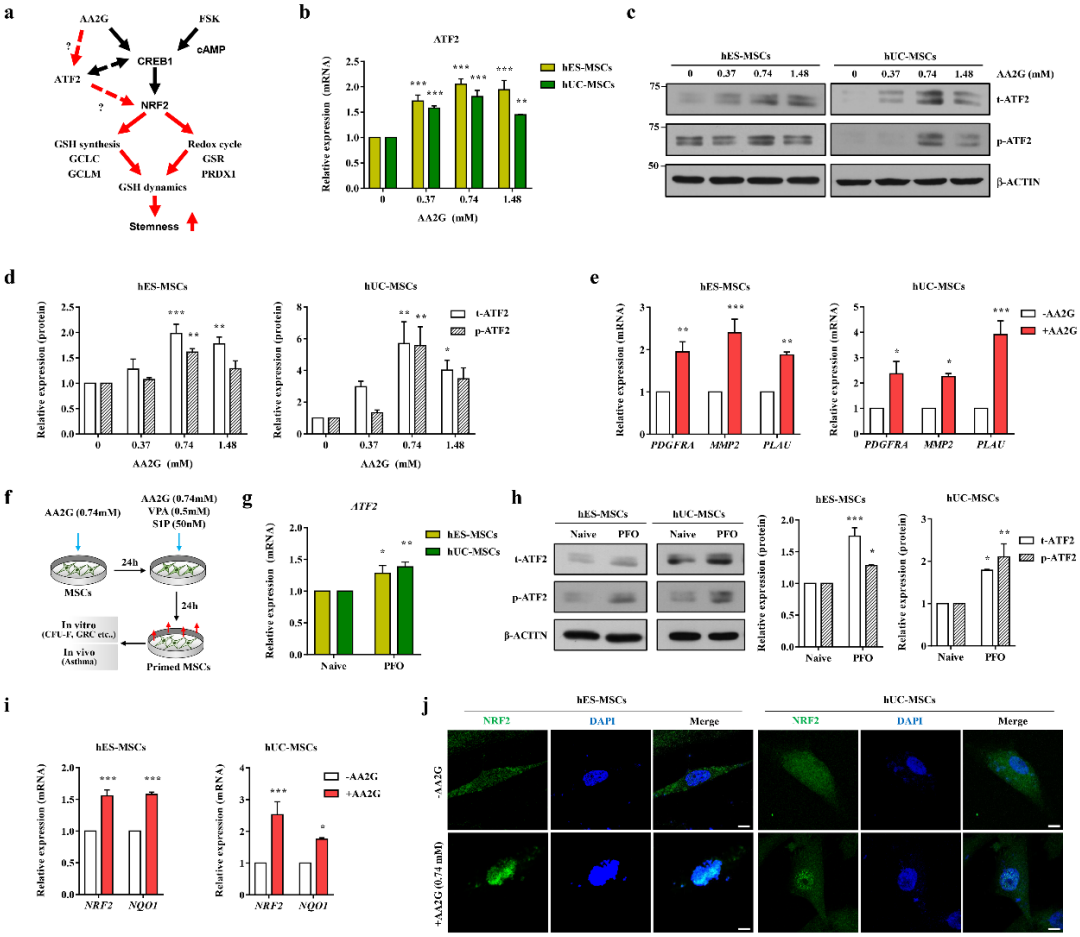

Figure 1-1. AA2G priming activates ATF2 and NRF2 in human MSCs

(**a**) A schematic overview of the ATF2 and CREB1-NRF2 cascades involved in GSH dynamics in human MSCs. (**b**) RQ-PCR analysis (n = 4) of the ATF2 transcript in the AA2G-treated hES-MSCs and hUC-MSCs. (**c**) Western blot analyses (n = 3) of total ATF2 (t-ATF2) and phosphorylated ATF2 (p-ATF2) proteins in the AA2G-treated hES-MSCs and hUC-MSCs. The expression level of β-actin was used as a loading control. Molecular weight marker sizes (kD) are shown on the left. (**d**) Quantification of the western blotting data described in (**c**, **e**) RQ-PCR analyses (n = 4) of ATF2 target genes following treatment of hES-MSCs and hUC-MSCs with AA2G for 72 h. (**f**) Schematic summary of the PFO procedure, which included supplementation with 0.74 mM AA2G for two days, followed by further stimulation with 50

nM sphingosine 1-phosphate (S1P) and 0.5 mM valproic acid (VPA) one day before functional evaluation. RQ-PCR (n = 4; **g**) and western blot analyses (n = 3; **h**) for the expression of ATF2 in hES-MSCs and hUC-MSCs under normal (naïve) or PFO culture conditions. (**i**) RQ-PCR analyses (n = 4) of NRF2 and NQO1 in the hES-MSCs and hUC-MSCs primed with 0.74 mM AA2G for 72 h. (**j**) Representative confocal microscopy images of the NRF2 protein (green) in the hES-MSCs and hUC-MSCs treated with or without AA2G. Magnification, ×1000. Scale bar, 10 μm. Nuclei were stained with DAPI (blue). (**b**, **d**–**i**) Data are represented as ratios relative to the nontreated cells (-AA2G). All quantification results are shown as the mean ± SEM (*$p < 0.05$, **$p < 0.01$, ***$p < 0.001$ compared with nontreated cells, via two-way ANOVA).

ATF2 regulates redox homeostasis in MSCs by crosstalking with the NRF2 pathway

We then investigated whether ATF2 can directly modulate the CREB1-NRF2 signaling cascade in MSCs. In both hES-MSCs and hUC-MSCs, AA2G priming increased the mRNA expression levels of NRF2 and NQO1, a well-known NRF2 target gene (Fig. 1-1i), and stimulated translocation of the NRF2 protein into the nucleus, indicating activation of the NRF2 pathway (Fig. 1-1j). Consistent with these results, AA2G priming also increased the expression levels of genes related to GSH synthesis (GCLC and GCLM) and redox cycling (GSR and PRDX1) (Fig. 1-2a), which have been reported as targets of the CREB1-NRF2 pathway that play a role in the maintenance of redox homeostasis in MSCs21. NRF2 and its targets (GCLC, GCLM, GSR, and PRDX1) were decreased at the mRNA and protein levels in MSCs harboring shRNAs targeting ATF2 (shATF2) (Fig. 1-2b). Notably, KD of ATF2 also impaired the AA2G-mediated nuclear translocation of the NRF2 protein (Fig. 1-2d) and induction of the GSH-related genes targeted by CREB1-NRF2 (GCLC, GCLM, PRDX1, and GSR) (Fig. 1-2e), suggesting an interplay between the ATF2 and CREB1-NRF2 signaling cascades in MSCs. The majority of ATF2 target genes activated by AA2G priming were downregulated by KD of ATF2.

To investigate the biological relevance of these findings, we used a high-throughput GRC assay (Fig. 1-3), which enables real-time monitoring of the qualitative and quantitative aspects of GSH dynamics in living cells using a reversible chemical probe [21]. Changes in the intracellular GSH level were monitored for approximately 1 h after exposure to diamide, a thiol-specific oxidant. KD of ATF2 decreased the basal level of GSH and impaired the GRC following diamide treatment in both hES-MSCs and hUC-MSCs (Fig. 1-2f), indicating a crucial role of ATF2 in maintaining GSH dynamics in MSCs. Collectively, these results demonstrate that ATF2 acts as a novel mediator of redox homeostasis in MSCs by crosstalking with the NRF2 signaling cascade.

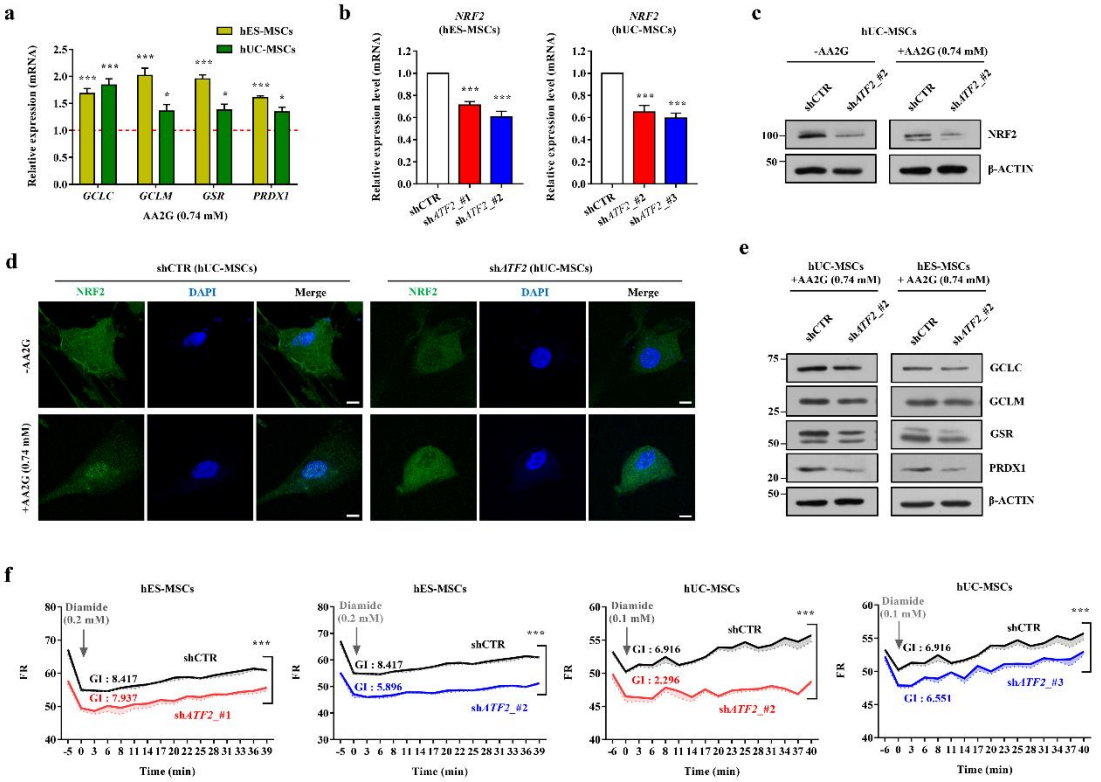

Figure 1-2. Crosstalk between the ATF2 and NRF2 pathways in AA2G-primed MSCs

(**a**) RQ-PCR analyses (n = 4) of CREB1-NRF2-dependent GSH synthesis (GCLC and GCLM) and redox cycling (GSR and PRDX1) genes in AA2G-primed MSCs. Expression levels were calculated as the ratio of the value of AA2G-primed MSCs to the nontreated cells (set to 1; see the red dotted line). RQ-PCR analysis (n = 4) of the NRF2 transcript (**b**) and western blot analyses of NRF2 protein (**c**) in the MSCs expressing a scrambled control shRNA (shCTR) or an ATF2-specific shRNA (shATF2). Two independent shATF2 constructs were used. (**d**) Representative confocal microscopy images of the NRF2 protein (green) in the hUC-MSCs treated with or without AA2G and expressing shCTR or shATF2. Nuclei were stained with DAPI (blue). Magnification, ×1000. Scale bar, 10 μm. (**e**) Western blot analyses of NRF2 target genes in the AA2G-primed hES-MSCs and hUC-MSCs expressing shCTR or shATF2. Molecular weight marker sizes (kD) are shown on the left of the blots. (**f**) F_{510}/F_{580} fluorescence ratio (FR) plots of the hES-MSCs and hUC-MSCs carrying the indicated shCTR or shATF2

constructs. The GSH dynamics index (GI) for each sample (n = 3) was quantified based on both the initial FR (representing the baseline of total GSH) and the slope after 0.1 or 0.2 mM diamide treatment (representing the GRC). Representative images of F_{510} (GSH bound) and F_{580} (GSH free) fluorescence are shown in Fig. 1-3b. All quantification results are shown as the mean ± SEM. Statistical analyses were performed via one-way (**b**) or two-way (**a** and **f**) ANOVA with Bonferroni post hoc tests (*$p < 0.05$, ***$p < 0.001$ compared with nontreated or shCTR cells).

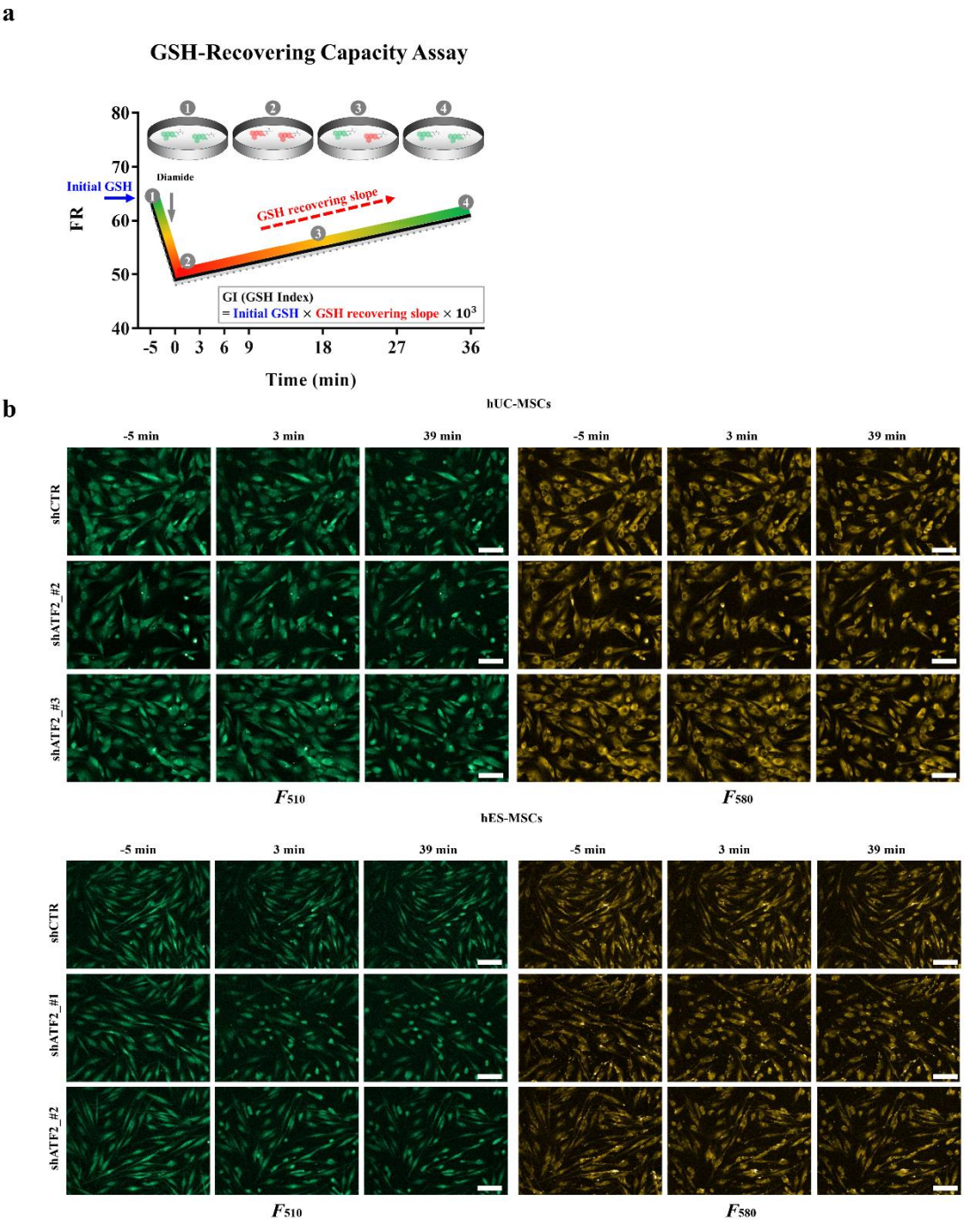

Figure 1-3. Real-time live-cell GSH recovery capacity assay

(**a**) A schematic overview for evaluating the GSH recovery capacity (GRC), an indicator of cellular antioxidant capacity. Changes in GSH dynamics in every living single cell were

monitored in real-time using an Operetta High-Content Imaging System and FreSHtracer (Fluorescent real-time thiol tracer), a reversible GSH fluorescent probe [1,2]. The GI of each sample following exposure to 0.1 or 0.2 mM diamide was quantified based on both the initial F_{510}/F_{580} fluorescence ratio (FR) (representing the baseline total GSH) and the slope after diamide treatment (representing the GRC), as described previously [2]. (**b**) Representative images of F_{510} (GSH bound) and F_{580} (GSH free) fluorescence in hES-MSCs and hUC-MSCs carrying the indicated shCTR or shATF2 constructs. The related FR plots with quantification results are shown in Fig. 1-2f.

ATF2 regulates the core functions of MSCs

To explore its role in maintaining the characteristics of MSCs that influence their therapeutic potency, we silenced ATF2 in hES-MSCs by infecting the cells with lentiviruses harboring two independent shATF2 constructs. KD of ATF2 had little effect on the expression of surface markers characteristic of MSCs, including CD29, CD73, and CD105. Furthermore, KD of ATF2 had little effect on the in vitro differentiation of hES-MSCs into the chondrogenic, adipogenic, and osteogenic lineages, which were evaluated by an increased level of cartilage proteoglycans (Alcian Blue staining), accumulation of lipid droplets (Oil Red O staining), and mineral deposition (Alizarin Red S staining), respectively.

KD of ATF2 in hES-MSCs decreased the potency of CFU-F, which represents the presence of true clonogenic progenitor cells (Fig. 1-4a) but did not significantly affect cell proliferation. A transwell chemotactic assay revealed that ATF2-KD hES-MSCs exhibited a severe defect in PDGF-stimulated cell migration (Fig. 1-4b). Furthermore, the ability of conditioned medium (CM) from ATF2-KD hES-MSCs to induce angiogenesis in a Matrigel tube formation assay was lower than that of CM from MSCs harboring a control shRNA (shCTR) construct (Fig. 1-4c). As observed in hES-MSCs, KD of ATF2 had minimal effects on the basic characteristics of MSCs, including surface marker phenotypes, multipotency, and cell proliferation (Fig. 1-5a), but significantly impaired the core functions of hUC-MSCs, including the potency of CFU-F (self-renewal) and PDGF-responsive chemotaxis capacity (Fig. 1-5b, c).

To examine the anti-inflammatory response of MSCs, we collected CM from hUC-MSCs and applied it to MH-S murine alveolar macrophages that were pretreated with lipopolysaccharide (LPS). As reported previously [10,21,23], CM from hUC-MSCs expressing shCTR significantly reduced secretion of the proinflammatory cytokines tumor necrosis factor-α (TNF-α) and interleukin-6 (IL-6) by LPS-stimulated MH-S cells, whereas CM collected from control cells (IMR90 human lung fibroblasts) did not (Fig. 1-5d). Notably, CM from ATF2-KD hUC-MSCs was less able to repress the secretion of TNF-α and IL-6 by LPS-stimulated MH-S cells than CM from control hUC-MSCs (Fig. 1-5d), indicating impairment of the anti-inflammatory potency of ATF2-KD cells. These results were validated further by examining the repressive effects of CM from the control and ATF2-KD cells on the

expression levels of various proinflammatory genes in the LPS-treated MH-S cells (Fig. 1-5e).

Importantly, the ectopic expression of ATF2 enhanced the PDGF-responsive chemotaxis activities in both hES- and hUC-MSCs (Fig. 1-6a–e). In addition, the proangiogenic or anti-inflammatory capacities were increased by the overexpression of ATF2 in hES- or hUC-MSCs, respectively (Fig. 1-7a, b). Collectively, the results of these in vitro functional assays indicate that ATF2 plays a critical role in preserving the primitive state of MSCs, as evidenced by their improved self-renewal, migratory, proangiogenic, anti-inflammatory, and immunomodulatory activities, all of which are related to their therapeutic potency.

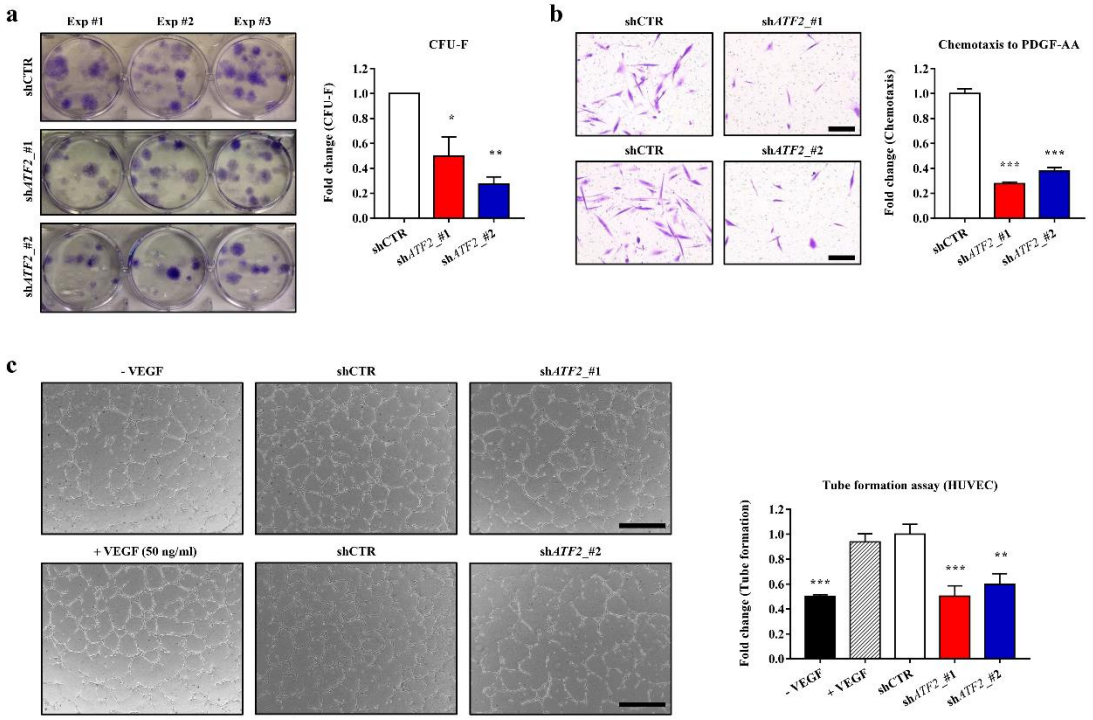

Figure 1-4. ATF2 is critical for maintaining the core functions of hES-MSCs

The effects of silencing ATF2 in hES-MSCs on colony forming unit fibroblast (CFU-F) potency (n = 3; **a**), chemotaxis (n = 7; **b**) in response to treatment with 10 ng/mL PDGF-AA, and angiogenesis in an in vitro Matrigel tube formation assay (n = 4; **c**). Cells expressed a scrambled control (shCTR) or ATF2-specific (shATF2) shRNA. Two independent shATF2 constructs were used. Representative results for each assay are shown on the left (**b**: magnification, ×200; scale bar, 100 μm; (**c**): magnification, ×40; scale bar, 200 μm). For the Matrigel tube formation assay, conditioned medium was prepared from the indicated hES-MSCs, and saline and recombinant human VEGF-A were used as negative and positive controls, respectively. Quantitative data are presented as ratios relative to the shCTR cells and are expressed as the mean ± SEM. Statistical analyses were performed via one-way ANOVA (*$p < 0.05$, **$p < 0.01$, ***$p < 0.001$ compared with shCTR cells).

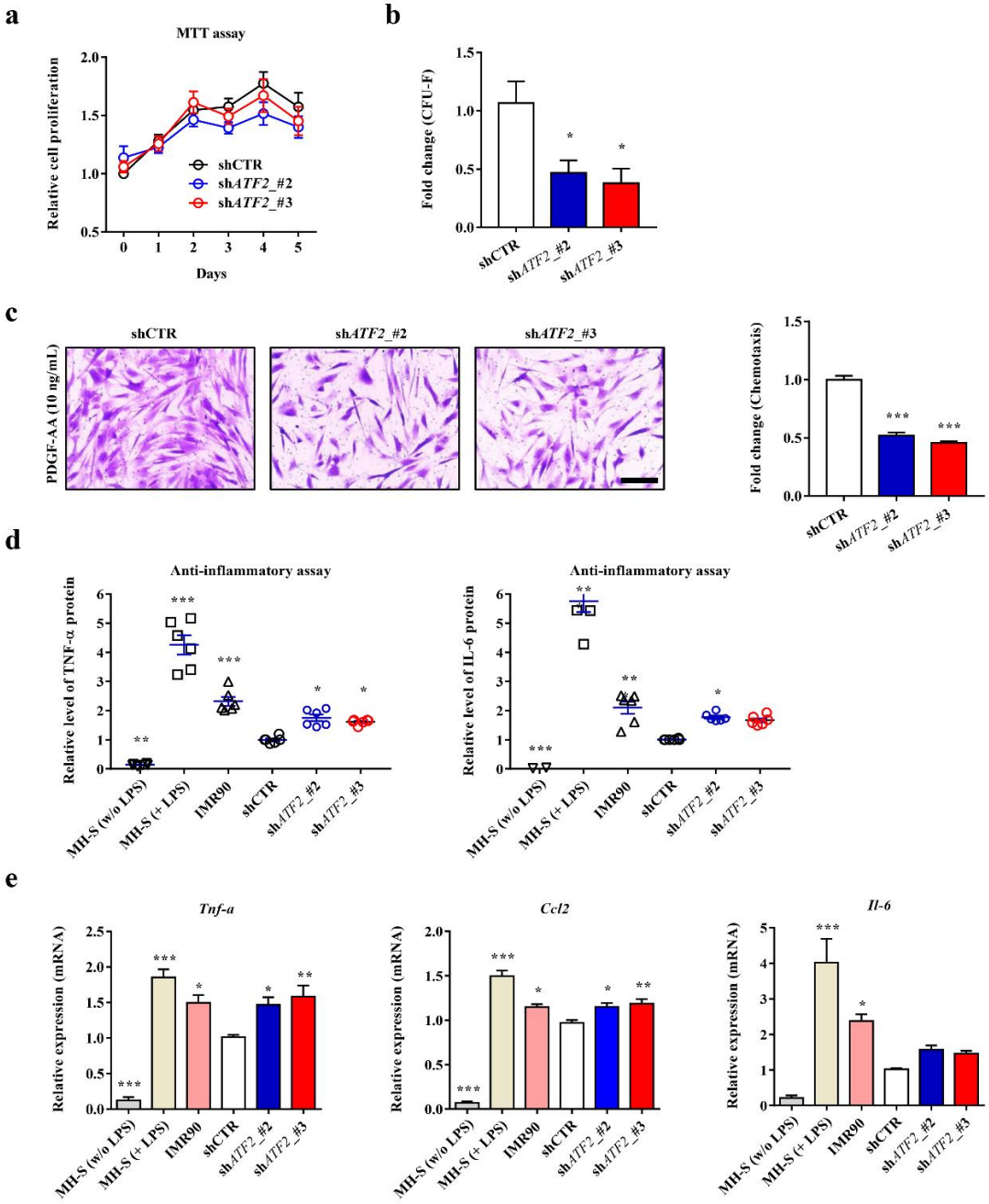

Figure 1-5. ATF2-silenced hUC-MSCs display defective therapeutic functions

Analyses of cell proliferation (n = 6; **a**), CFU-F potency (n = 5; **b**), and chemotaxis in response to treatment with 10 ng/mL PDGF-AA (n = 7; **c**) in hUC-MSCs harboring a scrambled (shCTR) or ATF2-specific (shATF2) shRNA. (**c**) Representative examples of chemotactic assays

(magnification, ×200; scale bar, 100 μm) are shown next to the corresponding quantitative data. (**d**, **e**) Anti-inflammation assays using conditioned medium (CM) prepared from the AA2G-treated hUC-MSCs. (**d**) Quantification of TNF-α and IL-6 proteins secreted from MH-S cells that were stimulated with LPS for 8 h in the absence or presence of CM harvested from the indicated cells (n = 6). CM from IMR90 normal primary fibroblasts was used as a control. (**e**) RQ-PCR analyses of the expression levels of selected murine inflammatory genes in the LPS-stimulated MH-S cells (n = 6). All quantitative data are represented as fold changes relative to the shCTR group and are displayed as the mean ± SEM. Statistical analyses were performed via one-way ANOVA (*$p < 0.05$, **$p < 0.01$, ***$p < 0.001$ compared with shCTR cells).

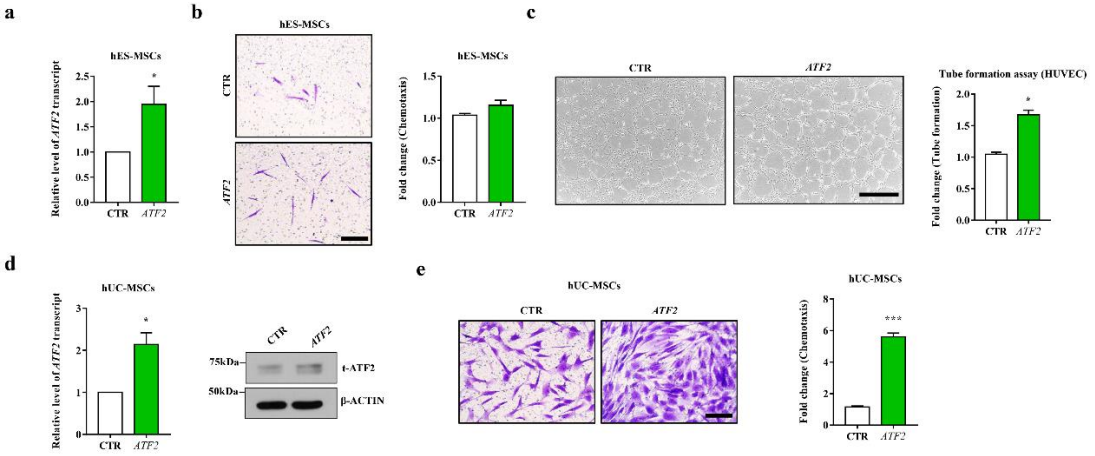

Figure 1-6. ATF2 ectopic expression enhanced PDGF-responsive chemotaxis in hES- and hUC-MSCs

(**a**) RQ-PCR (n = 4) analyses for the over-expression of ATF2 in hES-MSCs. (**b** and **c**) The PDGF-responsive chemotaxis (n = 7; **b**) and pro-angiogenesis (n = 4; **c**) activities in hES-MSCs harboring an empty control (CTR) or human ATF2 ORFs. (**d**) RQ-PCR (n = 4) and western blot analyses for the over-expression of ATF2 in hUC-MSCs. (**e**) The PDGF-responsive chemotaxis (n = 7) activity in hUC-MSCs over-expressing ATF2.

The expression levels of the indicated genes are represented as fold changes relative to the CTR group and are shown as the mean ± SEM. *$p < 0.05$; **$p < 0.01$; ***$p < 0.001$, compared with the CTR group, via nonparametric Mann-Whitney U tests (**a**–**e**) or one-way ANOVA with Bonferroni post hoc test.

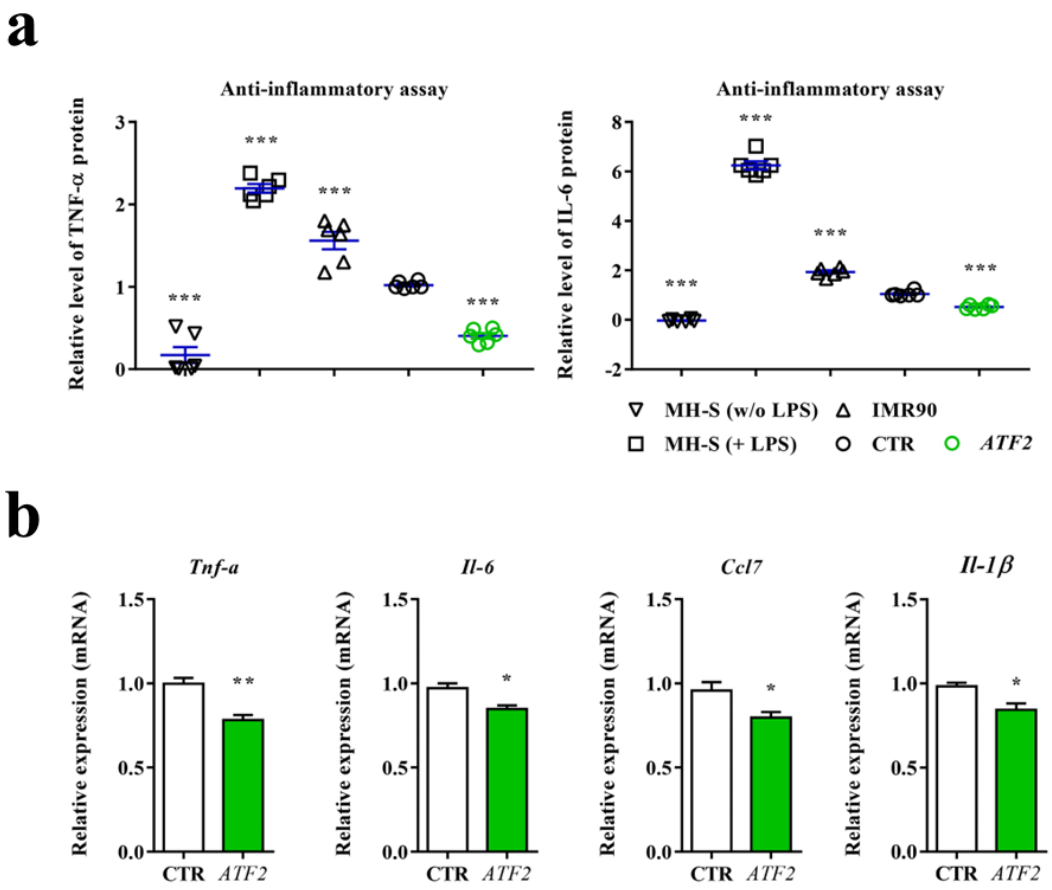

Figure 1-7. ATF2 overexpression increased pro-angiogenic and anti-inflammatory capacities in hES- and hUC-MSCs

(**a**) Quantification of TNF-α and IL-6 proteins (n = 6) from the LPS-stimulated MH-S cells by an ELISA assay. (**b**) RQ-PCR analysis of the proinflammatory genes in MH-S cells that were pretreated with the CM from the indicated cells (n = 6).

The expression levels of the indicated genes are represented as fold changes relative to the CTR group and are shown as the mean ± SEM. *$p < 0.05$; **$p < 0.01$; ***$p < 0.001$, compared with the CTR group, via nonparametric Mann-Whitney U tests (**b**) or one-way ANOVA with Bonferroni post hoc test (**a**).

The role of GSH dynamics in the ATF2-dependent functionality of MSCs

Next, we investigated whether the ATF2-mediated functionality of MSCs is dependent on the intracellular GSH level. To this end, ATF2-KD MSCs, which showed a reduced basal level of GSH and GRC (Fig. 1-2f), as well as impaired clonogenic and migratory capacities (Fig. 1-4 and 5), were treated with GSH-EE, a cell permeable form of GSH. Notably, the defects in the potency of CFU-F (self-renewal) and PDGF-responsive chemotaxis capacity observed in ATF2-KD MSCs were rescued by treatment with GSH-EE (Fig. 1-8a−c).

This result led us to explore whether ATF2 is involved in the beneficial effects of GSH-enhancing priming by supplementation with AA2G. Consistent with previous reports [10,23], AA2G priming increased PDGF-responsive migration and self-renewal (CFU-F potency) in both hES-MSCs and hUC-MSCs (Fig. 1-8d−f). These beneficial effects of AA2G were impaired significantly by silencing ATF2, indicating the critical role of ATF2 in the mode of action of AA2G priming of MSCs. As previously reported [23], the PFO procedure based on AA2G supplementation increased the core functions of MSCs, including self-renewal (CFU-F), PDGF-responsive cell migration, and the proangiogenic, anti-inflammatory, and immunomodulatory capacities of MSCs. Importantly, the silencing of ATF2 significantly impaired these beneficial effects of the PFO procedure in both hES-MSCs and hUC-MSCs (Fig. 1-9, 10, 11), further demonstrating the importance of ATF2 in AA2G-based GSH-enhancing priming conditions. Overall, these results demonstrate the importance of ATF2 as a novel mediator of GSH dynamics and related primitiveness during ex vivo expansion and priming of MSCs.

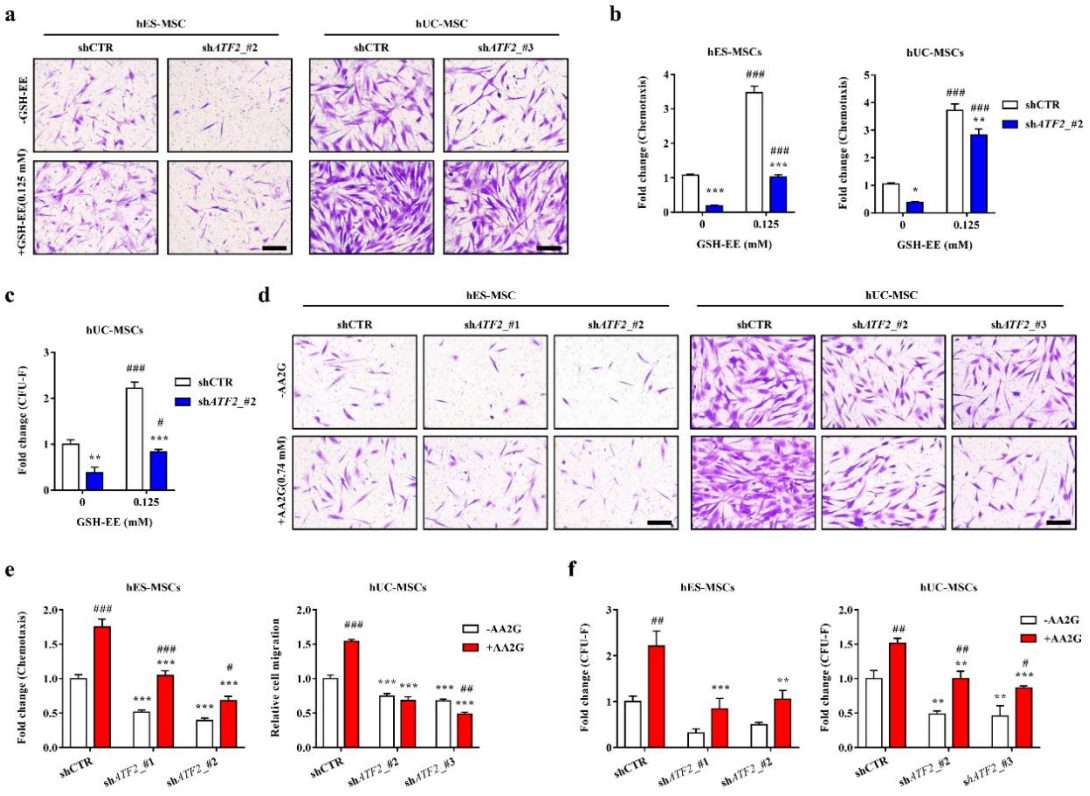

Figure 1-8. GSH dynamics play a role in ATF2-dependent MSC functionality

Chemotaxis (**a** and **b**) in response to treatment with 10 ng/ mL PDGF-AA (n = 7; **b**) and CFU-F potency (n = 3; **c**) in the control (shCTR) and ATF2-silenced (shATF2) MSCs with 0.125 mM GSH-EE. Chemotaxis (**d** and **e**) in response to treatment with 10 ng/mL PDGF-AA (n = 7; **e**) and CFU-F potency (n = 3; **f**) in the control (shCTR) and ATF2- silenced (shATF2) MSCs treated with 0.74 mM AA2G for 72 h. Representative images of the chemotaxis assays are presented on the left (magnification, ×200; scale bar, 100 μm). Quantitative data are represented as fold changes relative to the shCTR group and are displayed as the mean ± SEM. Statistical analyses were performed via two-way ANOVA (*$p < 0.05$, **$p < 0.01$, ***$p < 0.001$ compared with shCTR cells; #$p < 0.05$, ##$p < 0.01$, ###$p < 0.001$ compared with nontreated cells).

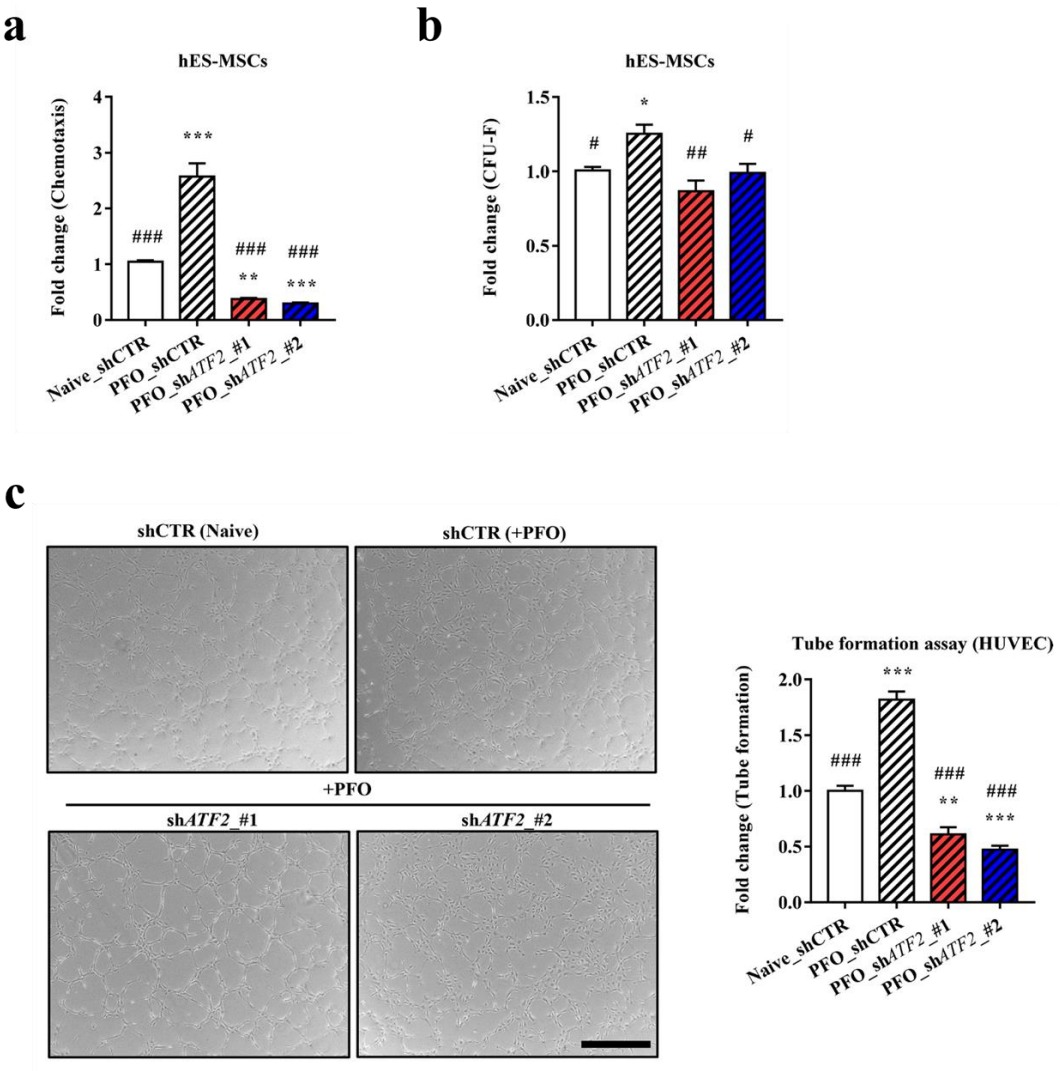

Figure 1-9. ATF2 silencing significantly impaired beneficial effects of the PFO procedure in hES- and hUC-MSCs

(**a**–**c**) PDGF-responsive chemotaxis (n = 7; **a**), Analyses of CFU-F (n = 3; **b**) and pro-angiogenesis (n = 4; **c**) activities in hES-MSCs after naïve culture or subjection to the PFO procedure with the supplement of AA2G for two days.

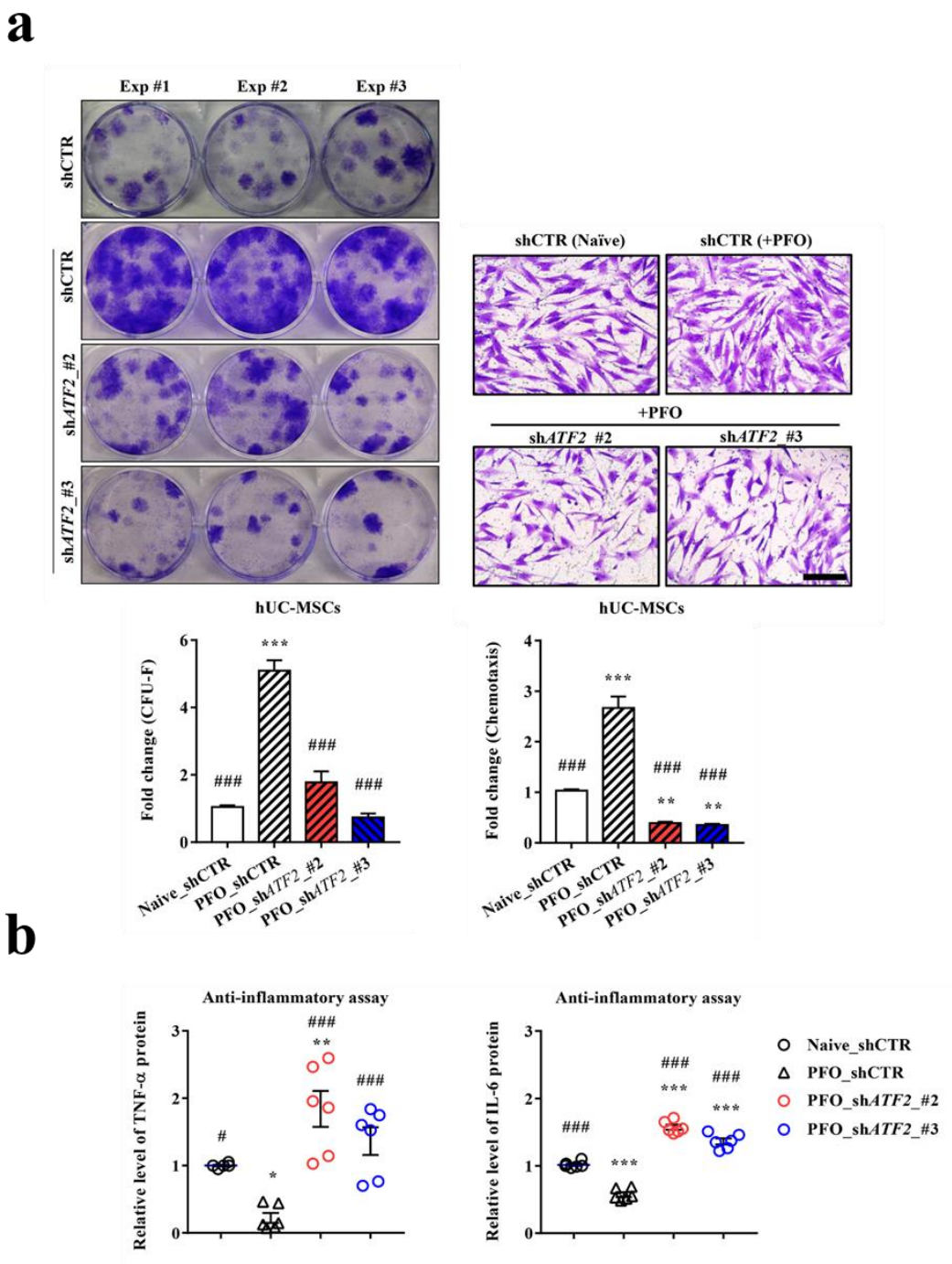

Figure 1-10. Role of ATF2 in the beneficial effects of the PFO procedure

(**a**) Analyses of CFU-F (n = 3), PDGF-responsive chemotaxis (n = 7), (**b**) Quantification of TNF-α and IL-6 proteins as anti-inflammation assays with lipopolysaccharide (LPS) and then incubated with conditioned medium (CM) (n = 6). The expression levels of the indicated genes

are represented as fold changes relative to the not treated (Naïve) shCTR group and are shown as the mean ± SEM (*$p < 0.05$; **$p < 0.01$; ***$p < 0.001$, compared with the naïve shCTR group; #$p < 0.05$; ##$p < 0.01$; ###$p < 0.001$, compared with the PFO shCTR group, via a one-way ANOVA with Bonferroni post hoc test).

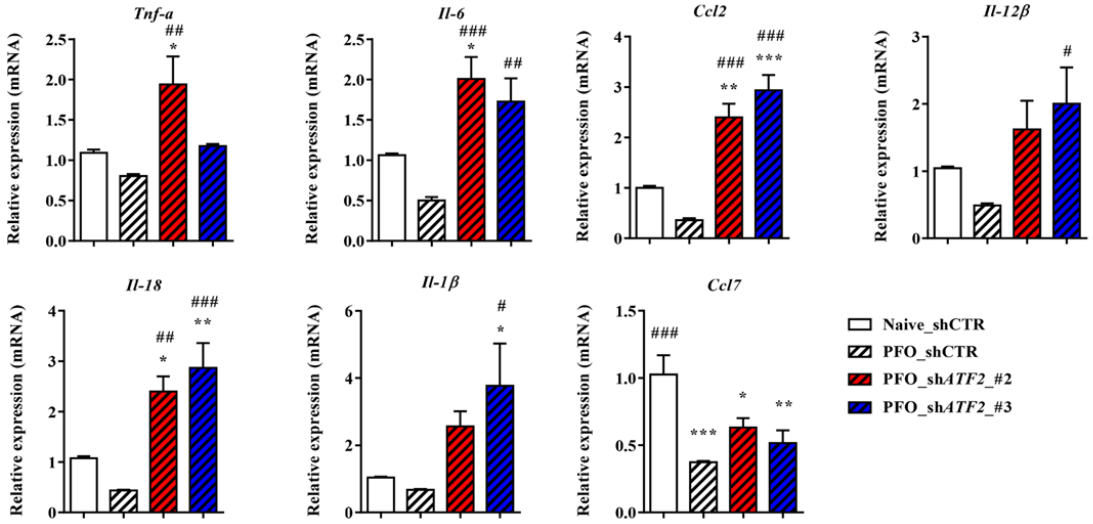

Figure 1-11. Role of ATF2 in the improved anti-inflammatory activity by the PFO procedure

RQ-PCR analyses (n = 6) of proinflammatory genes in MH-S cells that were pretreated with the CM from the indicated cells. The expression levels of the indicated genes are represented as fold changes relative to the not treated (Naïve) shCTR group and are shown as the mean ± SEM (*$p < 0.05$; **$p < 0.01$; ***$p < 0.001$, compared with the naïve shCTR group; #$p < 0.05$; ##$p < 0.01$; ###$p < 0.001$, compared with the PFO shCTR group, via a one-way ANOVA with Bonferroni post hoc test).

The importance of ATF2 for the use of MSCs in asthma therapy in vivo

To confirm the findings described above in vivo, we employed an OVA mouse model of allergenic asthma, which represents a Th2 immune cell-driven inflammatory airway allergic response [27] and compared the therapeutic potencies of a single intravenous injection of 3×10^5 hUC-MSCs expressing a control (shCTR) or ATF2-specific (shATF2) shRNA. As reported previously [33], severe inflammation in the bronchial and vascular areas of the lung tissues was observed in the OVA-sensitized asthmatic mice administered PBS vehicle (Fig. 1-12). Examination of the BALF revealed that these OVA-induced asthmatic mice displayed a significant increase in the overall cellularity and abundance of inflammatory cells (Fig. 1-13). Single administration of hUC-MSCs expressing shCTR attenuated the inflammation of the lung tissue and infiltration of inflammatory cells, including macrophages, neutrophils, and lymphocytes, in the BALF (Fig. 1-14). However, these beneficial effects were significantly defective in asthmatic mice injected with hUC-MSCs expressing shATF2.

Consistent with these findings, the levels of the IL-4, IL-5, and IL-13 proteins, all of which are Th2 immune response mediators, were lower in the BALF of asthmatic mice administered hUC-MSCs expressing shCTR than in that of asthmatic mice administered the vehicle control; however, this was not the case for mice administered hUC-MSCs expressing shATF2 (Fig. 1-14). The asthmatic mice were characterized by upregulation of genes related to the Th2-mediated immune response (e.g., Il-4, Il-5, and Il-13) and proinflammatory cytokines (e.g., Ccl7, Il6, Tnf-α, and Inf-γ); these increases were attenuated by single administration of hUC-MSCs expressing shCTR but not by administration of those expressing shATF2 (Fig. 1-15, 16). Overall, this preclinical study demonstrates that ATF2 plays a crucial role in MSCs to alleviate airway inflammatory responses.

Next, we examined whether ATF2 could modulate the in vivo engraftment of hUC-MSCs in the lung tissues of OVA-induced asthmatic mice. Staining of the lung tissues with an hB2M-specific antibody revealed that the frequencies of $hB2M^+$ engrafted cells were comparable in the mice administered hUC-MSCs expressing shCTR and those administered hUC-MSCs expressing shATF2 (Fig. 1-17a, b), indicating that ATF2 had a minimal effect on in vivo engraftment of the MSCs. Confocal microscopy analyses of the lung tissues revealed that the

hB2M^{+} engrafted cells were not stained with an antibody targeting SFTPC, a type 2 alveolar epithelial cell marker. Instead, the majority of hB2M^{+} cells were located in proximity to SFTPC^{+} cells in both the shCTR and shATF2 groups (Fig. 1-18a, b). Therefore, these results indicate that the engrafted cells protected against the airway inflammation response via a paracrine effect rather than by directly contributing to tissue resident cells.

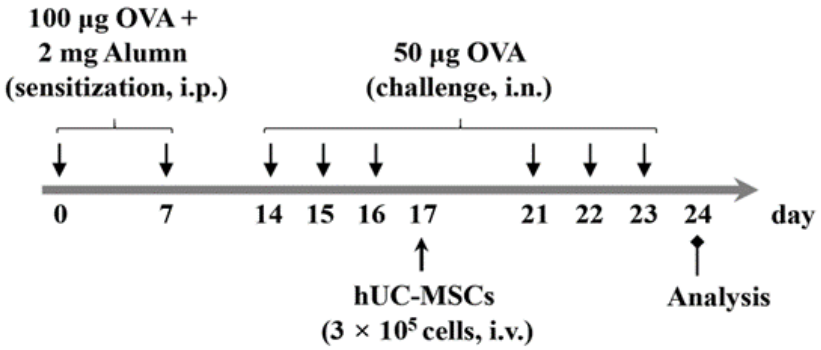

Figure 1-12. In vivo scheme for asthma induction and administration of MSCs

Schematic overview of the experimental protocols for the induction of asthma and the (i.v.) intravenous injection of 3×10^5 hUC-MSCs harboring a control (shCTR) or ATF2-specific shRNA (shATF2). OVA ovalbumin, alumn aluminum hydroxide, (i.p.) intraperitoneal injection, (i.n.) intranasal injection.

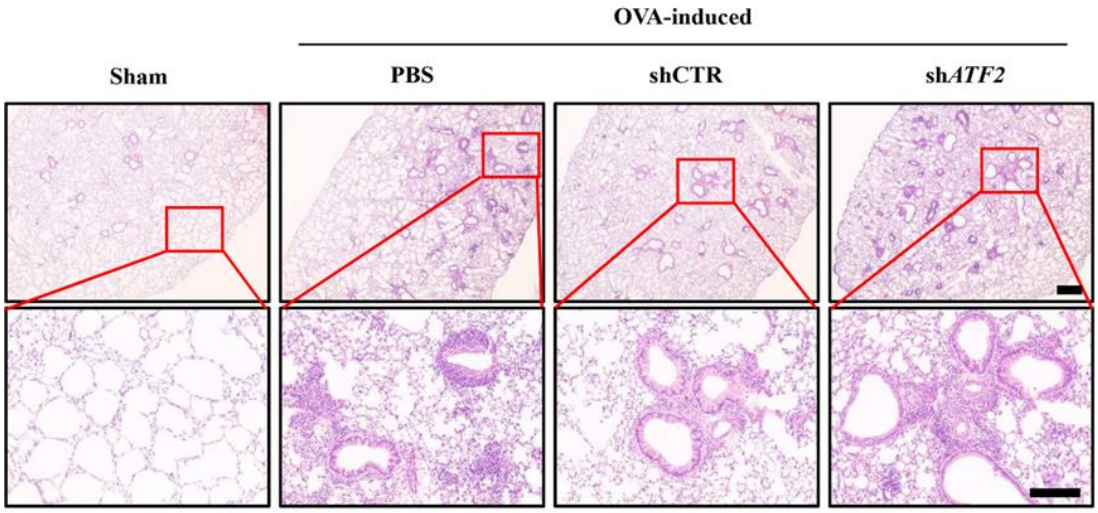

Figure 1-13. Severe inflammation in bronchial and vascular lung tissues of OVA-sensitized asthmatic mice

Hematoxylin and eosin staining of lung tissues (magnification, ×40, scale bar, 250 μm) from the sham mice and the OVA-induced mice injected with vehicle control (PBS) or hUC-MSCs expressing shCTR or shATF2. Higher magnification images (×200) are shown in the lower panels. Scale bar, 100 μm.

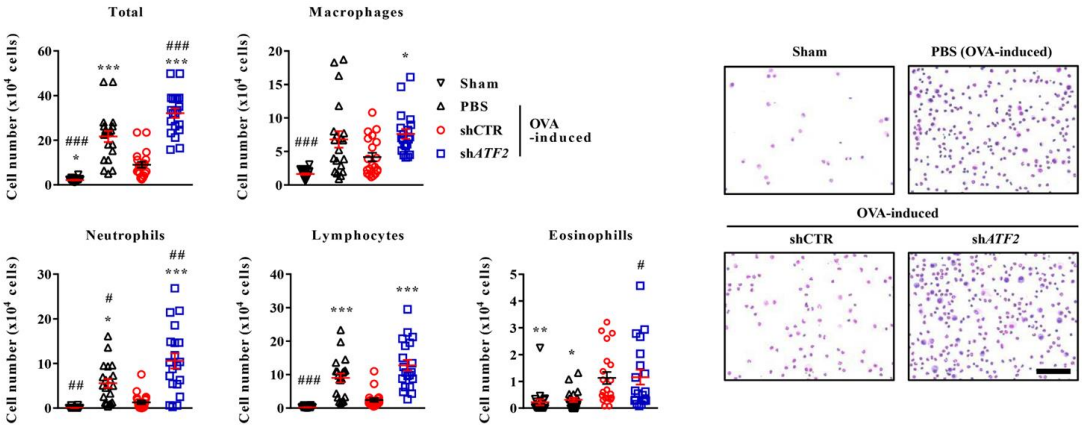

Figure 1-14. Increased cellularity and immune cells in OVA-induced asthmatic mice

The numbers of total cells, macrophages, neutrophils, lymphocytes, and eosinophils identified via cytospin staining of BALF from mice (n = 20) in the indicated groups. Representative images of cytospin staining (magnification, ×400) are also shown. Scale bar, 50 μm.

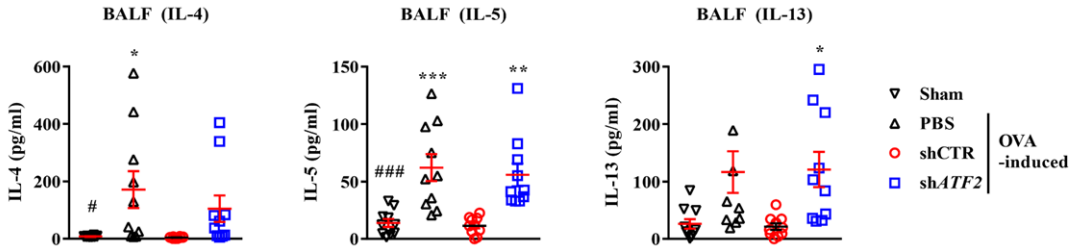

Figure 1-15. Impaired beneficial effects of shATF2-expressing hUC-MSCs in Th2 immune response mediators of asthmatic mice

Quantification of IL-4, IL-5, and IL-13 proteins in BALF from mice (n = 10) in the indicated groups. Quantitative data are represented as the mean ± SEM. Statistical significance was examined via one-way ANOVA with Bonferroni post hoc tests (*$p < 0.05$, **$p < 0.01$, ***$p < 0.001$ compared with the shCTR group; #$p < 0.05$, ##$p < 0.01$, ###$p < 0.001$ compared with the PBS group).

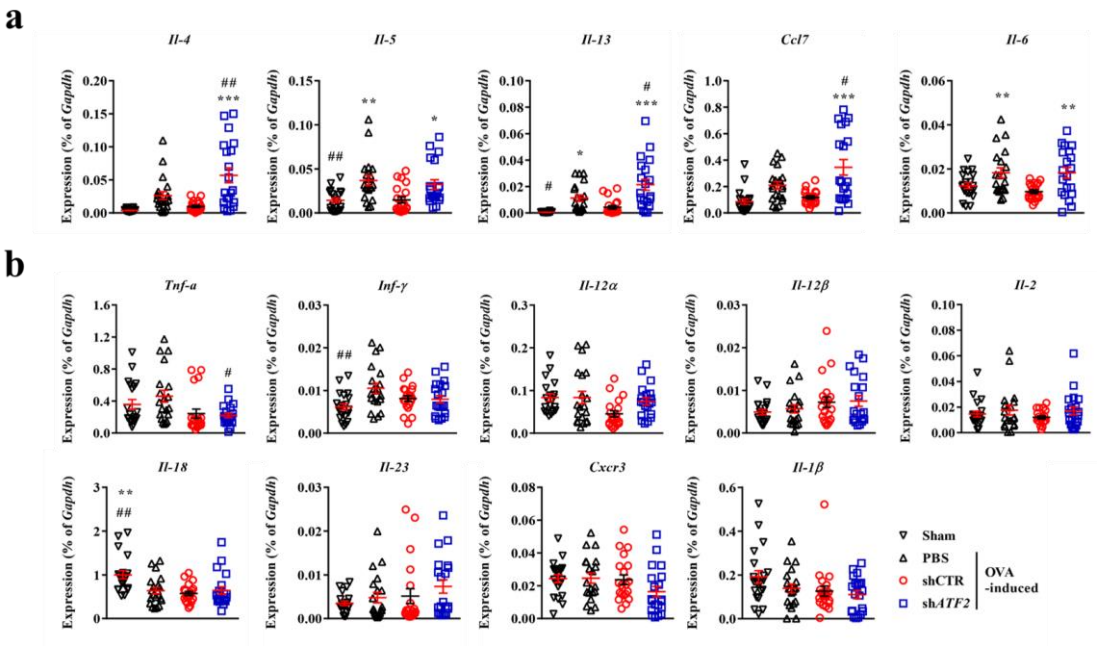

Figure 1-16. Up-regulation of Th2-related genes and pro-inflammatory cytokines in asthmatic mice

(**a**) RQ-PCR analyses of the indicated cytokines in lung tissues from mice (n = 20) in the indicated groups. (**b**) Expression of cytokine genes in the lungs of asthmatic mice. RQ-PCR analyses of 19 genes related to proinflammatory and Th1 immune responses in the lungs of asthmatic mice 1 week after injection of PBS vehicle or hUC-MSCs harboring a control (shCTR) or ATF2-specific (shATF2) shRNA (n = 20).

Quantitative data are represented as the mean ± SEM. Statistical significance was examined via one-way ANOVA with Bonferroni post hoc tests (*$p < 0.05$, **$p < 0.01$, ***$p < 0.001$ compared with the shCTR group; #$p < 0.05$, ##$p < 0.01$, ###$p < 0.001$ compared with the PBS group).

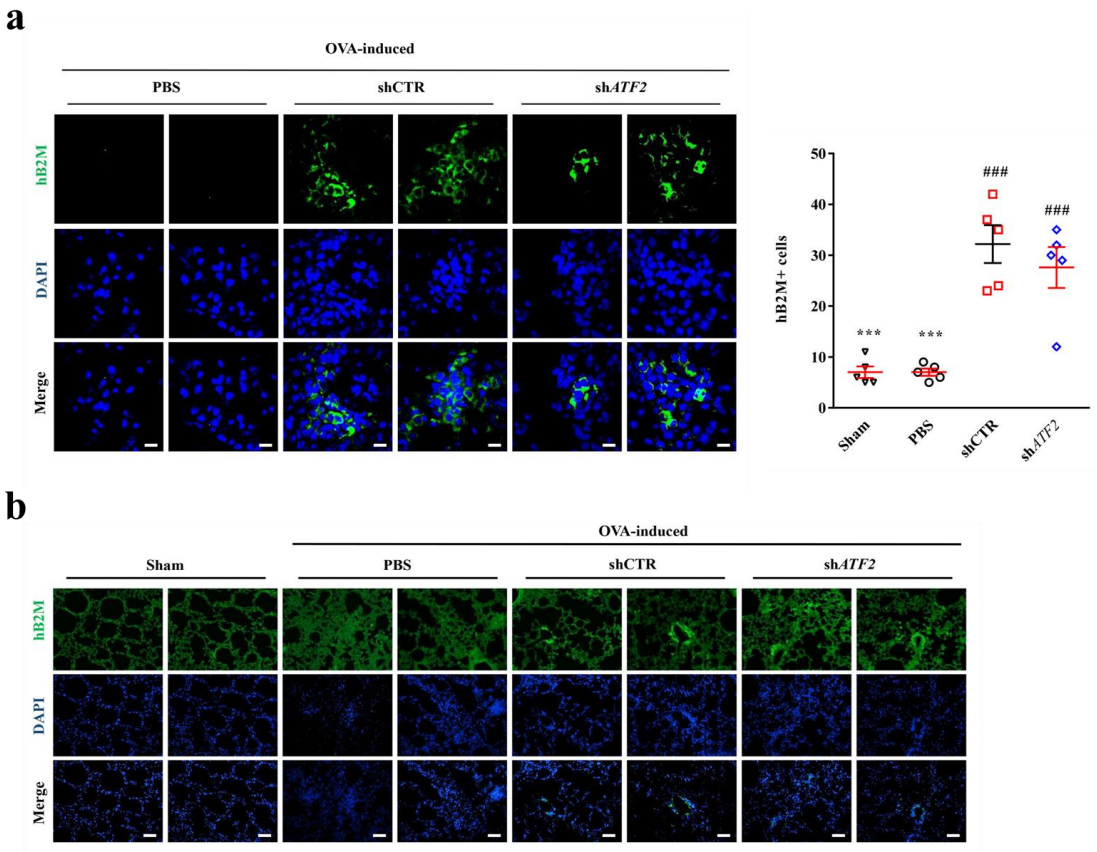

Figure 1-17. Immunostaining analysis of engraftment and cellular properties of transplanted hUC-MSCs

(**a**) Immunostaining to detect cells expressing hB2M (green) in the lung tissues of OVA-stimulated asthmatic mice 1 week after injection of PBS vehicle or hUC-MSCs harboring a control (shCTR) or ATF2-specific (shATF2) shRNA (magnification, ×1000; scale bar, 200 μm). (**b**) Representative images of immunostaining (magnification, ×200) to detect hB2M (green) in the lung tissues of OVA-stimulated asthmatic mice administered PBS vehicle or hUC-MSCs harboring a control (shCTR) or ATF2-specific (shATF2) shRNA. Scale bar, 200 μm.

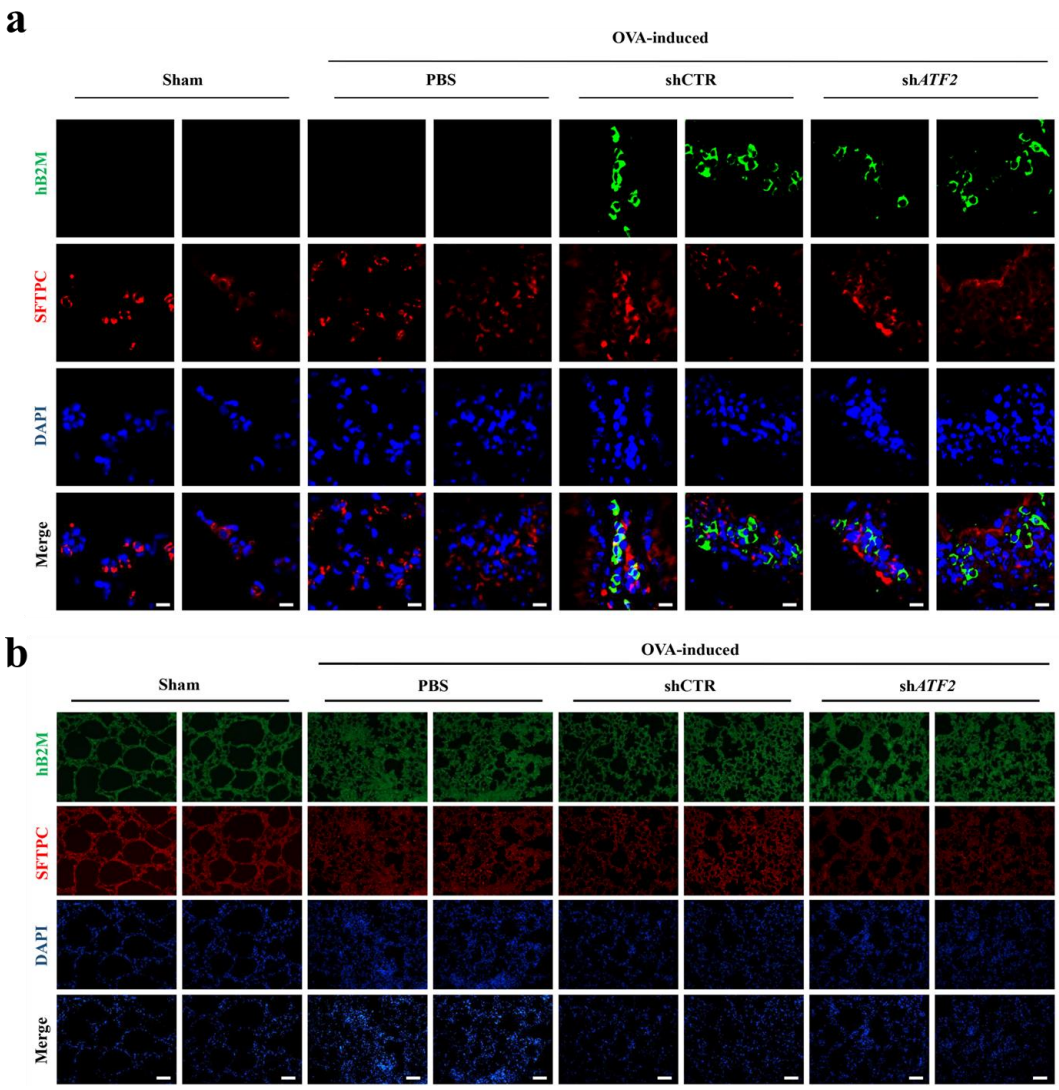

Figure 1-18. Co-staining of SFTPC and hB2M for the engrafted cells in lung tissues

(**a**) Representative confocal micrographs showing the immunohistochemical detection of hB2M (green) and the alveolar epithelial cell marker SFTPC (red) in lung tissues from mice in the indicated groups. Nuclei were stained with DAPI (blue). Two independent images are shown (magnification, ×1000; scale bar, 200 μm).

(**b**) To rule out the possibility of nonspecific staining, lung tissues of the OVA-induced asthmatic mice were costained with mouse and rabbit IgG control antibodies for hB2M (green)

and the alveolar epithelial cell marker SFTPC (red) as negative controls (magnification, ×200; scale bar, 200 μm. Nuclei were stained with DAPI (blue).

The Overexpression of ATF2 for the use of MSCs in asthma therapy in vivo

To confirm the findings described Overexpression of ATF2 for the use of MSC above in vivo, employed an OVA mouse model of allergenic asthma, which represents a Th2 immune cell-driven inflammatory airway allergic response and compared the therapeutic potencies of a single intravenous injection of 3×10^5 hES-MSCs, hUC-MSCs for ATF2 over-expression (Naive or PFO). As reported previously [33], severe inflammation in the bronchial and vascular areas of the lung tissues was observed in the OVA-sensitized asthmatic mice administered PBS vehicle (Fig. 1-19, Fig. 1-22). Examination of the BALF revealed that these Overexpression of ATF2 for the use of MSC with OVA-induced asthmatic mice displayed a significant increase in the overall cellularity and abundance of inflammatory cells. Single administration of MSC with ATF2 over-expression attenuated the inflammation of the lung tissue and infiltration of inflammatory cells, including macrophages, neutrophils, and lymphocytes, in the BALF (Fig. 1-20, Fig. 1-23).

Next, we examined whether Overexpression of ATF2 for the use of MSC could modulate the in vivo engraftment of the lung tissues of OVA-induced asthmatic mice. Staining of the lung tissues with an hB2M-specific antibody revealed that the frequencies of $hB2M^+$ engrafted cells were comparable in the mice administered Overexpression of ATF2 for the use of MSC (Fig. 1-21, Fig. 1-24), indicating that Overexpression of ATF2 had a dramatic effect on in vivo engraftment of the MSCs. Thus, Overexpression of ATF2 for the use of MSC, PFO-primed MSCs, indicating that the superior in vivo engraftment of PFO-MSCs could be responsible for their improved therapeutic potency compared with that of naïve MSCs.

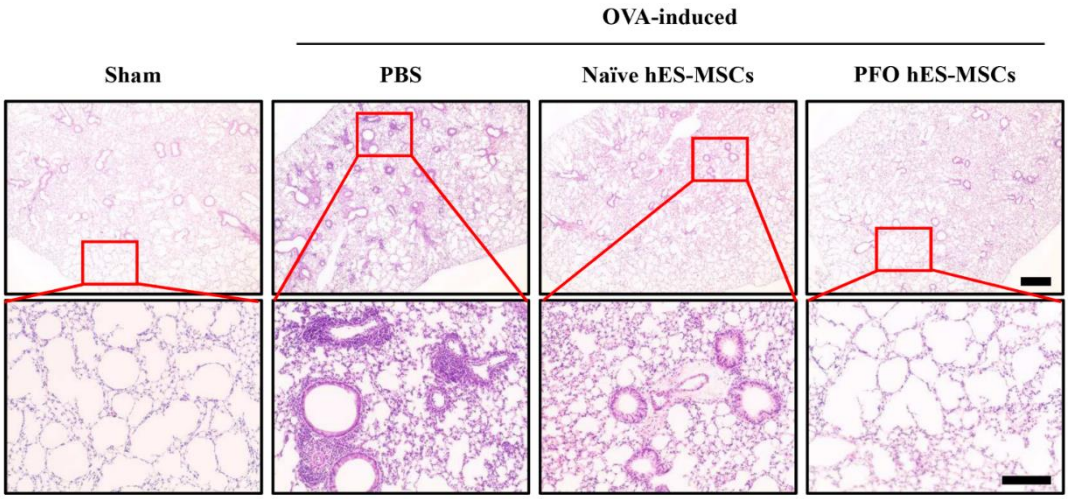

Figure 1-19. Inflammation in bronchial and vascular lung tissues of OVA-sensitized asthmatic mice administrated with ATF2 over-expression hES-MSCs

Hematoxylin and eosin staining of lung tissues (magnification, ×40, scale bar, 250 μm) from sham mice and OVA-induced mice injected with the vehicle control (PBS) or hES-MSCs in normal (Naïve) culture or subjected to the PFO procedure. Higher magnification images (×200) are shown in the lower panels. Scale bar, 100 μm.

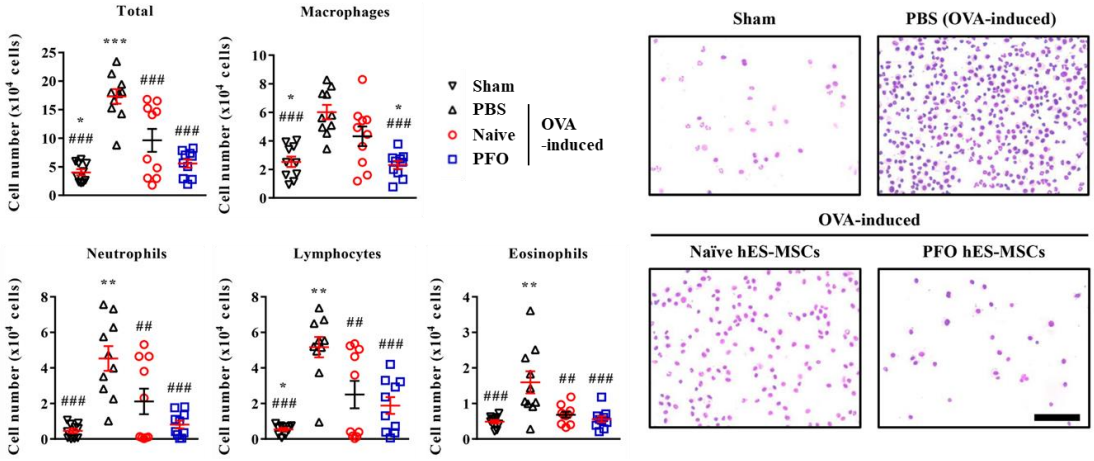

Figure 1-20. Decreased cellularity and immune cells in OVA-sensitized asthmatic mice administrated with ATF2 over-expression hES-MSCs

Representative images of the cytospin staining (magnification, ×400; scale bar, 50 μm) and the quantification of the numbers of total cells, macrophages, neutrophils, lymphocytes, and eosinophils in the BALF from mice (n = 10) in the indicated groups. All the quantitative data are shown as the mean ± SEM. Statistical significance was examined via a one-way ANOVA with Bonferroni post hoc tests (*$p < 0.05$, ***$p < 0.001$ compared with the naïve hES-MSC group; #$p < 0.05$, ###$p < 0.001$ compared with the PBS group).

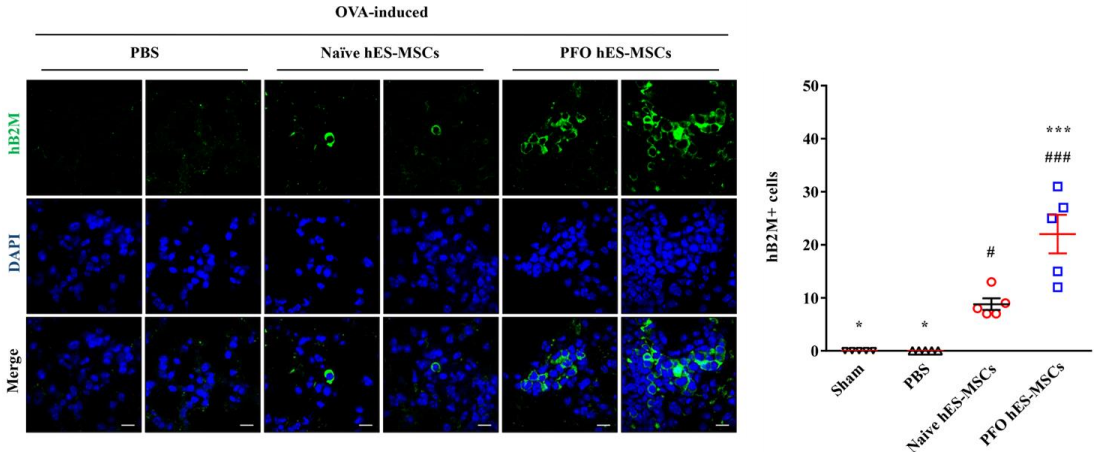

Figure 1-21. Immunostaining analysis of engraftment and cellular properties of transplanted OVA-sensitized hES-MSCs with ATF2 over-expression

Immunostaining to detect the engrafted cells expressing hB2M (green) in the lung tissues of OVA-stimulated asthmatic mice one week after injection of the PBS vehicle or the naïve or PFO hES-MSCs (magnification, ×1000; scale bar, 200 μm). The engrafted $hB2M^+$ cells in lung tissues from mice (n = 5) in the indicated groups were quantified and are shown in the right panel. All the quantitative data are shown as the mean ± SEM. Statistical significance was examined via a one-way ANOVA with Bonferroni post hoc tests (*$p < 0.05$, ***$p < 0.001$ compared with the naïve hES-MSC group; #$p < 0.05$, ###$p < 0.001$ compared with the PBS group).

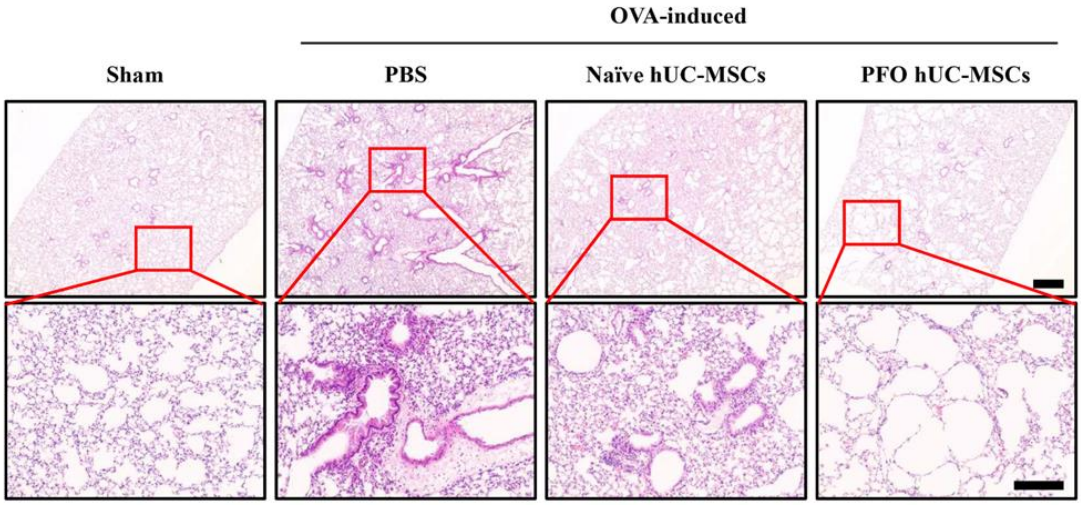

Figure 1-22. Inflammation in bronchial and vascular lung tissues of OVA-sensitized asthmatic mice transplanted with ATF2 over-expression hUC-MSCs

Hematoxylin and eosin staining of lung tissues (magnification, ×40, scale bar, 250 μm) from sham mice and OVA-induced mice injected with the vehicle control (PBS) or hUC-MSCs in normal (Naïve) culture or subjected to the PFO procedure. Higher magnification images (×200) are shown in the lower panels. Scale bar, 100 μm.

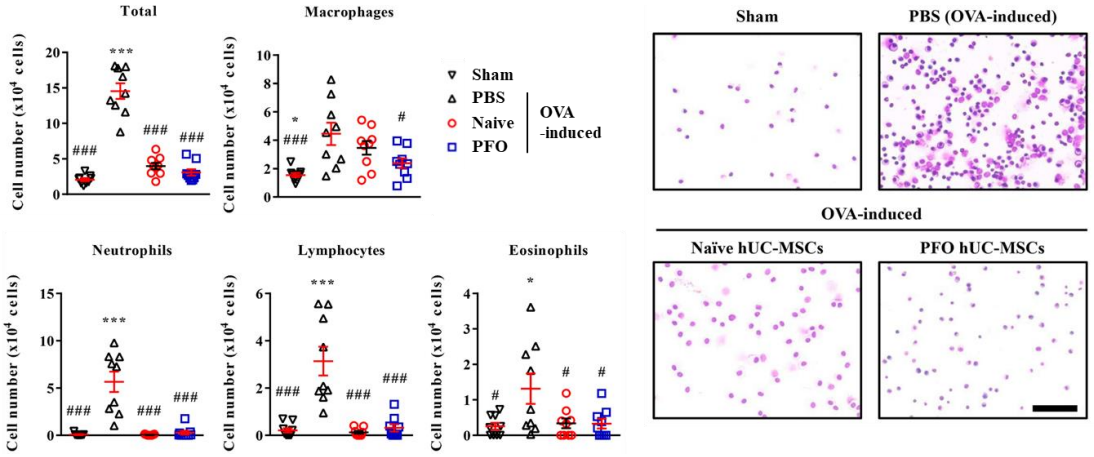

Figure 1-23. Decreased cellularity and inflammatory cell in OVA-sensitized asthmatic mice transplanted with ATF2 over-expression hUC-MSCs

Representative images of the cytospin staining (magnification, ×400; scale bar, 50 μm) and the quantification of the numbers of total cells, macrophages, neutrophils, lymphocytes, and eosinophils in the BALF from mice (n = 10) in the indicated groups. All the quantitative data are shown as the mean ± SEM. Statistical significance was examined via a one-way ANOVA with Bonferroni post hoc tests (*$p < 0.05$, ***$p < 0.001$ compared with the naïve hUC-MSC group; #$p < 0.05$, ###$p < 0.001$ compared with the PBS group).

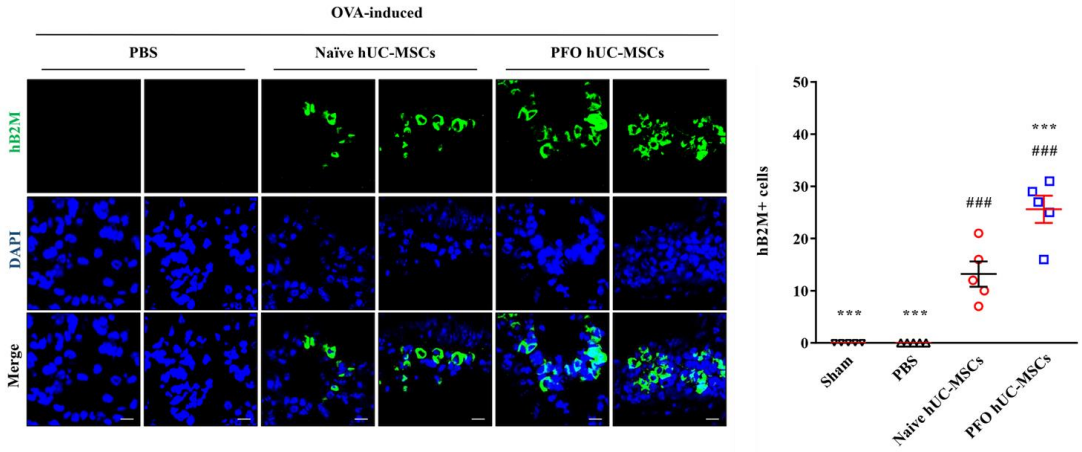

Figure 1-24. Immunostaining analysis of engraftment and cellular properties of transplanted OVA-sensitized hUC-MSCs with ATF2 over-expression

Immunostaining to detect the engrafted cells expressing hB2M (green) in the lung tissues of OVA-stimulated asthmatic mice one week after injection of the PBS vehicle or the naïve or PFO hUC-MSCs (magnification, ×1000; scale bar, 200 μm). The engrafted $hB2M^+$ cells in lung tissues from mice (n = 5) in the indicated groups were quantified and are shown in the right panel. All the quantitative data are shown as the mean ± SEM. Statistical significance was examined via a one-way ANOVA with Bonferroni post hoc tests (*$p < 0.05$, ***$p < 0.001$ compared with the naïve hUC-MSC group; #$p < 0.05$, ###$p < 0.001$ compared with the PBS group).

DISCUSSION

GSH dynamics are important for preserving both the primitive state of MSCs and their therapeutic efficacy toward several intractable disorders [9,21,23,34]. The results presented here demonstrate that ATF2 is a novel mediator of GSH dynamics in MSCs that acts via interplay with the NRF2 signaling cascade, thereby affecting the functionality and therapeutic potency of MSCs toward allergic asthma.

Several reports have described protocols for the stable preservation and ex vivo expansion of primitive MSCs with high therapeutic potency, for example, by enriching small-sized cells or enhancing the antioxidant capacity [9,10,20,21,23]. In these previous reports, transcriptome analyses revealed that MSCs with high levels of GSH displayed common molecular features, including activation of the CREB1-NRF2 pathway, resulting in the upregulation of genes related to GSH synthesis and redox cycling, as well as high expression levels of AP1 family transcription factors such as ATF2, JUN, JUNB, and FRA1. In our recent study, we found that the FOS proto-oncogene AP1 protein played a central role in maintaining both the core functions of hES-MSCs in vitro and the in vivo engraftment of transplanted hES-MSCs, thus affecting their therapeutic potency in a preclinical study of interstitial cystitis/bladder pain syndrome [16]. AP1 activity is responsive to extracellular signals [29], and the functions of AP1 complexes are diverse due to their ability to form distinct heterodimers. For example, ATF2 reportedly forms eight different complexes with other members of the ATF, JUN, and FOS families, whereas JUN can form 15 different dimeric complexes. Therefore, investigating the role of the interplay between these AP proteins in controlling GSH dynamics could not only advance our understanding of the molecular signature of the primitiveness of MSCs but also overcome the technical limitations of current MSC therapies.

Here, we found that ATF2 is a crucial mechanomediator of redox homeostasis in hES-MSCs and hUC-MSCs that acts by collaborating with the CREB1-NRF2 pathway. This finding is consistent with a previous report demonstrating that the ATF2 protein forms complexes with NRF2 and other multiple basic leucine zipper proteins and is recruited to promote the heme oxygenase-1 gene following arsenite treatment [35]. In addition, another study found that ectopic expression of ATF2 inhibited ferroptosis induced by a bromodomain and extraterminal

domain protein inhibitor in human breast cancer cells by upregulating NRF2. The clinical relevance of the positive correlation between ATF2 and NRF2 was demonstrated via The Cancer Genome Atlas Program (TCGA) dataset analysis of breast, lung, and cervical tissues36. ATF2 is a stress-response protein that is upregulated by oxidative, inflammatory, and DNA damage stresses [29]. In esophageal squamous epithelial cancer cells, activation of ATF2 via phosphorylation of threonine residues 69 and 71 reduces oxidative stress-induced apoptosis and consequently reinforces cell cycle arrest by upregulating $p21^{WAF1}$ and JUN [37]. In addition, resveratrol (3,5,4'-trihydroxystilbene), a naturally occurring polyphenol with antioxidant activity, reportedly increases the transcriptional activation potentials of CREB and ATF2 to mediate cytoprotective and tumor suppressive outcomes [38]. Therefore, the activation of ATF2 by diverse extracellular stimuli could affect the intracellular level and dynamics of GSH to modulate various biological processes, including inflammation, aging, tumorigenesis, and the primitiveness of stem cells.

In our current study, the expression level and activity of ATF2 were stimulated by priming human MSCs with AA2G, a VitC derivative, to enhance GSH dynamics. In previous study [10], we found that AA2B stably promoted the primitive state of MSCs and the naïve pluripotency of murine ESCs and overcame the critical drawbacks of VitC, which is extremely unstable in aqueous solution because it readily oxidizes to dehydroascorbate, leading to cellular toxicity. We also found that AA2G reproduced the known biological effects of VitC, including TET-dependent DNA demethylation in murine ESCs and suppression of p53 during the generation of murine iPSCs, and that activation of the CREB1 pathway accounted for the beneficial effects of AA2G in ESCs and MSCs [10]. Furthermore, priming with AA2G promoted the core functions of MSCs, including self-renewal (based on CFU-F activity), PDGF-responsive cell migration, and anti-inflammatory potency. The in vivo importance of these findings was demonstrated by using a polyinosinic:polycytidylic acid (poly-I:C)-induced murine asthma model representing viral infection pathogenesis [10]. In this study, ATF2 played a crucial role in the beneficial effects of the PFO procedure based on the combination of three small molecules, AA2G, S1P, and VPA, which significantly improved the therapeutic potency of MSCs from different sources for treating allergic asthma. In this regard, the present study elucidates a novel mode of action of various AA2G-based priming procedures, namely, the

role of ATF2 in preserving GSH dynamics and the related primitiveness of MSCs. Therefore, we postulate that ATF2 might be responsible for the effects of AA2G priming in other populations of stem cells, such as human PSCs, neural stem cells, and hematopoietic stem cells. Further studies are required to verify this hypothesis. In addition, the direct target(s), or critical mediator(s) of ATF2 in controlling GSH dynamics should be identified in different cellular or microenvironmental contexts.

GSH-enhancing priming conditions, such as AA2G priming and the PFO procedure, could connect cellular redox signaling via numerous common pathways, such as the receptor tyrosine kinase and G protein-coupled receptor (GPCR) pathways [39]. GPCRs activate heterotrimeric G proteins in the plasma membrane; unlike the Gi (Gαi/o) subunit, the Gs alpha subunit protein (Gαs) is responsible for stimulating cAMP- and protein kinase (PKA) dependent pathways by activating adenylyl cyclase [39]. Notably, we previously found that the beneficial effects of AA2G priming in murine ESCs and human MSCs were prevented by treatment with melittin, which inhibits Gαs and stimulates Gαi/o, underlining the critical role of Gαs in AA2G priming-mediated effects. Furthermore, the GPCR-related genes G protein subunit α (GNAI1) and Hydroxytryptamine Receptor 2B (HTR2B) were identified as components of the CREB1-associated gene networks generated to characterize the transcriptome of AA2G treated murine ESCs and human MSCs [10]. Therefore, GPCR signaling could play a crucial upstream role in modulating ATF2-mediated GSH dynamics and the related functionality of MSCs following AA2G priming. Additional studies are required to investigate the importance of GPCRs in the ATF2-NRF2 pathway, focusing on the specific roles of Gα subunit proteins in MSCs under different ex vivo expansion conditions.

Since the burden of uncontrolled asthma is substantial and growing continuously [40], the identification of pathway-specific approaches for the prevention and treatment of this disease is required to reduce costs and improve the quality of life of patients. Due to their strong anti-inflammatory and immunomodulatory effects on innate and adaptive immune cells, MSCs have been used to treat intractable asthma, which is a major cause of morbidity and mortality worldwide [1,5]. In preclinical studies using animal models representing different pathogeneses, including asthma caused by house dust mites, poly-I:C, or OVA stimulation, MSC therapy was effective in alleviating airway inflammatory responses,

hyperresponsiveness, and remodeling [7]. In our current study, we used an OVA-stimulated murine asthma model to demonstrate the in vivo importance of ATF2 in the therapeutic potency of MSCs, particularly toward airway inflammation, which is an important pathophysiological feature of asthma. The results of this preclinical study are consistent with our previous studies showing that AA2G-primed MSCs or those with high levels of GSH exhibit enhanced therapeutic potency in a mouse model of virus associated asthma [9,10].

In these previous preclinical studies, the in vivo engraftment capacity of MSCs with high GSH dynamics was superior to that of control MSCs. In contrast, ATF2-silenced MSCs were engrafted into the lung at considerably higher levels than control MSCs. To further examine this unexpected finding, we investigated the properties and locations of the engrafted cells by costaining the hB2M and SFTPC proteins. When hES-MSCs were sorted based on the intracellular level of GSH, the MSCs that survived in the lungs expressed the SFTPC protein, indicating their direct contribution to the alveolar epithelium [9]. Although MSCs reportedly take on the gene expression profile of lung epithelial cells both in vitro and in vivo [41–47] and are stimulated by tissue injury [42], the transdifferentiation of mesodermal MSCs into surfactant protein-producing cells is rare in a normal physiological environment. In this regard, our previous study showed that AA2G-primed hES-MSCs engrafted into mouse lungs showed little expression of SFTPC [10]. Similarly, in our current study, we found that the $hB2M^+$ engrafted cells were negative for SFTPC expression but were located in the proximity of $SFTPC^+$ type 2 alveolar epithelial cells. Importantly, the anti-inflammatory capacity of hUC-MSCs was severely impaired by ATF2 silencing but enhanced by ATF2 overexpression. Taken together, these findings indicate that the MSCs engrafted into mouse lungs induced an anti-inflammatory response via a paracrine effect rather than by directly transdifferentiating into tissue-resident cells. The anti-inflammatory and immunosuppressive activities of MSCs are mediated by cell contact-dependent mechanisms involving Programmed Death-Ligand 1 (PD-L1 & B7-H1) [48] and by the secretion of soluble factors such as IL-10, transforming growth factor-β, nitric oxide, prostaglandin E2, and indoleamine 2,3-dioxygenase [49,50]. Therefore, for determination of the mode of action of MSC therapies in asthma, further studies are required to investigate which mediators could be affected by ATF2. In summary, this study demonstrates that ATF2 mediates GSH dynamics and the related functional and therapeutic

ability of MSCs to alleviate inflammatory responses in an experimental asthma model. Moreover, this study provides an in vivo proof of concept that the expression or activity of ATF2 can be used as a biomarker for predicting and evaluating the functions of MSCs for their ex vivo expansion and therapeutic applications.

CHAPTER 2

A Preclinical Study of Human Embryonic Stem Cell Derived Mesenchymal Stem cells for Treating Detrusor Underactivity by Chronic Bladder Ischemia

INTRODUCTION

Detrusor underactivity (DUA) is defined as “low detrusor pressure or short detrusor contraction time, usually in combination with a low urine flow rate resulting in prolonged bladder emptying and/or failure to achieve complete bladder emptying within a normal time span” by the international continence society standardization [1,2]. To date, the available therapeutic options for DUA are suboptimal, with the majority of patients suffering from persistent discomfort, severely deteriorated quality of life, and complications, including recurrent urinary tract infections and urinary retention [3]. Research to develop more effective, long-term therapies for DUA with improved patient outcomes is ongoing.

Stem cell therapy is emerging as a potential treatment option for a wide range of intractable diseases including bladder voiding dysfunction disorders [4,5]. Stem cells are characterized as cells that can self-renew and possess differentiation potency, which can be capitalized on to replace the damaged cells. Among the different types of stem cells, mesenchymal stem cells (MSCs) are considered as a reliable source for stem cell therapy. Besides their regenerative capacity, the MSCs can migrate to the damaged tissues and exhibit paracrine effects, such as recruitment of endogenous progenitor cells and secretion of growth-factors that can favor tissue regeneration. MSCs can been isolated from adult or fetal tissues [5], or they can be also derived from pluripotent stem cells (PSCs) such as embryonic stem cells (ESCs) and induced PSCs (iPSCs) [6–8]. The beneficial effects of MSC therapy include the generation of various preclinical bladder dysfunction models and reports of positive patient outcomes from clinical trials [9–17].

Previously, we investigated the therapeutic effects of multipotent MSCs (M-MSCs) derived from human ESCs in a streptozotocin-induced diabetic rat model of DUA. The transplanted M-MSCs integrated into pericytes, which provided favorable micro-environments for detrusor muscle regeneration [12]. In the present study, we aimed to investigate the therapeutic effects of M-MSC treatment in a DUA rat model with extensive vascular endothelial damage (VED) of the iliac arteries. Further, we aimed to investigate the underlying pathophysiological mechanisms of DUA for targeted therapeutics.

MATERIALS AND METHODS

Ethics Statement and Study Approval

Animal experiments were approved by the Institutional Animal Care and Use Committee of the University of Ulsan College of Medicine (IACUC-2019-12-004) and performed in accordance with the guidelines and regulations.

Study Design

Sixteen-week-old male Sprague–Dawley rats were divided into five groups: sham (n = 9), DUA (n = 9), DUA + 250 K M-MSCs (n = 10), DUA + 500 K M-MSCs (n = 9), and DUA + 1000 K M-MSCs (n = 10) (K = a thousand). All animals were anesthetized by intraperitoneal injection of 30 mg/kg Zoletil (Virbac Laboratories, Carros, France) prior to operation. Rats in the DUA groups had a 2-French Fogarty arterial embolectomy catheter (E-060-2F; Edwards Lifesciences, Irvine, CA, USA) inserted into the common iliac artery via the femoral artery. The balloon was passed from the common iliac artery to the femoral artery over 30 repetitions in the inflated state, and then the same procedure was repeated bilaterally. The sham group underwent sham operation. All rats received a 1.25 % cholesterol diet (D12336; Research Diets, New Brunswick, NJ, USA) for 8 weeks. Seven weeks after the operation, the DUA plus stem cell treatment groups were injected with 2.5, 5.0, or 10.0×10^5 M-MSCs (250 K, 500 K, or 1000 K, respectively) directly at the serosa of the anterior bladder wall. For the sham and DUA groups, phosphate-buffer solution (PBS) was injected. Animals that did not survive in catheter implantation or bladder manipulation were excluded from subsequent analyses. Additional rats (n = 6) were used for the organ bath study. The M-MSCs used in the stem cell treatments were maintained up to seven passages only to ensure their functionality as previously described [9,10,18].

Evaluation of Bladder Voiding Function

One week after M-MSC injection, the experimental groups were evaluated by awake cystometry. Bladder voiding function was evaluated in unrestrained, awake-state rats in metabolic cages as previously described [9,10,12]. Detrusor pressure was defined as

[intravesical pressure (IVP) – intraabdominal pressure (IAP)]. The contractility of the bladder tissues was measured by the organ bath study, as previously described [12,19]. In brief, longitudinal strips of posterior bladder wall were normalized to weight per 1 g and then mounted in 5 mL organ baths containing Krebs solution (118 mM NaCl, 5.0 mM KCl, 2.5 mM $CaCl_2$, 1.0 mM $MgSO_4$, 30 mM $NaHCO_3$, 1.0 mM KH_2PO_4, and 11.4 mM glucose, pH 7.4), and maintained at 37 °C with 5 % CO_2 and 95 % O_2 continuously supplied. The contractile response to 80 mM KCl (P9333; Sigma-Aldrich, St. Louis, MO, USA), EFS (electrical field stimulation, 1, 2, 4, 8, 16, and 32 Hz), 1 mM ATP (A2383; Sigma-Aldrich), or carbachol concentration (PHR1511; Sigma-Aldrich; 1 nM to 1 mM) were recorded as previously described [12,19]. An electrical pulse (1 millisecond pulse width and 80 V in bath) was delivered using a stimulator (D-7806; Hugo Sachs Elektronik, Germany) for 5 s at increasing frequencies (1, 2, 4, 8, 16, and 32 Hz), with 5 min intervals between electrical field stimulations.

Histological and Immunostaining Analysis

Next, the bladder tissues were harvested for histological and gene expression analyses. For histological analysis, collagen deposition, bladder muscle atrophy, and angiogenesis were assessed with Masson's trichrome staining (Junsei Chemical, Tokyo, Japan) and immunohistochemistry with anti-α smooth muscle actin (α-SMA) (ab7817; Abcam, Cambridge, UK), and anti-CD31 (sc-376,764; Santa Cruz Biotechnology, Dallas, TX, USA) antibody staining, respectively. Apoptosis in each layer of bladder (urothelium and muscle layer) was assessed by terminal deoxynucleotidyl transferase dUTP nick end labeling staining (1,684,795; TUNEL, Roche, Mannheim, Germany), and the nuclei were counterstained with 4′6-diamnio-2-phenylindole quantification analysis using Image Pro 5.0 software (Media-Cybernetics, Rockville, MD, USA). The distribution and cellular properties of transplanted M-MSCs were evaluated by immunohistochemical analysis of the bladders with human β2-microglobulin (hB2MG) (SC80668; Santa Cruz Biotechnology, Dallas, TX, USA) and by co-staining with antibodies specific for vimentin (#5741; Cell Signaling Technology, Danvers, MA, USA), α-SMA (ab5694; Abcam), NG2 (ab129051; Abcam) and CD31 (ab28364; Abcam). These proteins were visualized by Alexa Fluor 488-conjugated (A11001) or Alexa Fluor 564-

conjugated (A11010) anti-mouse or anti-rabbit secondary antibodies (Molecular Probes, Grand Island, NY, USA). Images were acquired using a ZEISS LSM800 confocal microscope system (Carl Zeiss, Munich, Germany).

Transcriptome and Gene Expression Analysis

Publicly available transcriptome datasets (GEO series accession number: GSE122060) [19] were used to compare gene expression data from CBI and sham-operated rat bladders. Differentially expressed genes were determined as 1.5-fold up- or down-regulation, with $p < 0.05$ defined as the cutoff values. Transcriptomic features were analyzed using MetaCore (Clarivate Analytics, Philadelphia, PA, USA) with default settings, which provided gene networks, biofunctions, and canonical pathways for representing CBI bladders. The significance of each candidate gene was individually validated by real-time quantitative PCR (RQ-PCR) analysis, as previously described [20,21].

Statistical Analysis

Data are reported as the mean standard error of the mean (SEM) and were analyzed using GraphPad Prism 7.0 software (GraphPad Software, La Jolla, CA, USA). Differences and significance were verified by one- or two-way ANOVA followed by Bonferroni post-hoc tests. A p value < 0.05 was considered as statistically significant.

RESULTS

Bladder Function Evaluation

Previously, we reported that DUA could be induced in a rat model of CBI with 30 bilateral repetitions of iliac arterial injury (AI), followed by a 1.25 % high cholesterol diet for 8 weeks [19]. In the present study, we investigated whether M-MSCs derived from human ESCs can show the therapeutic potency for treating DUA in this rat model. To address this issue, we transplanted three different cell dosages (0.25, 0.5, and 1.0×10^6 cells; denoted 250 K, 500 K, and 1000 K, respectively) of M-MSCs directly into the bladders at 7 weeks post-CBI injury. As a control, we administered PBS to the CBI-induced DUA rat model (DUA group) and the sham-operated rats (Sham group). In line with our previous report [19], the DUA group presented with decreased detrusor pressure and larger micturition volume, post-void residual, and bladder capacity (BC) than the sham group (Fig. 2-1a and b). A single administration of M-MSCs restored detrusor pressure in a dose dependent manner; however, the beneficial effects of M-MSC therapy were suboptimal for restoring micturition interval (MV) and volume. Conversely, injection of 1000 K M-MSCs significantly reduced the residual volume (RV), resulting in decreased bladder capacity, compared with the DUA group (Fig. 2-1b).

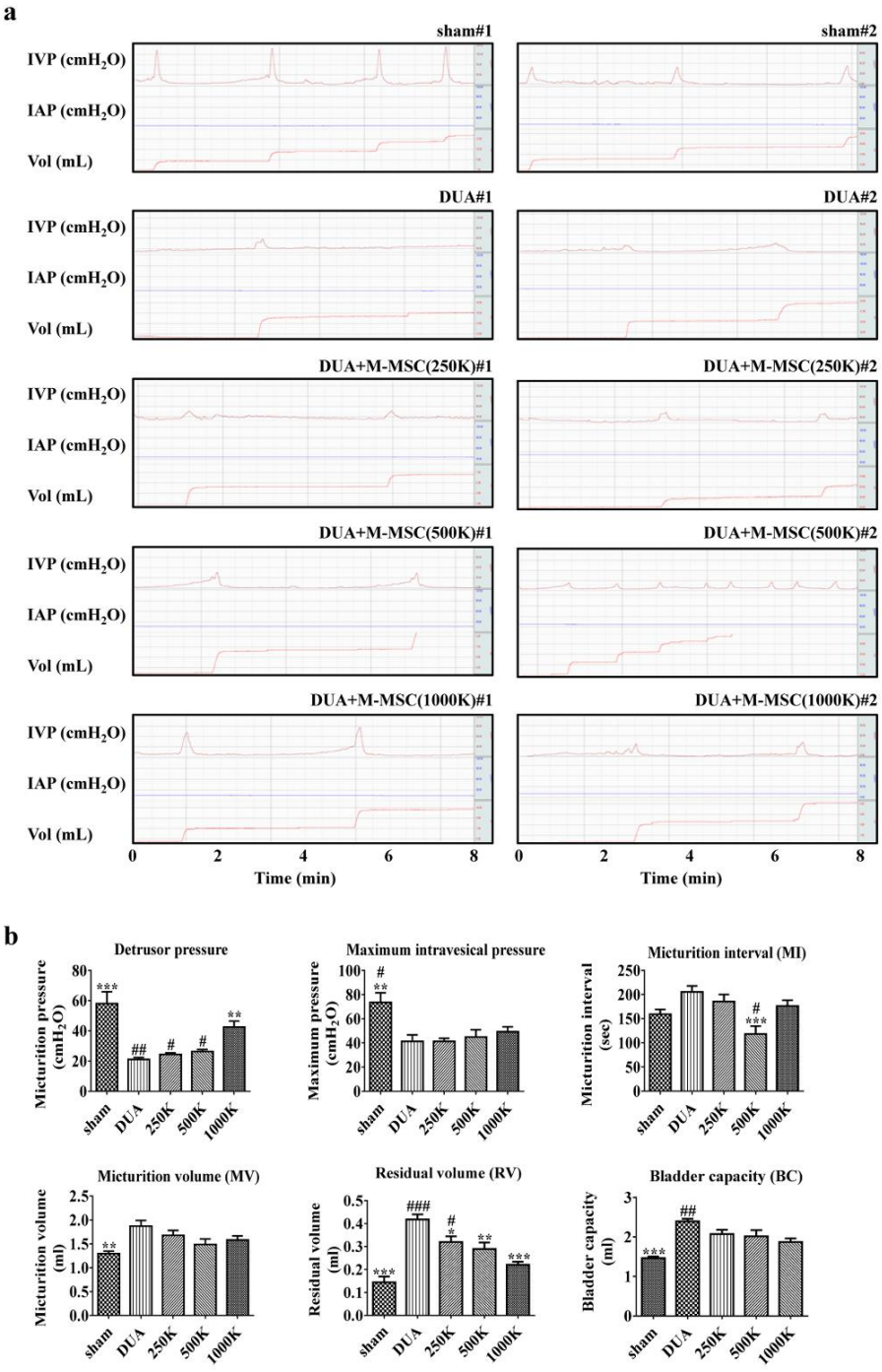

Figure 2-1. M-MSC injection restored bladder function in DUA rat models

(**a**) Representative awake cystometry results and (**b**) Quantitative analysis of bladder voiding parameters 1-week post-injection of either 0.25 ×, 0.5 ×, or 1.0 × 10^6 M-MSCs (250 K, 500 K, or 1000 K groups, K = a thousand) into rat bladders. All quantitative data are presented as

mean ± SEM. *$p < 0.05$, **$p < 0.01$, ***$p < 0.001$ compared with the DUA group; #$p < 0.05$, ##$p < 0.01$, ###$p < 0.001$ compared with the 1000 K group. One-way ANOVA with Bonferroni post-hoc test was used for statistical analysis. IVP, intravesical pressure; IAP, intra-abdominal pressure.

Organ Bath Study

Bladder strips from the DUA group overall demonstrated significantly deteriorated contractile responses to various stimuli including 80 mM KCl, electrical field stimulation, 1 mM ATP, and carbachol concentration response, compared with the sham group (Fig. 2-2a–d). In line with the awake cystometry results, M-MSC injection restored these contractility defects in a dose-dependent manner, with 1000 K M-MSC treatment exhibiting the highest potency in all the stimulations. Taken together, these results demonstrate that a single local administration of 1.0×10^6 M-MSCs was more effective at restoring bladder voiding function and contractibility induced by a high degree of atherosclerotic occlusion.

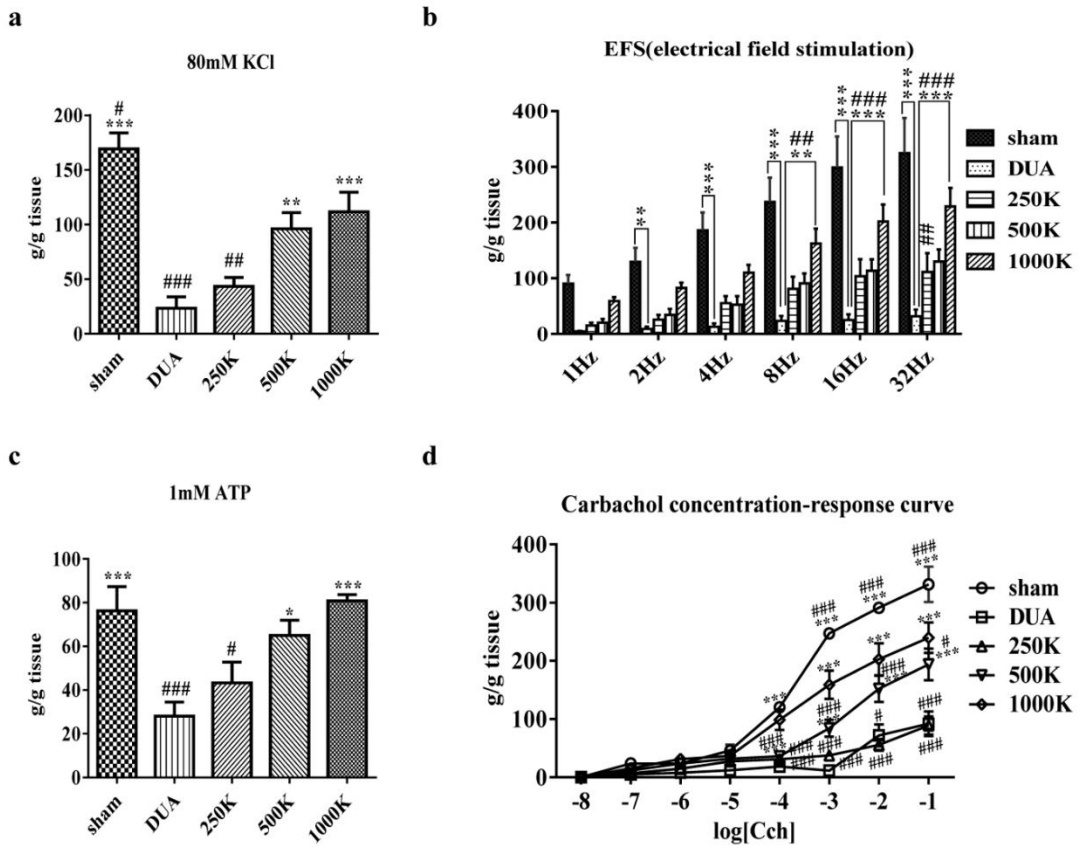

Figure 2-2. Repair of bladder contractility by M-MSC therapy

(**a**–**d**) Organ bath analysis for evaluating the contractile response of bladder muscle strips to either 80 mM KCl (**a**), electrical field stimulation (**b**), 1 mM ATP (**c**), or carbachol, as indicated (**d**). All quantification data are presented as mean ± SEM (12 bladder strips from six independent rats). *$p < 0.05$, **$p < 0.01$, ***$p < 0.001$ compared with the DUA group; #$p < 0.05$, ##$p < 0.01$, ###$p < 0.001$ compared with the 1000 K group with one- (**a** and **c**) or two- (**b** and **d**) ANOVA with Bonferroni post-tests.

Histological Analysis

We next examined whether M-MSC therapy can regenerate the histological damage characteristic of DUA bladders. Rat bladders in the DUA group presented with atrophy of bladder muscle (Fig. 2-3a) and accompanied fibrosis indicated by accumulation of collagen fibers based on strong Masson's trichrome staining (Fig. 2-3b). The muscular degeneration was confirmed by immunohistochemical staining of α-SMA protein (Fig. 2-3c).

Consistent with these histological injuries, the DUA bladders showed a significant increase of apoptosis in both the urothelial and muscular layer of the bladder along with endothelium of bladder vasculature (Fig. 2-4a). Of importance, M-MSC injection into the rats alleviated the characteristic DUA histological injuries including fibrosis, muscular degeneration, and increased apoptosis of the bladder muscle tissue (Fig. 2-3 and 2-4). Rat bladders treated with 1000 K M-MSCs had a significant improvement of tissue fibrosis and muscle atrophy, and reduced apoptosis of muscle fibers, compared with the 250 K and 500 K MSC treatment groups (Fig. 2-3e and d; Fig. 2-4b–d). These results indicate a dose-dependent therapeutic effect of M-MSC therapy for DUA.

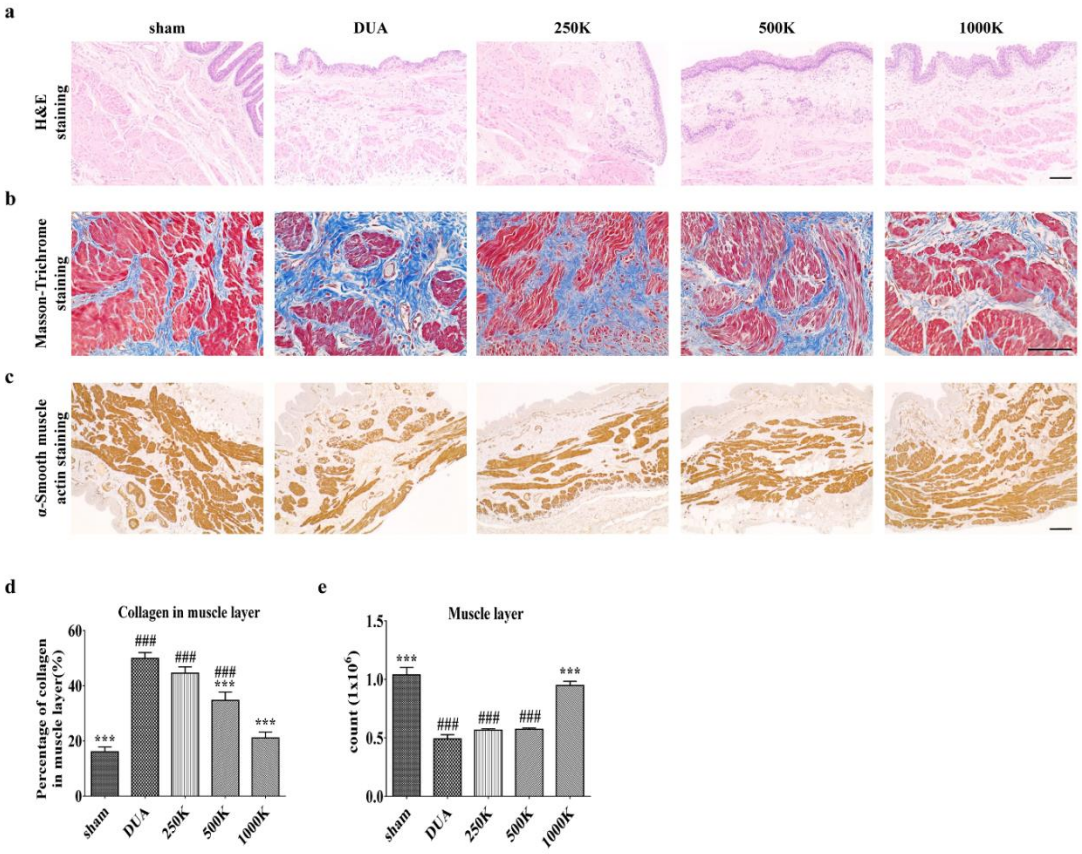

Figure 2-3. M-MSCs injection repaired histological injury in CBI bladders

(**a** and **b**) Representative images for hematoxylin and eosin (H&E; magnification ×100, scale bar = 200 μm, **a**) and Masson's trichrome (magnification ×400, scale bar = 200 μm, **b**) staining in the bladder tissues 1 week after transplantation of the indicated dosage M-MSCs. The tissue fibrosis was stained in blue. (**c**) Representative images for immuno-histochemical staining of α-smooth muscle actin (α-SMA, magnification ×100, scale bar = 200 μm) in the indicated bladders. Nuclei were stained with Mayer's hematoxylin. (**d** and **e**) Quantification of histological examinations for fibrosis (**d**) and α-SMA stained muscle fiber (**e**). All quantitative data are presented as the mean ± SEM (n = 9 or 10). *$p < 0.05$, **$p < 0.01$, ***$p < 0.001$ compared with the DUA group; #$p < 0.05$, ##$p < 0.001$, ###$p < 0.001$ compared with the 1000 K group with one-way ANOVA with Bonferroni post-tests.

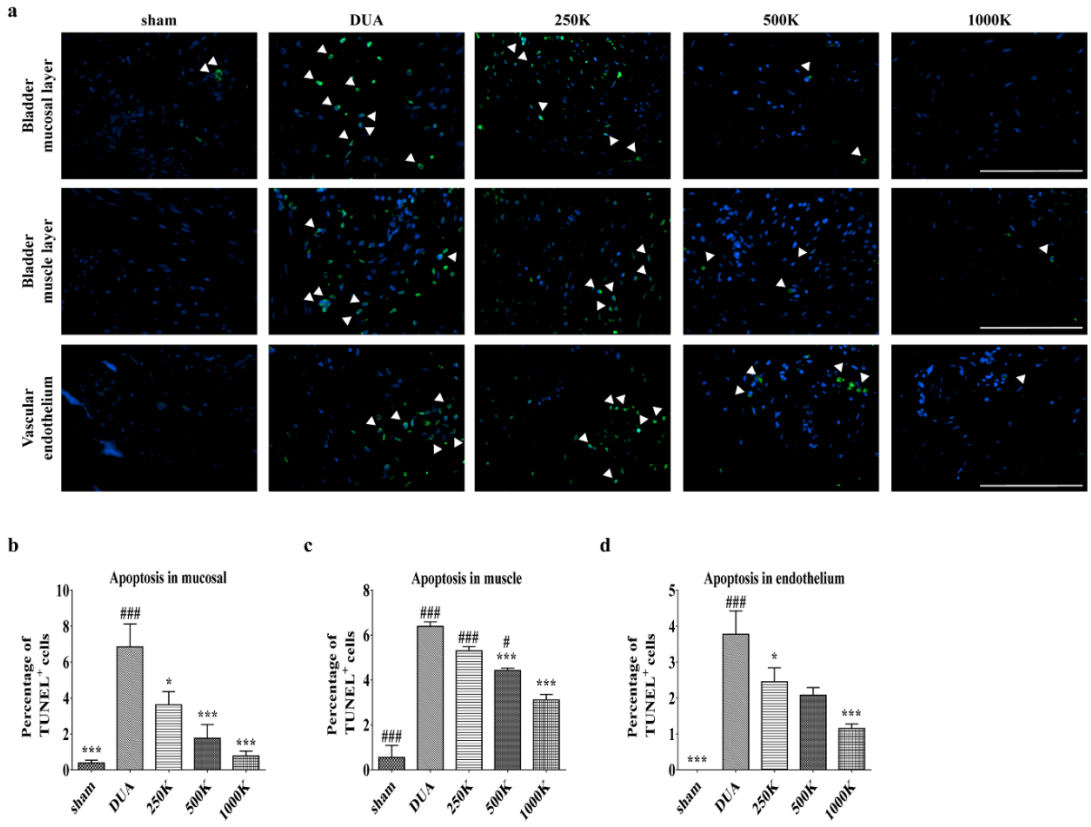

Figure 2-4. M-MSC therapy protected the apoptotic response in CBI bladders

(**a**) Representative images of TUNEL staining for apoptotic cells (green, magnification ×400, scale bar = 200 μm) in the mucosal and muscle layers, and vascular endothelium of bladders in the indicated groups. Nuclei were stained with DAPI. (**b**–**d**) Quantification of percentage of apoptotic cells (arrowhead in a) by calculating the ratio of apoptotic cells (TUNEL positive) to total cells (DAPI-stained nuclei). All quantitative data are presented as the mean ± SEM (n = 9 or 10). *$p < 0.05$, **$p < 0.01$, ***$p < 0.001$ compared with the DUA group; #$p < 0.05$, ##$p < 0.001$, ###$p < 0.001$ compared with the 1000 K group with one-way ANOVA with Bonferroni post-tests.

Characterization of Cellular Properties of the Engrafted M-MSCs

Next, to determine the in vivo distribution and cellular differentiation lineage of the transplanted M-MSCs, the engrafted M-MSCs were detected by immunostaining with the human antigen hB2MG, and co-stained with either α-SMA, a muscle marker; vimentin, a mesenchymal marker; or NG2, a pericyte maker. The majority of $hB2MG^{+}$ engrafted cells were localized between muscle and serosa of the bladder at the site of M-MSCs injection. In particular, the engrafted hB2MG positive ($^{+}$) cells were frequently observed near but not in the muscle fibers, and they expressed minimal α-SMA protein (Fig. 2-5a), suggesting that the transplanted M-MSCs may not contribute toward the myocyte in the CBI-injured bladders. Instead, the $hB2MG^{+}$ cells were localized in close proximity to bladder vessels and co-stained with the NG2 pericyte and vimentin stromal marker proteins (Fig. 2-5b and c). The results indicated that M-MSCs mainly engrafted as pericytes to support paracrine effects for repairing tissue damage in the CBI bladders.

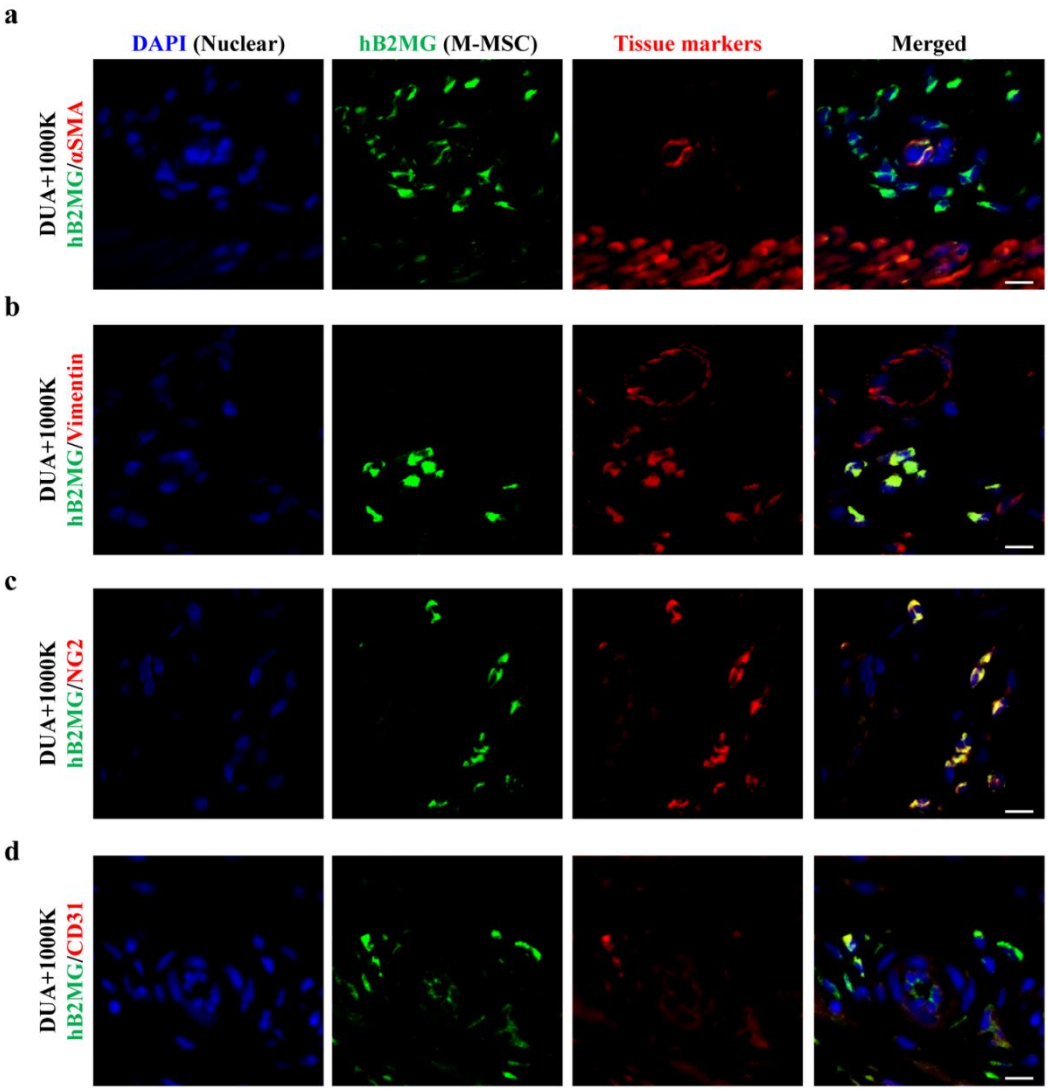

Figure 2-5. Cellular lineages of transplanted M-MSCs in the CBI bladders

(**a**–**c**) Representative confocal microscopic images (magnification ×1000, scale bar = 10 μm) of human B2MG (hB2MG, green) co-stained with either α-SMA myocyte (**a**), vimentin stromal cell (**b**), NG2 pericyte (**c**), or CD31 endothelial cell (**d**) markers in bladder sections harvested from DUA + 1000 K rats at 1-week post-transplant. Nuclei were stained with DAPI (blue). Note that M-MSCs mainly engrafted as pericytes, not endothelial cells in vessels near muscle fibers in the CBI bladders.

The Role of M-MSC Therapy in Angiogenesis of the CBI Bladders

Induction of angiogenesis is an important mechanism for elucidating the beneficial outcome of MSC therapy [22]. To address this issue, we quantified the blood vessel content in the rat bladders by immunohistochemical analysis with CD31, an endothelial cell marker. In line with the engraftment of M-MSCs as a pericyte (Fig. 2-5b and c), the content of $CD31^+$ vessels in the CBI-injured bladders were increased by the administration of M-MSCs (Fig. 2-6a and b). However, the majority of $hB2MG^+$ cells expressed practically no CD31 antigen (Fig. 2-5d), indicating that pericytes near blood vessels, not endothelial cells, were the major cellular fate of the engrafted M-MSCs in the CBI bladders.

To obtain more mechanistic insights, we examined the expression level of several factors related to angiogenesis and the repair of the bladder injury [4,23]. The gene expression analysis revealed that M-MSCs, compared with IMR90, a differentially normal fibroblast cell, had significantly increased expression of a subset of pro-angiogenic factors and their cognate receptors, including vascular endothelial growth factor-A (VEGFA), platelet-derived growth factors (PDGF-A, -B, and -D), fibroblast growth factor-2 (FGF2), transforming growth factor β-1 (TGFB1), VEGF receptor-1 (VEGFR1), integrin subunit α-V (ITGAV), angiopoietin-1 receptor (TEK), and CD44 (Fig. 2-7 and Fig. 2-8). In addition, M-MSCs up-regulated their expression of WNT family member genes (e.g., WNT2, WNT4, and WNT5B), which play an important role in repair of the bladder injury [9,10,14,24]. Taken together, these results support the finding that M-MSCs, mainly engrafted as pericytes in blood vessels near bladder muscle fibers, stimulate angiogenesis in the CBI injured bladder, which might be crucial for their therapeutic potency.

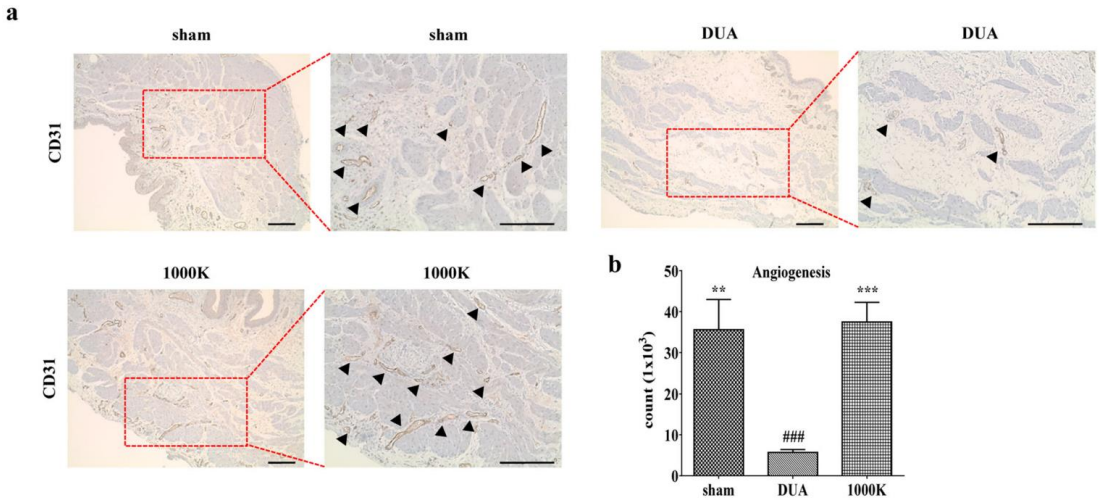

Figure 2-6. M-MSCs injection stimulated angiogenesis in CBI bladders

(**a**) Representative images of immuno-histochemical staining of CD31 (magnification ×100, scale bar = 200 μm) in the bladder tissues 1 week after transplantation of the indicated dosage of M-MSCs. Photomicrographs with higher magnification (magnification ×200, scale bar = 200 μm) are shown in the right corner of each panel. The arrowheads indicate the CD31 positive ($CD31^+$) vessels. The nuclei were stained with Mayer's hematoxylin. (**b**) Quantification of the $CD31^+$ vessels in the indicated bladders. Quantitative data are presented as the mean ± SEM (n = 9 or 10). $^{**}p < 0.01$, $^{***}p < 0.001$ compared with the DUA group; $^{###}p < 0.001$ compared with the 1000 K group with one-way ANOVA with Bonferroni post-tests.

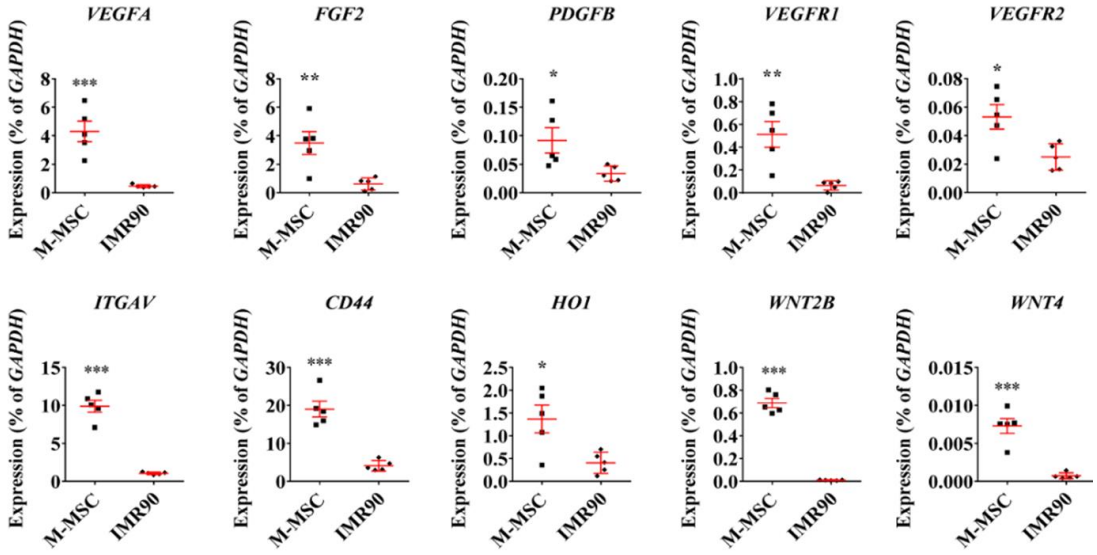

Figure 2-7. Gene expression analysis revealed that M-MSCs

Expression of transcripts of genes related to the angiogenesis and WNT signaling pathways in the M-MSCs and IMR90, a human primary lung fibroblast. Expression is presented as % GAPDH and shown as a dot plot of mean ± SEM (n = 5). *$p < 0.05$, **$p < 0.01$, ***$p < 0.001$ compared by the non-parametric Mann–Whitney U test.

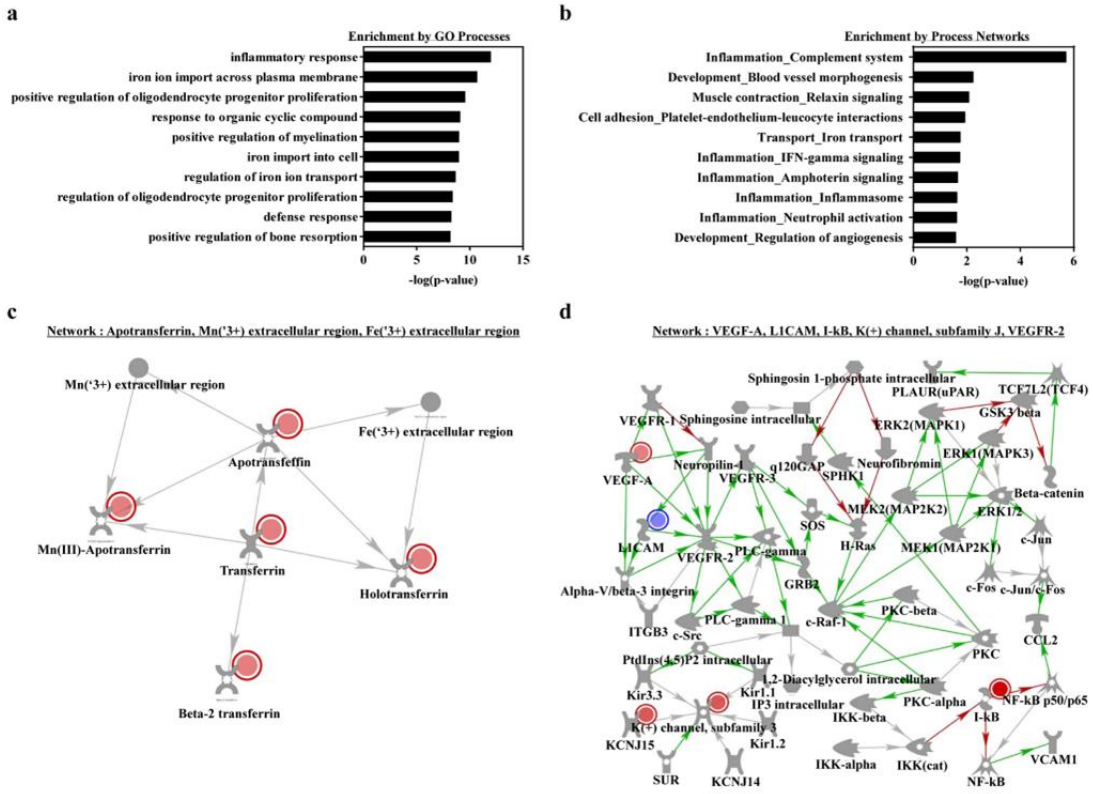

Figure 2-8. Expression of a subset of pro-angiogenic factors

(**a** and **b**) The top Gene Ontology (GO) processes (**a**) and process networks (**b**) as revealed by MetaCore analysis comparing CBI and sham bladders. (**c** and **d**) Two representative gene networks related to iron ion import (**c**) or VEGF- and NFκB-mediated cellular response to growth factor stimulus (**d**), as determined by MetaCore analysis. Gene networks are illustrated by overlaying the experimental values as fold changes in CBI versus sham samples. Up- and down-regulated genes are indicated in red and green, respectively.

Gene Expression Analysis

A previous transcriptomic study reported that CBI-induced bladder injury characteristically up-regulated the genes involved in the IL-17 and HIF-1 signaling pathways [19]. For example, the expression of NFKB inhibitor-alpha (Nfkbia), C-X-C motif hemokine ligand-2 (Cxcl-2), and S100 calcium binding protein-A9 (S100a9) representing the IL-17 pathway was significantly increased in the CBI-injured bladders. In addition, the expression of interferon gamma receptor-1 (Ifngr-1) and Vegfa were up-regulated as HIF-1 pathways. Of importance, M-MSC therapy significantly prevented the dysfunction of these IL-17- or HIF-1-related genes (Fig. 2-9).

To identify the driving genes underlying DUA pathogenesis induced by ischemic vascular injury, we further analyzed the published transcriptome datasets for sham and DUA bladders [19] using the MetaCore transcriptome analysis tool that provides the gene networks, biological processes, and pathway maps. Compared with the sham group, CBI bladders exhibited characteristic changes in the complement immune response-, inflammation-, and ion transport-related pathways (Fig. 2-10a-d). The molecular features of CBI bladders were elucidated by examining the altered expression of complement factor-B or -H (Cfb and Cfh), complement C2 (C2), Angiopoietin 1 (Angpt-1), colony stimulating factor 3 receptor (Csf3r), C-X-C motif chemokine ligand-3 (Cxcl-3) genes, interleukin-33 (Il-33), and transferrin (Tf) (Fig. 2-10d The transplantation of M-MSCs significantly restored the altered expression of Cfh and Tf as well as the majority of the inflammatory genes in the bladders.

Furthermore, MetaCore gene network analysis revealed that the CBI bladders were characterized by the VEGF-A and I-κB associated gene networks involving Vegf-a, Ikb, and the L1 cell adhesion molecule (L1cam) (Fig. 2-11), as well as networks related to the sensory perception of chemical stimuli, including claudin-23 (Cldn23), alkylglycerone phosphate synthase (Agps, also known as Adas), Angpt-1, transmembrane Channel Like 7 (Tmc7), and interferon induced protein with tetratricopeptide repeats-1 (Ifit-1, also known as Ifi-56) (Fig. 2-12). Accordingly, CBI injury significantly down-regulated Cldn23 and up-regulated Tmc7 in the bladders treated with M-MSCs (Fig. 2-7e). Collectively, these results demonstrate the

novel significance of the complement system and ion transport-related pathways. Further, these results indicate that CBI-induced DUA pathogenesis leads to an NF-κB- and VEGF-A-mediated inflammatory response, which may be important when considering the applications of M-MSC therapy.

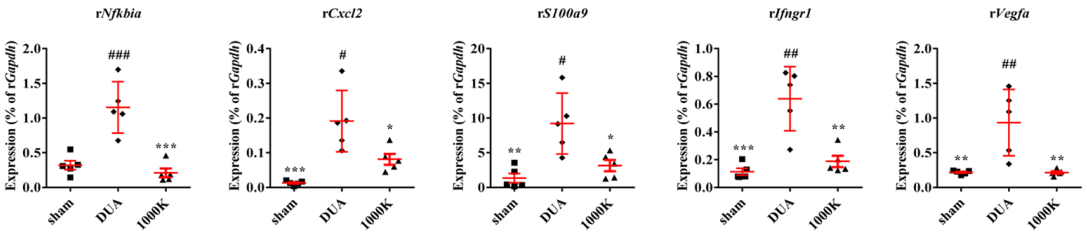

Figure 2-9. Expression of HIF-1 signaling pathways

Real-time qPCR analysis of genes relating to the IL-17 and HIF-1 signaling pathways in the indicated bladders. Expression is presented as % of Gapdh expression and shown as a dot plot of mean SEM (n = 5). *$p < 0.05$, **$p < 0.01$, ***$p < 0.001$ compared with the DUA group; #$p < 0.05$, ##$p < 0.01$, ###$p < 0.001$ compared with the 1000 K group with one-way ANOVA with Bonferroni post-tests.

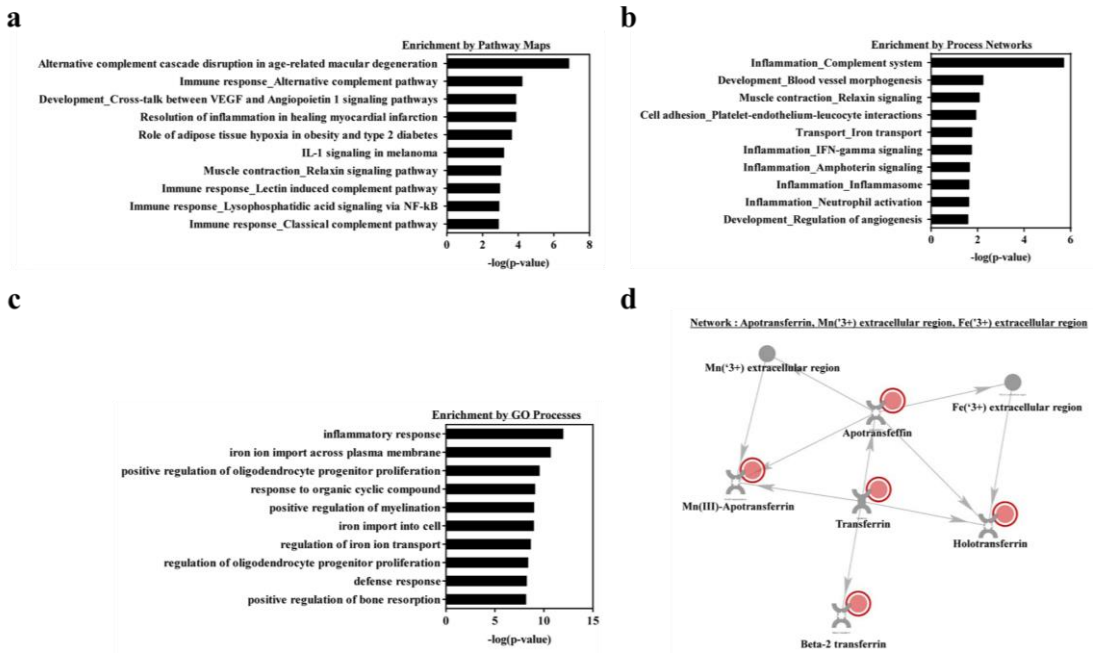

Figure 2-10. Characteristic changes in complement immune response, inflammation, and ion transport pathways in CBI bladders

(**a** and **b**) The top Gene Ontology (GO) processes (**a**) and process networks (**b**) as revealed by MetaCore analysis comparing CBI and sham bladders. Gene networks are illustrated by overlaying the experimental values as fold changes in CBI versus sham samples. Up- and down-regulated genes are indicated in red and green, respectively.

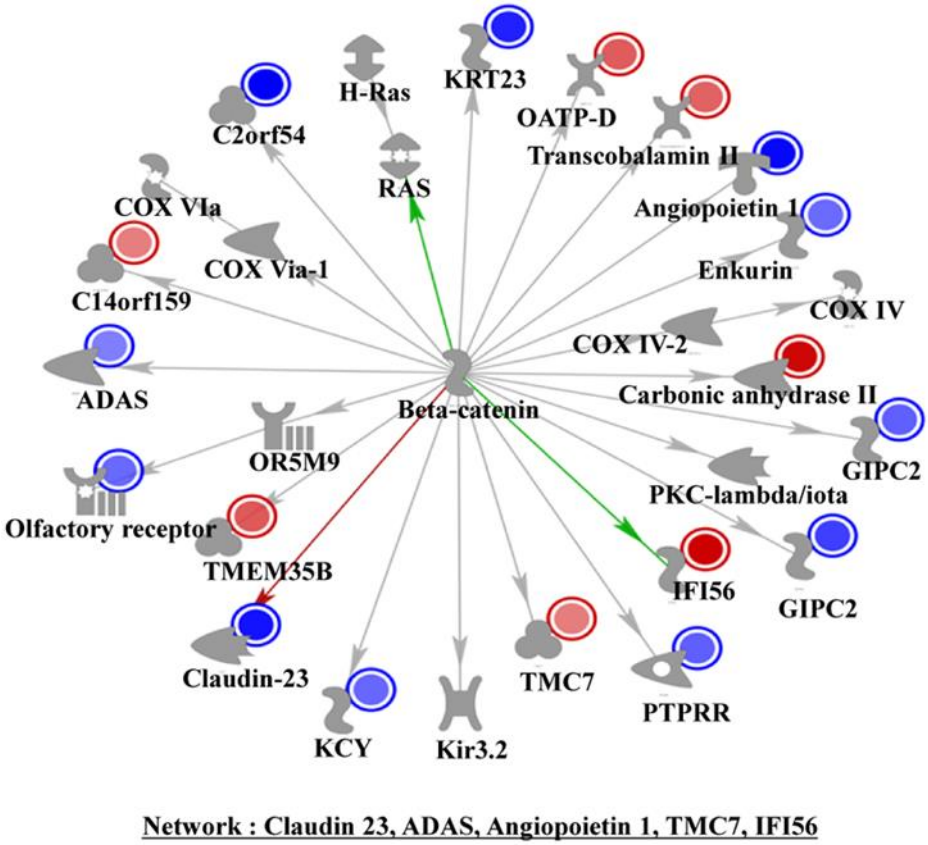

Figure 2-11. Pathway maps revealed in networks related to chemical sensory perception in DUA and sham bladders

Representative gene network associated with the sensory perception of chemical stimuli. The gene network is illustrated by overlaying experimental values as fold changes in CBI versus sham samples. Up- and down-regulated genes are indicated in red and green, respectively genes involved in networks characteristic of CBI in the indicated bladders. Expression is presented as % of Gapdh expression and shown as a dot plot of mean SEM (n = 5). *$p < 0.05$, **$p < 0.01$, ***$p < 0.001$ compared with the DUA group; #$p < 0.05$, ##$p < 0.01$, ###$p < 0.001$ compared with the 1000 K group with one-way ANOVA with Bonferroni post-tests.

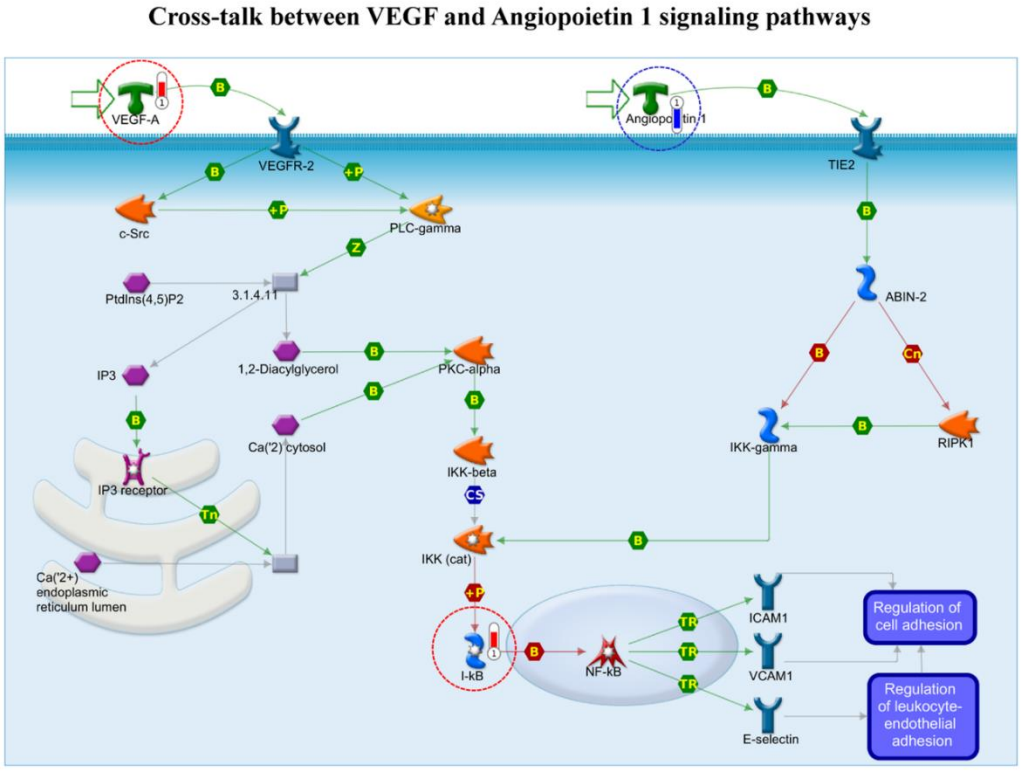

Figure 2-12. Cross-talk between VEGF and Angiopoietin 1 signaling pathways

A schematic overview of the cross-talk between VEGF and angiopoietin 1 signaling pathways in MetaCore analysis of the CBI bladder transcriptome dataset. The gene expression fold changes in CBI versus sham samples are overlaid in the pathway map. Up- and down-regulated genes are indicated in red and green, respectively.

DISCUSSION

In this preclinical study, we demonstrate the therapeutic effects of M-MSC transplantation in a CBI-induced rat model of DUA. Following transplantation, the injected M-MSCs mainly integrated into pericytes nearby muscle fibers of the rat bladders and exhibited paracrine effects to repair vascular insult and detrusor muscle damage. Mechanistically, M-MSC therapy prevented the NF-κB-mediated inflammatory and complement system response in the CBI-induced bladders. In human DUA patients, a common symptom is an underactive bladder that is characterized by a slow urine stream, hesitancy, and straining to void, with or without a feeling of incomplete bladder emptying [25]. Diagnosis of underactive bladder is frustrating as current therapeutic options have suboptimal and limited efficacy. In the early phase of DUA, patients are able to void with abdominal straining and oral medication but might complain of a weak stream and residua urine sensation. However, as DUA persists, progressive bladder remodeling results in a decompensated state with urothelial dysfunction, neuron and smooth muscle degeneration, and high levels of extracellular matrix deposition in the bladder [26]. Timely intervention to prevent irreversible changes of detrusor is necessary.

The current treatment strategies for DUA aim to improve detrusor contractility, reducing bladder outlet resistance or direct drainage of urine. Surgical intervention to reduce bladder outlet resistance and direct drainage of urine is relatively invasive compared with medical therapy. Direct drainage of urine is not a definite resolution for DUA as it only circumvents the existing problem [27]. In addition, effective bladder emptying cannot be achieved if adequate detrusor contraction is absent. Considering that normal voiding is achieved by adequate, continuous detrusor contraction, which leads to complete bladder emptying within a normal time span, future investigations to fulfill the unmet needs of DUA should focus on restoring the detrusor contractility before the golden time.

Stem cell therapy seems to be an adequate candidate for restoring detrusor contractility [4, 12]. Contemporary concepts in the pathogenesis of DUA are complex, such that its etiological factors can be classified as idiopathic, neurogenic, myogenic, iatrogenic, and functional [28]. Our CBI DUA model presented with myogenic degeneration, increased apoptosis in both the urothelial and muscular layers of the bladder, and increased collagen deposition. A single

administration of M-MSCs successfully alleviated both the histological and functional abnormalities by reversing muscle atrophy and reducing the inflammatory and complement system response in CBI-induced rat bladders. Therefore, the present study provides an in vivo proof of concept that MSC therapy is a viable option for treating DUA.

The application of autologous muscle-derived mesenchymal stem cells (AMDC) has been reported in several clinical trials to treat stress urinary incontinence patients. Recently, Gilleran et al., reported the first regulatory approved clinical trial, which evaluated the safety and efficacy of intradetrusor injected AMDCs in 20 non-neurogenic DUA patients [29]. The study subjects received approximately 30 transurethral injections of 0.5 mL delivered to the bladder (125 million AMDC/15 mL). The initial end point was post-injection 6 months; however, all participants asked for a second injection due to satisfactory results, so the follow-up assessments were made at post-injection 1, 3, 6, and 12 months. At the primary outcome point of 12 months, 11 out of 19 patients (58 %) reported a global response assessment ≥ 5, showing slight to marked improvement in their symptoms. In addition, improvement of voiding efficiency was observed in many subjects who were catheter dependent at baseline. No AMDC-related serious adverse events were reported. The reported adverse events included injection related and biopsy related complications. The main differences between this clinical trial and our preclinical study are the injection route and the type of stem cells used. As there are no currently available devices, such as a cystoscope with an injection channel for rats, the M-MSCs were directly injected into the rat bladder. However, if our study is clinically applied, M-MSCs will be injected via a transurethral route as it is familiar to urologists and is minimally invasive.

Large-scale production of MSCs from adult tissues adversely resulted in the loss of their primitive functions. In addition, adult-tissue derived MSCs, especially those from aged donors, have limited proliferative capacity in vitro due to replicative senescence [30–33], and MSCs at high passage number are more likely to trigger an innate immune attack upon transplantation [34]. To overcome these issues, M-MSCs used in this study were derived from hESCs, which have been suggested as a cost-effective alternative source due to their pluripotency and unlimited expansion potential [6]. Indeed, the M-MSCs used in this study could be expanded for more than 30 passages without adverse genetic or functional abnormalities and exhibited

several typical MSC features, including fibroblast-like morphology and expression of surface markers characteristic to MSCs (CD73 and CD105) or pericytes (PDGFRB, CD146, and NG2), and chondrogenic, osteogenic, and adipogenic differentiation ability [9]. More importantly, M-MSCs showed superior therapeutic efficacy and long-term in vivo engraftment to adult-tissue counterparts in several animal models of interstitial cystitis/bladder pain syndrome (IC/BPS) [9,10,13], ketamine cystitis [11], and diabetes mellitus associated DUA, as well as asthma [33,35]. Moreover, hESC-derived M-MSCs do not need tissue biopsy or sampling from subjects in a clinical setting, so biopsy-related adverse events can be avoided. In the present study, we demonstrate that hESC-derived M-MSCs can be also effective for treating DUA induced by chronic vascular endothelial damage.

In several preclinical and clinical trials using adult-tissue derived MSCs, poor engraftment and survival of the transplanted cells under in vivo conditions have impeded transferring MSC therapy into clinical practice. The preceding data reporting advantages of M-MSCs might be attribute able to enhanced in vivo engraftment and survival [9,10]. In the CBI-injured bladders, $hB2MG^+$ engrafted cells were detected 7 days after transplantation, mainly located between the muscle and serosa of the bladder. The engrafted M-MSCs contributed little to the α-SMA^+ myocyte. Instead, they were engrafted into pericytes or stromal cells near blood vessels and muscle fibers, suggesting that their prolonged paracrine effects repair the damaged muscle fibers. The several trophic factors secreted by MSCs are responsible for paracrine effects by mediating immune-suppressive, anti-inflammatory, and pro-angiogenic responses, which have significantly contributed to the beneficial outcomes of MSC therapy targeting several diseases. Gene expression analysis revealed that M-MSCs, compared with the differentiated fibroblast cell line, up-regulated the expression of several angiogenic genes (e.g., VEGFA, PDGF-A, and FGF2) and tissue regenerating WNT family genes (e.g., WNT2B and WNT4). WNT signaling plays a key role in angiogenesis and vascular remodeling or maturation in the tissue development, homeostasis and repair processes [36–39]. In particular, the secreted Frizzled-related protein-1, a modulator of the WNT pathway, stimulates the angiogenic functions of MSCs, leading to vessel maturation and functionality. Therefore, further in-depth characterization of the paracrine factors of M-MSCs, including WNT related factors, could advance our understanding of the mode of action of M-MSC therapy targeted to DUA. In

addition, further study is warranted to investigate the underlying mechanisms and key player(s) that modulate the perivascular engraftment of M-MSCs in the DUA pathological condition.

To date, the pathophysiology of CBI-induced DUA has not been fully elucidated [40,41]. In the present study, transcriptome analysis of CBI-injured bladders was characterized by the alternation of the complement system (e.g., Cfb, Cfh, and C2), and the inflammatory (e.g., Csf3r, Cxcl-3, and Il-33), ion transport (Tf), IL-17 (Nfkbia, Cxcl2, and S100a9), and HIF-1 (Vegfa and Angpt-1) signaling pathways. In response to CBI damage, VEGF and ANGPT-1 signaling can crosstalk to stimulate NF-κB activation, enhancing leukocyteendothelial adhesion and aggravating vascular endothelial damage (Fig. 2-12). Furthermore, inflammatory signals, including interleukin-1, can activate VEGF-A expression and angiogenesis in the tumor micro-environments [42–44]. Since M-MSC therapy effectively restored the dysfunction of genes related to VEGF-A and NF-κB signaling, a further study is required to determine whether the interplay between these signaling pathways is involved in CBI-induced DUA. It would also be interesting to further investigate the role of the complement system in the pathophysiology of DUA, which is relatively unknown.

The main limitation of current study is its preclinical design. The pathophysiology of DUA is multifactorial and our CBI model might not reflect the entire and complex pathogenesis. In addition, despite the promising results from this preclinical study, one major obstacle to the therapeutic application of hESC-derivatives is the safety issues, including the possible formation of teratoma or other tumors, immune rejection, and the risk that the cell will differentiate into unwanted cell types [45]. However, recent successful clinical studies for the therapy of eye disorders could alleviate this general concern of hESC-based therapeutics [46,47]. Likewise, the aforementioned adverse outcomes were not detected in longterm monitoring up to 1 year in both acute and chronic IC/BPS animal models treated with M-MSC therapy [9, 10]. However, safety issues surrounding hESC-based therapies must still be thoroughly investigated before clinical application of these cells [45].

In conclusion, this study findings provide an in vivo proof of concept for treating CBI-induced DUA with hESC-derived M-MSCs that restore bladder voiding functions, contractibility, and histological features. Further, we optimized dosage and elucidated the underlying molecular mechanisms of M-MSC therapy.

REFERENCE

Chapter 1. Reference

1. Holgate, S. T. et al. *Asthma*. Nat. Rev. Dis. Prim, **1**, 15025 (2015)
2. Yang, J., Kim, E. K., Park, H. J., McDowell, A. & Kim, Y. K. *The impact of bacteria derived ultrafine dust particles on pulmonary diseases*. Exp. Mol. Med, **52**, 338–347 (2020).
3. Wilhelm, C. & Stockinger, B. *Innate lymphoid cells and type 2 (th2) mediated immune responses - pathogenic or beneficial?* Front. Immunol, **2**, 68 (2011).
4. Lambrecht, B. N. & Hammad, H. *The immunology of asthma.* Nat. Immunol, **16**, 45–56 (2015).
5. Holgate, S. T. & Polosa, R. *Treatment strategies for allergy and asthma.* Nat. Rev. Immunol, **8**, 218–230 (2008).
6. Zhang, L. B. & He, M. *Effect of mesenchymal stromal (stem) cell (MSC) transplantation in asthmatic animal models: a systematic review and meta-analysis.* Pulm Pharmacol Ther, **54**, 39–52 (2019).
7. Srour, N. & Thebaud, B. *Stem cells in animal asthma models: a systematic review.* Cytotherapy, **16**, 1629–1642 (2014).
8. Jin, H. J. et al. *Senescence-associated MCP-1 secretion is dependent on a decline in BMI1 in human mesenchymal stromal cells.* Antioxid Redox Signal, **24**, 471–485 (2016).
9. Jeong, E. M. et al. *Real-time monitoring of glutathione in living cells reveals that high glutathione levels are required to maintain stem cell function.* Stem Cell Rep, **10**, 600–614 (2018).
10. Lee, S. et al. *Ascorbic acid 2-glucoside stably promotes the primitiveness of embryonic and mesenchymal stem cells through ten-eleven translocation- and cAMP-responsive element-binding protein-1-dependent mechanisms.* Antioxid Redox Signal, **32**, 35–59 (2020).
11. Hong, K. S. et al. *A porous membrane-mediated isolation of mesenchymal stem cells*

from human embryonic stem cells. Tissue Eng. Part C. Methods, **21**, 322–329 (2015).

12. Kim, J. M. et al. *Perivascular progenitor cells derived from human embryonic stem cells exhibit functional characteristics of pericytes and improve the retinal vasculature in a rodent model of diabetic retinopathy.* Stem Cells Transl. Med, **5**, 1268–1276 (2016).
13. Ryu, C. M. et al. *Longitudinal intravital imaging of transplanted mesenchymal stem cells elucidates their functional integration and therapeutic potency in an animal model of interstitial cystitis/bladder pain syndrome.* Theranostics, **8**, 5610–5624 (2018).
14. Shin, J. H. et al. *Safety of human embryonic stem cell-derived mesenchymal stem cells for treating interstitial cystitis: a phase I study.* Stem Cells Transl. Med, **11**, 1010–1020 (2022).
15. Huang, Y. et al. *miR-19b enhances osteogenic differentiation of mesenchymal stem cells and promotes fracture healing through the WWP1/Smurf2-mediated KLF5/β-catenin signaling pathway.* Exp. Mol. Med, **53**, 973–985 (2021).
16. Yu, H. Y. et al. *Intravital imaging and single cell transcriptomic analysis for engraftment of mesenchymal stem cells in an animal model of interstitial cystitis/ bladder pain syndrome.* Biomaterials, **280**, 121277121277 (2022).
17. ArefNezhad, R., *Motedayyen, H. & Mohammadi, A. Therapeutic aspects of mesenchymal stem cell-based cell therapy with a focus on human amniotic epithelial cells in multiple sclerosis: a mechanistic review.* Int. J. Stem Cells, **14**, 241–251 (2021).
18. Kiaie, N., Ghanavati, S. P. M., Miremadi, S. S., Hadipour, A. & Aghdam, R. M. *Mesenchymal stem cell-derived exosomes for COVID-19 therapy, preclinical and clinical evidence.* Int. J. Stem Cells, **14**, 252–261 (2021).
19. Heo, J. et al. *Sirt1 regulates DNA methylation and differentiation potential of embryonic stem cells by antagonizing Dnmt3l.* Cell Rep, **18**, 1930–1945 (2017).
20. Kim, Y. et al. *Small hypoxia-primed mesenchymal stem cells attenuate graft versus-host disease*. Leukemia, **32**, 2672–2684 (2018).
21. Lim, J. et al. *Glutathione dynamics determine the therapeutic efficacy of mesenchymal stem cells for graft-versus-host disease via CREB1-NRF2 pathway.* Sci. Adv, **6**,

eaba1334 (2020).

22. Lim, J. et al. *Valproic acid enforces the priming effect of sphingosine-1 phosphate on human mesenchymal stem cells.* Int. J. Mol. Med, **40**, 739–747 (2017).

23. Lim, J. et al. *Small-sized mesenchymal stem cells with high glutathione dynamics show improved therapeutic potency in graft-versus-host disease.* Clin. Transl. Med, **11**, e476 (2021).

24. Mushahary, D., Spittler, A., Kasper, C., Weber, V. & Charwat, V. *Isolation, cultivation, and characterization of human mesenchymal stem cells.* Cytom. A, **93**, 19–31 (2018).

25. Heo, J. et al. *The CDK1/TFCP2L1/ID2 cascade offers a novel combination therapy strategy in a preclinical model of bladder cancer.* Exp. Mol. Med, **54**, 801–811 (2022).

26. Jeong, E. M. et al. *Monitoring glutathione dynamics and heterogeneity in living stem cells.* Int. J. Stem Cells, **12**, 367–379 (2019).

27. Kang, H. et al. *Effect of Acinetobacter lwoffii on the modulation of macrophage activation and asthmatic inflammation.* Clin. Exp. Allergy, **52**, 518–529 (2021).

28. Heo, J. et al. *Phosphorylation of TFCP2L1 by CDK1 is required for stem cell pluripotency and bladder carcinogenesis.* EMBO Mol. Med, **12**, e10880 (2020).

29. Lopez-Bergami, P., Lau, E. & Ronai, Z. *Emerging roles of ATF2 and the dynamic AP1 network in cancer.* Nat. Rev. Cancer, **10**, 65–76 (2010).

30. Kim, J. & Wong, P. K. *Loss of ATM impairs proliferation of neural stem cells through oxidative stress-mediated p38 MAPK signaling.* Stem cells, **27**, 1987–1998 (2009).

31. Yu, T. et al. *The regulatory role of activating transcription factor 2 in inflammation.* Mediators Inflamm, **950472** (2014).

32. Huebner, K., Prochazka, J., Monteiro, A. C., Mahadevan, V. & Schneider-Stock, R. *The activating transcription factor 2: an influencer of cancer progression.* Mutagenesis, **34**, 375–389 (2019).

33. Ha, E. H. et al. *Endothelial Sox17 promotes allergic airway inflammation.* J. Allergy Clin. Immunol, **144**, 561–573 e566 (2019).

34. Watanabe, J. et al. *Preconditioning of bone marrow-derived mesenchymal stem cells with N-acetyl-L-cysteine enhances bone regeneration via reinforced resistance to oxidative stress.* Biomaterials, **185**, 25–38 (2018).

35. Gong, P., Stewart, D., Hu, B., Vinson, C. & Alam, J. *Multiple basic-leucine zipper proteins regulate induction of the mouse heme oxygenase-1 gene by arsenite.* Arch. Biochem. Biophys, **405**, 265–274 (2002).

36. Wang, L. et al. *ATF2 inhibits ani-tumor effects of BET inhibitor in a negative feedback manner by attenuating ferroptosis. Biochem.* Biophys. Res. Commun, **558**, 216–223 (2021).

37. Walluscheck, D. et al. *ATF2 knockdown reinforces oxidative stress-induced apoptosis in TE7 cancer cells.* J. Cell Mol. Med, **17**, 976–988 (2013).

38. Thiel, G. & Rössler, O. G. *Resveratrol stimulates cyclic AMP response element mediated gene transcription. Mol.* Nutr. Food Res, **60**, 256–265 (2016).

39. Petry, A. & Görlach, A. *Regulation of NADPH oxidases by G protein-coupled receptors.* Antioxid Redox Signal, **30**, 74–94 (2019).

40. Yaghoubi, M., Adibi, A., Safari, A., FitzGerald, J. M. & Sadatsafavi, M. *The projected economic and health burden of uncontrolled asthma in the United States.* Am. J. Respir. Crit. Care Med, **200**, 1102–1112 (2019).

41. Krause, D. S. et al. *Multi-organ, multi-lineage engraftment by a single bone marrow-derived stem cell.* Cell, **105**, 369–377 (2001).

42. Rojas, M. et al. *Bone marrow-derived mesenchymal stem cells in repair of the injured lung.* Am. J. Respir. Cell Mol. Biol, **33**, 145–152 (2005).

43. Krause, D. S. *Bone marrow–derived cells and stem cells in lung repair.* Proc. Am. Thorac. Soc, **5**, 323–327 (2008).

44. Kassmer, S. H., Bruscia, E. M., Zhang, P.-X. & Krause, D. S. *Nonhematopoietic cells are the primary source of bone marrow-derived lung epithelial cells.* Stem Cells, **30**, 491–499 (2012).

45. Cerrada, A. et al. *Human decidua-derived mesenchymal stem cells differentiate into functional alveolar type II-like cells that synthesize and secrete pulmonary surfactant complexes.* PLoS One, **9**, e110195 (2014).

46. Carraro, G. et al. *Human amniotic fluid stem cells can integrate and differentiate into epithelial lung lineages.* Stem Cells, **26**, 2902–2911 (2008).

47. Liu, A. et al. *Wnt5a through noncanonical Wnt/JNK or Wnt/PKC signaling*

contributes to the differentiation of mesenchymal stem cells into type II alveolar epithelial cells in vitro. PLoS One, **9**, e90229 (2014).

48. Sheng, H. et al. *A critical role of IFNgamma in priming MSC-mediated suppression of T cell proliferation through up-regulation of B7-H1.* Cell Res, **18**, 846–857 (2008).

49. Krampera, M. et al. *Role for interferon-γ in the immunomodulatory activity of human bone marrow mesenchymal stem cells.* Stem Cells, **24**, 386–398 (2006).

50. Wang, Y., Chen, X., Cao, W. & Shi, Y. *Plasticity of mesenchymal stem cells in immunomodulation: pathological and therapeutic implications.* Nat. Immunology, **15**, 1009–1016 (2014).

Chapter 2. Reference

1. Abrams, P., Cardozo, L., Fall, M., Griffiths, D., Rosier, P., Ulmsten, U., van Kerrebroeck, P., Victor, A. et al. *The standardisation of terminology of lower urinary tract function: Report from the standardisation subcommittee of the international continence society.* Neurourology and Urodynamics, **21(2)**, 167–178 (2002).
2. Smith, P. P. et al. *Detrusor underactivity and the underactive bladder: Symptoms, function, cause-what do we mean? ICI-RS think tank 2014.* Neurourology and Urodynamics, **35(2)**, 312–317 (2016).
3. Osman, N. I., Esperto, F. et al. *Detrusor underactivity and the underactive bladder: A systematic review of preclinical and clinical studies.* European Urology, **74(5)**, 633–643 (2018).
4. Shin, J. H., Ryu, C. M., Yu, H. Y., Shin, D. M. et al. *Current and future directions of stem cell therapy for bladder dysfunction.* Stem Cell Reviews and Reports, **16(1)**, 82–93 (2020).
5. Kim, Y., Jin, H. J., Heo, J., Ju, H., Lee, H. Y., Kim, S., Lee, S., Lim, J., Jeong, S. Y., Kwon, J. H., Kim, M., Choi, S. J., Oh, W., Yang, Y. S., Hwang, H. H., Yu, H. Y. et al. *Small hypoxia-primed mesenchymal stem cells attenuate graft-versus-host disease.* Leukemia, **32(12)**, 2672–2684 (2018).
6. E., H. K., Michelangelo, C., Kate, D., M., R. A., Filipa, V., KwanLeong, H., et al. *Embryonic stem cell-derived mesenchymal stem cells (MSCs) have a superior neuroprotective capacity over fetal MSCs in the hypoxic-ischemic mouse brain.* Stem Cells Translational Medicine, **7(5)**, 439–449 (2018).
7. Sheyn, D., Ben-David, S., Shapiro, G., De Mel, S., Bez, M., Ornelas, L. et al. *Human induced pluripotent stem cells differentiate into functional mesenchymal stem cells and repair bone defects.* Stem Cells Translational Medicine, **5(11)**, 1447– 1460 (2016).
8. Zhang, Y., Liang, X., Liao, S., Wang, W., Wang, J., Li, X., Ding, Y., Liang, Y., Gao, F., Yang, M., Fu, Q., Xu, A., Chai, Y. H., He, J. et al. *Potent paracrine effects of human induced pluripotent stem cell-derived mesenchymal stem cells attenuate doxorubicin-induced cardiomyopathy.* Scientific Reports, **5**, 11235 (2015).

9. Kim, A., Yu, H. Y., Lim, J., Ryu, C. M., Kim, Y. H., Heo, J., Han, J. Y., Lee, S., Bae, Y. S., Kim, J. Y., Bae, D. J., Kim, S. Y., Noh, B. J., Hong, K. S., Han, J. Y., Lee, S. W., Song, M., Chung, H. M., Kim, J. K. et al. *Improved efficacy and in vivo cellular properties of human embryonic stem cell derivative in a preclinical model of bladder pain syndrome.* Scientific Reports, **7(1)**, 8872 (2017).

10. Ryu, C. M., Yu, H. Y., Lee, H. Y., Shin, J. H., Lee, S., Ju, H., Paulson, B., Lee, S., Kim, S., Lim, J., Heo, J., Hong, K. S., Chung, H. M., Kim, J. K., Shin, D. M., & Choo, M. S. *Longitudinal intravital imaging of transplanted mesenchymal stem cells elucidates their functional integration and therapeutic potency in an animal model of interstitial cystitis/bladder pain syndrome.* Theranostics, **8(20)**, 5610–5624 (2018).

11. Lee, S. W., Ryu, C. M., Shin, J. H., Choi, D., Kim, A., Yu, H. Y., Han, J. Y., Lee, H. Y., Lim, J., Kim, Y. H., Heo, J., Lee, S., Ju, H., Kim, S., Hong, K. S., Han, J. Y., Song, M., Chung, H. M., Kim, J. K., Shin, D. M., & Choo, M. S. *The therapeutic effect of human embryonic stem cell-derived multipotent mesenchymal stem cells on chemical-induced cystitis in rats.* International Neurourology Journal, **22**(Suppl 1), S34–S45 (2018).

12. Shin, J. H., Ryu, C.-M., Ju, H., Yu, H. Y., Song, S., Hong, K.-S., Chung, H. M., Park, J., Shin, D. M., & Choo, M. S. et al. *Therapeutic efficacy of human embryonic stem cell-derived multipotent stem/stromal cells in diabetic detrusor underactivity: A preclinical study*. Journal of Clinical Medicine, **9(9)** (2020).

13. Ryu, C. M., Shin, J. H., Yu, H. Y., Ju, H., Kim, S., Lim, J., Heo, J., Lee, S., Shin, D. M. et al. *N-acetylcysteine prevents bladder tissue fibrosis in a lipopolysaccharide-induced cystitis rat model.* Scientific Reports, **9(1)**, 8134 (2019).

14. Song, M., Lim, J., Yu, H. Y., Park, J., Chun, J. Y., Jeong, J., Heo, J., Kang, H., Kim, Y. H., Cho, Y. M., Kim, S. W., Oh, W., Choi, S. J., Jang, S. W., Park, S., Shin, D. M., & Choo, M. S. *Mesenchymal stem cell therapy alleviates interstitial cystitis by activating Wnt signaling pathway.* Stem Cells and Development, **24(14)**, 1648–1657 (2015).

15. Kim, A., Yu, H. Y., Heo, J., Song, M., Shin, J. H., Lim, J., Yoon, S. J., Kim, Y. H., Lee, S., Kim, S. W., Oh, W., Choi, S. J., Shin, D. M. et al. *Mesenchymal stem cells protect against the tissue fibrosis of ketamine-induced cystitis in rat bladder.* Scientific

Reports, **6**, 30881 (2016).

16. Shin, J. H., Ryu, C.-M., Ju, H., Yu, H. Y., Song, S., Shin, D.-M., & Choo, M. S. *Synergistic effects of N-acetylcysteine and mesenchymal stem cell in a lipopolysaccharide-induced interstitial cystitis rat model.* Cells, **9(1)**, 86 (2019).
17. Song, M., Heo, J., Chun, J.-Y., Bae, H. S., Kang, J. W., Kang, H., Cho, Y. M., Kim, S. W., Shin, D. M., & Choo, M. S. *The paracrine effects of mesenchymal stem cells stimulate the regeneration capacity of endogenous stem cells in the repair of a bladderoutlet-obstruction-induced overactive bladder.* Stem Cells and Development, **23(6)**, 654–663 (2013).
18. Lim, J., Heo, J., Ju, H., Shin, J.-W., Kim, Y., Lee, S. et al. *Glutathione dynamics determine the therapeutic efficacy of mesenchymal stem cells for graft-versus-host disease via CREB1-NRF2 pathway.* Science Advances, **6(16)**, eaba1334 (2020).
19. Kim, M., Yu, H. Y., Ju, H., Shin, J. H., Kim, A., Lee, J., Ryu, C. M., Yun, H. D., Lee, S., Lim, J., Heo, J., Shin, D. M. et al. *Induction of detrusor underactivity by extensive vascular endothelial damages of iliac arteries in a rat model and its pathophysiology in the genetic levels.* Scientific Reports, **9(1)**, 16328 (2019).
20. Heo, J., Noh, B. J., Lee, S., Lee, H. Y., Kim, Y., Lim, J., Ju, H., Yu, H. Y., Ryu, C. M., Lee, P. C., Jeong, H., Oh, Y., Kim, K., Kim, S. Y., Son, J., Hong, B., Kim, J. S., Cho, Y. M. et al. *Phosphorylation of TFCP2L1 by CDK1 is required for stem cell pluripotency and bladder carcinogenesis.* EMBO Molecular Medicine, **12(1)**, e10880 (2020).
21. Heo, J., Lim, J., Lee, S., Jeong, J., Kang, H., Kim, Y., Kang, J. W., Yu, H. Y., Jeong, E. M., Kim, K., Kucia, M., Waigel, S. J., Zacharias, W., Chen, Y., Kim, I. G., Ratajczak, M. Z., & Shin, D. M. *Sirt1 regulates DNA methylation and differentiation potential of embryonic stem cells by antagonizing Dnmt3l.* Cell Reports, **18(8)**, 1930–1945 (2017).
22. Kang, H., Kim, K.-H., Lim, J., Kim, Y.-S., Heo, J., Choi, J., Jeong, J., Kim, Y. H., Kim, S. W., Oh, Y. M., Choo, M. S., Son, J., Kim, S. J., Yoo, H. J., Oh, W., Choi, S. J., Lee, S. W. et al. *The therapeutic effects of human mesenchymal stem cells primed with Sphingosine-1 phosphate on pulmonary artery hypertension.* Stem Cells and

Development, **24(14)**, 1658–1671 (2015).

23. Bastakoty, D., & Young, P. P. *Wnt/beta-catenin pathway in tissue injury: Roles in pathology and therapeutic opportunities for regeneration.* The FASEB Journal, **30(10)**, 3271–3284 (2016).

24. Shin, K., Lee, J., Guo, N., Kim, J., Lim, A., Qu, L., Mysorekar, I. U., & Beachy, P. A. Hedgehog/Wnt feedback supports regenerative proliferation of epithelial stem cells in bladder. Nature, **472(7341)**, 110–114 (2011).

25. Osman, N. I., Chapple, C. R., Abrams, P. et al. *Detrusor underactivity and the underactive bladder: A new clinical entity? A review of current terminology, definitions, epidemiology, aetiology, and diagnosis.* European Urology, **65(2)**, 389–398. (2014).

26. Osman, N. I., & Chapple, C. R. *Contemporary concepts in the aetiopathogenesis of detrusor underactivity.* Nature Reviews. Urology, **11(11)**, 639–648 (2014).

27. Bayrak, Ö., & Dmochowski, R. R. *Underactive bladder: A review of the current treatment concepts.* Turkish Journal of Urology, **45(6)**, 401–409 (2019).

28. Aizawa, N., & Igawa, Y. *Pathophysiology of the underactive bladder. Investig Clin Urol*, **58(Suppl 2)**, S82–S89 (2017).

29. Gilleran, J., Diokno, A. C. et al. *Improved global response outcome after intradetrusor injection of adult muscle-derived cells for the treatment of underactive bladder.* International Urology and Nephrology, **53**, 1331–1338 (2021).

30. Zaim, M., Karaman, S. et al. *Donor age and long-term culture affect differentiation and proliferation of human bone marrow mesenchymal stem cells.* Annals of Hematology, **91(8)**, 1175–1186 (2012).

31. Kretlow, J. D., Jin, Y.-Q., Liu, W., Zhang, W. J., Hong, T.-H., Zhou, G. et al. *Donor age and cell passage affects differentiation potential of murine bone marrow-derived stem cells.* BMC Cell Biology, **9(1)**, 60 (2008).

32. Wagner, W., Bork, S., Horn, P., Krunic, D., Walenda, T. et al. *Aging and replicative senescence have related effects on human stem and progenitor cells.* PLoS One, **4(6)**, e5846 (2009).

33. Lee, S., Lim, J., Lee, J. H., Ju, H., Heo, J., Kim, Y., Kim, S., Yu, H. Y., Ryu, C. M., Lee, S. Y., Han, J. M., Oh, Y. M., Lee, H., Jang, H., Yoon, T. J., Ahn, H. S., Kim, K., Kim, H. R., Roe, J. S., Chung, H. M., Son, J., Kim, J. S., & Shin, D. M. *Ascorbic acid 2- glucoside stably promotes the primitiveness of embryonic and mesenchymal stem cells through ten-eleven translocation- and cAMPresponsive element-binding Protein-1-dependent mechanisms.* Antioxidants & Redox Signaling, **32(1)**, 35–59 (2020).

34. Moll, G., Rasmusson-Duprez, I., von Bahr, L., Connolly-Andersen, A.-M., Elgue, G., Funke, L., Hamad, O. A., Lönnies, H., Magnusson, P. U., Sanchez, J., Teramura, Y., Nilsson-Ekdahl, K., Ringdén, O., Korsgren, O., Nilsson, B., & le Blanc, K. *Are therapeutic human mesenchymal stromal cells compatible with human blood*? Stem Cells, **30(7)**, 1565–1574 (2012).

35. Jeong, E. M., Yoon, J. H., Lim, J., Shin, J. W., Cho, A. Y., Heo, J., Lee, K. B., Lee, J. H., Lee, W. J., Kim, H. J., Son, Y. H., Lee, S. J., Cho, S. Y., Shin, D. M., Choi, K., & Kim, I. G. *Real-time monitoring of glutathione in living cells reveals that high glutathione levels are required to maintain stem cell function.* Stem Cell Reports, **10(2)**, 600–614 (2018).

36. Chen, Q., Zhang, H., Liu, Y., Adams, S., Eilken, H. et al. *Endothelial cells are progenitors of cardiac pericytes and vascular smooth muscle cells.* Nature Communications, **7**, 12422 (2016).

37. Gaskill, C. F., Carrier, E. J., Kropski, J. A., Bloodworth, N. C., Menon, S., Foronjy, R. F., Taketo, M. M., Hong, C. C., Austin, E. D., West, J. D., Means, A. L., Loyd, J. E., Merryman, W. D., Hemnes, A. R., de Langhe, S., Blackwell, T. S., Klemm, D. J., & Majka, S. M. *Disruption of lineage specification in adult pulmonary mesenchymal progenitor cells promotes microvascular dysfunction.* The Journal of Clinical Investigation, **127(6)**, 2262–2276 (2017).

38. Lee, S., Elaskandrany, M., Lau, L. F., Lazzaro, D., Grant, M. B., & Chaqour, B. *Interplay between CCN1 and Wnt5a in endothelial cells and pericytes determines the angiogenic outcome in a model of ischemic retinopathy.* Scientific Reports, **7(1)**, 1405 (2017).

39. Mazzoni, J., Smith, J. R., Shahriar, S., Cutforth, T., Ceja, B., & Agalliu, D. *The Wnt*

inhibitor Apcdd1 coordinates vascular remodeling and barrier maturation of retinal blood vessels. Neuron, **96(5)**, 1055–1069 e1056 (2017).

40. Nomiya, M., Yamaguchi, O., Akaihata, H., Hata, J., Sawada, N., Kojima, Y., & Andersson, K. E. *Progressive vascular damage may lead to bladder underactivity in rats.* The Journal of Urology, **191(5)**, 1462–1469 (2014).
41. Sagawa, K., Aikawa, K., Nomiya, M., Ogawa, S., Akaihata, H., Takahashi, N., et al. *Impaired detrusor contractility in a rat model of chronic bladder ischemia.* Urology, **81(6)**, 1379 e1379-1314 (2013).
42. Lebovic, D. I., Bentzien, F., Chao, V. A., Garrett, E. N., Meng, Y. G., & Taylor, R. N. *Induction of an angiogenic phenotype in endometriotic stromal cell cultures by interleukin-1beta.* Molecular Human Reproduction, **6(3)**, 269–275 (2000).
43. Zhou, W., Guo, S., & Gonzalez-Perez, R. R. *Leptin proangiogenic signature in breast cancer is linked to IL-1 signalling.* British Journal of Cancer, **104(1)**, 128–137 (2011).
44. Kolb, R., Phan, L., Borcherding, N., Liu, Y., Yuan, F., Janowski, A. M., Xie, Q., Markan, K. R., Li, W., Potthoff, M. J., Fuentes-Mattei, E., Ellies, L. G., Knudson, C. M., Lee, M. H., Yeung, S. C. J., Cassel, S. L., Sutterwala, F. S., & Zhang, W. *Obesity associated NLRC4 inflammasome activation drives breast cancer progression.* Nature Communications, **7**, 13007 (2016).
45. Cho, S. J., Kim, S. Y., Jeong, H. C., Cheong, H., Kim, D., Park, S. J., Choi, J. J., Kim, H., Chung, H. M., Moon, S. H., & Cha, H. J. *Repair of ischemic injury by pluripotent stem cell based cell therapy without Teratoma through selective photosensitivity.* Stem Cell Reports, **5(6)**, 1067–1080 (2015).
46. Schwartz, S. D., Regillo, C. D., Lam, B. L., Eliott, D., Rosenfeld, P. J., Gregori, N. Z., Hubschman, J. P., Davis, J. L., Heilwell, G., Spirn, M., Maguire, J., Gay, R., Bateman, J., Ostrick, R. M., Morris, D., Vincent, M., Anglade, E., del Priore, L. V., & Lanza, R. *Human embryonic stem cell-derived retinal pigment epithelium in patients with age-related macular degeneration and Stargardt's macular dystrophy: Follow-up of two open-label phase 1/2 studies.* Lancet, **385(9967)**, 509–516 (2015).
47. Schwartz, S. D., Hubschman, J. P., Heilwell, G., Franco-Cardenas, V., Pan, C. K., Ostrick, R. M., Mickunas, E., Gay, R., Klimanskaya, I., & Lanza, R. *Embryonic stem*

cell trials for macular degeneration: A preliminary report. Lancet, **379(9817)**, 713–720 (2012).

Abstract in Korean

CHAPTER 1

풍부한 비단백질 티올 항산화제인 글루타치온(GSH)은 여러 생물학적 과정에 참여하며 줄기세포의 기능을 결정한다. 하지만 현재까지 GSH 역학을 매개하는 네트워크에 대한 자세한 연구는 아직까지 부족한 실정이다. 본 연구에서는 cAMP 반응 요소 결합 단백질(CREB)인 전사 활성화 인자-2(ATF2)가 핵 인자와의 누화를 통해 인간 중간엽 줄기 세포(MSC)에서 GSH 의 수준과 활성을 유지하는 데 중요한 역할을 한다는 것을 보여준다. Nuclear factor (erythroid-derived 2) like-2 (NRF2)는 세포 산화환원 항상성에 관여하는 것으로 잘 알려진 마스터 조절인자이다. 안정적인 비타민 C 유도체인 AA2G(ascorbic acid 2-glucoside)를 사용한 프라이밍은 인간 배아 줄기 세포와 탯줄에서 유래한 중간엽 줄기세포에서 ATF2 의 발현과 활성을 증가시켰다. 그리고 활성화된 ATF2 는 CREB1-NRF2 경로와 누화되어 GSH 합성(GCLC 및 GCLM) 및 산화환원 순환(GSR 및 PRDX1)에 관여하는 유전자의 유도를 통해 중간엽 줄기세포의 GSH 역학을 보존한다. 따라서, ATF2 의 shRNA-매개 침묵화는 중간엽 줄기세포의 자기 재생, 이동, 혈관형성 및 항 염증 능력을 현저하게 손상시켰고, 이러한 결함은 GSH 로 중간엽 줄기세포를 보충함으로써 구제되었다. 또한, ATF2 를 억제하면 오브 알부민으로 유발된 알레르기성 천식 마우스 모델에서 기도 염증반응을 완화시키는 중간엽 줄기세포의 능력이 약화되었다. 일관되게 과발현 또는 AA2G 기반 프라이밍 절차에 의한 ATF2 의 활성화는 중간엽 줄기세포의 핵심 기능을 향상시켜, 중간엽 줄기세포의 천식 치료에 대한 생체 내 치료 효능을 향상시켰다.

결과적으로, 논문의 연구 결과는 ATF2 가 알레르기성 천식을 치료하는 데 사용되는 중간엽 줄기세포의 핵심 기능과 치료 효능을 결정하는 GSH 역학의 새로운 조절자임을 시사한다.

CHAPTER2

본 연구에서는 인간 배아 줄기 세포 유래 다능성 중간엽 줄기 세포(M-MSCs)의 치료 효과를 통해 죽상경화증으로 유발된 만성 방광 허혈(CBI) 및 관련 메커니즘이 있는 In vivo 모델에서 배뇨근 기능저하(DUA)에 대해 평가했다.

16 주령의 수컷 Sprague‑Dawley Rat model 을 5 개 그룹(n = 10)으로 나누었다. DUA 그룹은 CBI 를 유도하기 위해 장골 동맥에 대한 내피 손상의 양측 반복을 30 회 반복했다.

본 연구에 사용된 모든 Rat 은 8 주 동안 1.25 % 콜레스테롤 식이요법을 진행했으며, 2.5, 5.0 또는 10.0 × 10^5 세포(250K, 500K 또는 1000K, K = 1000) 밀도의 M-MSC 를 손상 후 7 주째에 방광에 직접 주입한 반면 sham 및 DUA 그룹 vehicle(인산완충액) 로만 처리했다. M-MSC 주입 1 주 후, 방광측정법을 Rat 에게 수행한 후, 방광조직을 확보하여 장기 인큐베이터에서 근육장력 평가를 수행하고 면역조직 화학염색법 및 유전자 발현 분석을 진행했다.

장골 동맥 손상에 의한 CBI 는 감소된 배뇨 압력, 증가된 배뇨 간격 및 더 큰 장기 부피와 함께 DUA 의 특징인 배뇨 결손을 재현했다. 병리학적 DUA 특성은 M-MSC 처리에 의해 용량 의존적으로 개선되었으며, 1000K 그룹이 최고의 효능을 나타냈다. 조직학적 분석에 따르면 M-MSC 요법은 방광 섬유증, 근육 손실 및 세포자살을 포함한 CBI 유발 손상을 감소시켰다. 이식된 M-MSC 는 근세포보다는 주로 Vimentin 및 NG2 양성 혈관주위세포로 이식되어 CBI 방광에서 Wnt signaling 과 매개하여 혈관신생을 증가시켰다. CBI 손상 방광의 전사체는 M-MSC 요법으로 회복된 보체 시스템, 염증 및 이온 수송 관련 경로를 특징으로 가진다.

CBI 유도 DUA Rat 모델의 방광에 직접 M-MSC 를 주입하면 배뇨 프로파일이 개선되고 용량 의존 방식으로 방광 근육 위축이 복구되는 연구결과를 확인할 수 있었다.

결과적으로, 논문의 연구 결과는 M-MSC 가 CBI 유도 DUA 질환을 손상된 방광에서 Wnt signaling 과 매개하여 혈관신생을 증가시킴을 통해 치료효능에 있어 중요한 key factor 로써 작용함을 시사한다.

Acknowledgments

박사학위 졸업논문을 작성함에 있어, 많은 지원과 도움을 받아 이에 진심을 담아 감사의 말씀을 올립니다.

우선, 본 연구의 완성을 위해 지도해주신 저의 지도교수님인 서울아산병원, 울산대의과대학, 세포치료센터 센터장이신, 신동명 교수님께 깊은 감사의 말씀을 드립니다. 신동명 교수님의 연구에 대한 열정과 지혜로운 조언, 인내심 있는 지도, 그리고 항상 초심을 잃지 말라는 말씀 덕분에 긴 연구 생활의 탄탄한 밑거름이 되어 학문적으로 성장할 수 있었습니다.

그리고, 멀리서 늘 응원해주시고 따뜻하게 격려해주시는 경희대 의과대학 박용식 교수님께도 깊은 감사의 말씀을 드립니다. 석사학위 과정부터 이어진 교수님의 따뜻한 말씀과 지지 덕분에 여러 어려움에도 흔들리지 않고 연구에 임할 수 있었습니다.

그리고, 바쁘신 와중에도 시간을 내어 저의 박사학위 졸업논문을 심사해주신 교수님들께도 감사의 말씀드립니다.

또한, 연구를 진행하면서 많은 도움을 주신 실험실 식구들에게 깊은 감사의 말씀을 전합니다. 밤낮을 함께 하며 실험데이터를 분석하고, 어려움을 극복하며 열정적으로 논의했던 시간들로 인해, 연구에 대한 창의적인 관점을 키울 수 있었습니다. 또한 많이 부족한 저에게 다양한 연구 관점을 밝혀주고, 연구 뿐만 아니라 인생에 있어 많은 것들을 배울 수 있는 시간들이었습니다.

그리고, 연구생활에 지칠 때마다, 저의 엔돌핀이 되어준 친구들에게 감사의 말을 전합니다. 같은 분야를 공부하며 연구적인 조언도 스스럼없이 할 수 있어 큰 도움이 되었고, 같은 길을 걸어가며 외롭지 않을 수 있어, 항상 힘이 되고 있다고 말해주고 싶습니다.

긴 시간동안 기다려 주시고 묵묵히 지지와 격려를 보내주신 사랑하는 어머니, 사랑하는 아버지, 그리고 사랑하는 동생에게 깊은 감사의 말씀을 드립니다. 항상 사랑과 응원으로 자신감과 힘을 실어 주셔서 긴 시간동안 전진할 수 있었습니다.

또한, 묵묵히 지지해주신 사랑하는 장인어른, 장모님, 그리고 처제에게 깊은 감사의 말씀을 드립니다. 관심 어린 애정과 배려 덕분에 연구에 집중할 수 있었습니다.

마지막으로, 사랑하는 아내이자 풍납동 귀염둥이 솔이에게 진심 어린 감사의 인사를 전합니다. 긴 시간동안 밤낮없는 학위생활에 많은 일들이 있었고, 함께 희로애락을 보내주어, 늘 힘이 되었고 고마웠다는 말을 전합니다.

함께한 10 년 동안 모든 순간들이 저에게 원동력이 되었고, 앞으로 많은 역경이 닥쳐도 이겨낼 수 있는 용기를 가지게 해주었습니다. 연구자가 아닌 한 사람으로써, 지혜로울 수 있게 옆에서 많은 도움을 준 사랑하는 아내에게 그 간의 노고와 희생에 진심으로 고맙다고 감사의 말을 전합니다.

끝으로 항상 마음에 새기며 연구에 임한 문구가 있습니다. **“Attitude is everything”** 이제 새로운 연구의 길이 또 열리겠지만, **“모든 것은 자세에 달려있다”** 저 문구를 매일 다짐하며 사회에 도움이 되는 연구자가 되겠습니다.

윤 홍 덕 올림